UNIVERSITY OF OKLAHOMA

GRADUATE COLLEGE

SHEAR STRESS-INDUCED ALTERATIONS IN RED BLOOD CELL CALCIUM ACCUMULATION, MICROVESICLE FORMATION, AND DEFORMABILITY UNDER MECHANICAL CIRCULATORY SUPPORT CONDITIONS

A THESIS

SUBMITTED TO THE GRADUATE FACULTY

in partial fulfillment of the requirements for the
Degree of
MASTER OF SCIENCE

By
PAIGE ELIZABETH FREY
Norman, Oklahoma
2025

SHEAR STRESS-INDUCED ALTERATIONS IN RED BLOOD CELL CALCIUM ACCUMULATION, MICROVESICLE FORMATION, AND DEFORMABILITY UNDER MECHANICAL CIRCULATORY SUPPORT CONDITIONS

A THESIS APPROVED FOR THE

SCHOOL OF SUSTAINABLE CHEMICAL, BIOLOGICAL, AND MATERIALS ENGINEERING

BY THE COMMITTEE CONSISTING OF

Dr. Edgar O'Rear, Chair

Dr. Vassilios Sikavitsas

Dr. Roger Harrison

Acknowledgments

I want to thank my advisor, Dr. Edgar O'Rear, for his encouragement, endless amount of great ideas, and for always believing in my abilities. I could not be more grateful to have such an attentive, caring, and motivating mentor, whose support has meant more to me than words can fully express.

I also would like to thank Dr. Roger Harrison and Dr. Vassilios Sikavitsas for serving on my committee and for their valuable feedback, which enhanced the quality of this work.

Kylie Foster has been an invaluable friend and mentor to me. I am extremely grateful for her guidance, support, and the thoughtful conversations that helped me throughout this journey. She is exceptionally intelligent and capable, and I look forward to witnessing all that she will undoubtedly accomplish in her life.

Madena and Jennifer's administrative support was essential to the progress of my research, as was Annette's assistance at Goddard Health Center in coordinating phlebotomy appointments for my study participants. I am also grateful to Andrew D'Amico for his development of the LabView program used in my deformability experiments, and to Dr. Gu for her assistance with confocal microscopy.

To all who have supported me throughout this journey, I extend my sincere thanks.

List of Tables

List of Figures

Abstract

Red blood cells (RBCs) are susceptible to damage from mechanical forces, particularly shear stress, which can impair their function and lead to complications in patients supported by mechanical circulatory devices like heart pumps (LVADs & RVADs) and veno-arterial extracorporeal membrane oxygenation (VA-ECMO). Calcium is a central focus of this work because increases in calcium within RBCs have been observed following both physiological and supraphysiological shear exposures and have been associated with decreased RBC deformability and microvesicle (MV) formation. When an RBC has impaired deformability, anemia may occur due to the inability of RBCs to traverse the slits in the spleen. Erythrocyte-derived microvesicles are known to be increased in MCS patients and have been linked to thrombosis and inflammation. This work investigates the effects of shear stress on RBC intracellular calcium accumulation, MV formation, and deformability under conditions relevant to mechanical circulatory support. In the first study, RBCs were exposed to varying shear durations (0 ms, 5 ms, and 10 ms) in microfluidic channels at a shear rate of 100,000 s^{-1}. The microfluidic devices mimic medical devices in their high-shear stresses with short exposure times. Intracellular calcium levels, measured by flow cytometry using the calcium indicator Fluo-4, AM, showed a transient increase (160%) shortly after shear exposure that normalized within hours, suggesting an attempt to return to calcium homeostasis. Microvesicle formation did not change with exposure time in the microchannel, but decreased over time post-shear, potentially due to vesicle adhesion to cells or collection tubes, warranting further investigation. To further investigate the role of calcium in MV formation in conditions of shear stress, MV concentration was assessed in a CentriMag mock loop system, circulating bovine RBCs for 6 hours in media with and without calcium. This set-up allowed the cells to repeatedly experience the high shear areas of the

CentriMag centrifugal pump at short, singular exposure times. Results demonstrated that CFSE-positive microvesicle production increased over six hours (214% in calcium media, 172% in no-calcium media) due to shear stress, independent of extracellular calcium presence. Plasma free hemoglobin (PFH) levels also rose steadily, indicating hemolysis driven primarily by mechanical stress rather than calcium-mediated processes. The third study evaluated deformability, PFH, and mean cell volume (MCV) in both bovine and human RBCs during prolonged circulation through the CentriMag pump. Deformability was relatively stable over time, but there was a detectable, significant impairment at 4.5 hours for bovine (10%) and 6 hours for human (9%). PFH levels increased consistently. Collectively, these findings emphasize how shear stress affects red blood cell integrity. Monitoring intracellular calcium, microvesicle formation, and deformability may help assess red blood cell damage in artificial organs, and this knowledge can guide the development of strategies to mitigate related complications.

Table of Contents

Chapter 1: Calcium increase in red blood cells in response to shear stress exposure

Abstract

Introduction of calcium into the erythrocyte leads to loss of potassium and cell volume with a resulting decrease in deformability. It can also cause the formation of microvesicles. This study aimed to explore intracellular calcium content of erythrocytes after short term exposure to shear rates like those found during mechanical circulatory support. Shear stress at 100,000 s^{-1} was induced by microfluidic channels of different shear exposures (0 ms, 5 ms, and 10 ms). The intracellular calcium level was measured by median fluorescence intensity from flow cytometry with the use of a fluorescent calcium probe, Fluo-4 AM. Results showed an increase in median fluorescence intensity (160%) in RBCs measured shortly after shear exposure, but the differences leveled out by 2.5- and 5-hours post-shear. This can be explained by the red blood cells' intracellular mechanisms that control calcium concentration. This study also aimed to explore microvesicle formation in response to shear stress since currently, it is not known if microvesicles form from an increase in intracellular calcium under high shear rates. Concentrations of microvesicles in the size range of 0.4 – 1 μm were measured by flow cytometry. Microvesicle formation experienced a decrease with respect to incubation time. This might be explained by microvesicles' adhering to the cells in the suspension, indicating a need for further study. Overall, this study provides evidence that a shear rate of 100,000 s^{-1} for up to 10 ms induces a transient calcium increase within the cell. This information is useful to understand certain complications that originate from mechanical trauma on blood in artificial organs.

Introduction

Artificial organs, such as ventricular assist devices or extracorporeal membrane oxygenation (ECMO) systems, play a crucial role in the survival of many patients; however, they can introduce shear stresses on the blood that exceed normal physiological levels. Shear stress is the force applied parallel to the surface of the cell, and it elicits varied responses from red blood cells. Stresses that are within physiological limits have been observed to increase the deformability of the red blood cell [1], but stresses exceeding physiological limits are known to decrease red blood cell deformability [1, 2]. The interplay between shear stress and intracellular calcium within RBCs has been recognized many times [3, 4], and the correspondence of calcium levels in changes in deformability, as well as microvesicle formation, have been observed [2, 5]. Since calcium plays an important role in red blood cell dynamics, this study aims to examine how intracellular calcium varies with increasing shear stress exposure time at higher shear rates.

Calcium handling in the RBC depends on ATP availability. To prevent calcium accumulation, excess calcium must be actively removed from the cell, a process that depends on ATP. Larsen found that ATP-rich erythrocytes experienced less calcium accumulation compared to ATP-depleted erythrocytes when exposed to the same amount of shear stress [6]. The difference is likely explained by the activity of the plasma membrane calcium ATPase (PMCA), which relies on ATP to pump calcium out of the cell. In the same study, Larsen also reported that calcium-dependent ATPase activity increased with shear rate, showing the need to remove excess calcium when under mechanical stress. At shear rates on the order of 1,000 s^{-1}, Wan found that no measurable ATP was released for exposure times less than 3 ms [7]. These findings are important because the calcium pump needs ATP to function, especially at high shear stresses where calcium entry is elevated. PMCA has a calcium/calmodulin binding site, allowing it to sense when

calcium levels rise and use energy from ATP hydrolysis to provide energy to the calcium pump [8]. If ATP is depleted, the PMCA will not function properly, and calcium is expected to accumulate within the cell. Overall, calcium removal through PMCA depends on ATP availability, making ATP important for keeping calcium in balance.

If shear stress-induced intracellular calcium accumulation induces two effects that decrease ATP, the RBC might experience energy depletion. Energy depletion would result in a shorter RBC lifespan, as ATP is a critical regulator of red blood cell deformability and intracellular calcium homeostasis [9]. Increased intracellular calcium along with impaired cell shape, and decreased deformability occur with ATP depletion , all being able to be partially reversed by restoring ATP and chelating calcium [10]. This relationship highlights the importance of ATP, not only in managing calcium transport mechanisms like PMCA, but also in preserving the mechanical properties of the RBC membrane. Without sufficient ATP, red blood cells become less deformable, more rigid, and are ultimately cleared from circulation sooner. Although an increase of intracellular calcium might cause energy depletion, red blood cells can restore ATP through glycolysis when in the presence of glucose [11], offering the potential for recovery. However, when the calcium load is high, the PCMA consumes ATP faster than it can be replenished by glycolysis, leading to ATP depletion [8]. This might make it more difficult for the cell to recover.

Shear stress at physiologic levels is shown to impact erythrocytes' intracellular calcium levels through Piezo1, mechanosensitive cation channel protein. The link to Piezo1 is present in studies with conditions of low shear stresses at short exposure times (~4 Pa for 9.6 ms) as well as long exposure times (<0.01 Pa for 2-3 seconds, calculated based on given flow rate and channel

dimensions) [12, 13]. To our knowledge, calcium studies with conditions closer to that of medical devices, with high shear stress and short exposure times [14], have not been completed.

Expanding the understanding of these cellular responses leads to further exploration of the role of shear stress on the calcium levels in red blood cells. While Piezo1 and PMCA are both at work when a red blood cell is mechanically stimulated, so is the Gardos channel. Calmodulin not only triggers PMCA but also triggers the Gardos effect. An accumulation of intracellular calcium leads to potassium efflux by the Gardos channel, leading to a hyperpolarized erythrocyte membrane. This was observed to activate anion channels as well [15]. The osmotic pressure within the cell decreases due to the efflux of potassium and chlorine, leading to an efflux of water from the cell [5, 16-19]. The result is a calcium-filled, dehydrated and less deformable red cell.

While the activation of these channels provides one explanation for the increase in intracellular calcium observed in response to shear stress, another potential mechanism is the direct formation of transient pores in the red blood cell membrane due to mechanical trauma. The release of hemoglobin during shear has been attributed to transient pore formation [20]. Such pore formation could allow extracellular calcium to enter the cell independently of channel-regulated transport. Evidence for this phenomenon has been demonstrated in shock wave lithotripsy [21] where extreme mechanical forces rapidly induced pore formation. This is especially relevant to conditions of high shear stress and short exposure times. Moreover, sustained high shear stress for long exposure times also has been shown to result in sodium and calcium influxes into the red blood cell [3]. Taken together, these observations suggest that at lower shear rates, calcium entry is more likely to occur through mechanosensitive channels,

whereas at higher shear rates, particularly with brief but intense exposure, pore formation may be the mechanism responsible for ion influxes.

Under mechanical circulatory support conditions (high shear rates, short exposure times), the RBC membrane may become structurally compromised. This disruption of the membrane could lead to externalization of PS on the outer leaflet of the membrane without changes in intracellular calcium. Externalized PS provides a negative surface charge, electrostatically attracting extracellular calcium ions [22]. The presence of PS has been shown to significantly increase the local calcium concentration near lipid membranes by enhancing calcium binding under normal physiologic ionic conditions (0.15 M NaCl) [23]. Furthermore, calcium binding to PS-rich membranes forms phospholipid-calcium complexes, effectively concentrating calcium ions at the membrane surface [24]. When it is exposed, PS not only serves as a signal for coagulation and cell-cell interactions [25], but in the case of high shear rates, may provide a platform that facilitates further calcium accumulation at sites of membrane injury. In the cells subjected to extremely high shear stress, PS exposure that occurs due to the structurally compromised membrane could amplify calcium influx by attracting extracellular calcium to areas of membrane damage. This could potentially enhance passive calcium entry through the transient pores formed by mechanical trauma. This theory is further supported by the study of O'Rear et al., which demonstrated that at high shear stresses (100-130 Pa) applied for 2 minutes, RBCs exhibited increased sodium influx, potassium efflux, and calcium accumulation. This non-selective ion movement in response to high shear stresses points away from Piezo1 as the mechanism of calcium accumulation.

Even though all red blood cells have these mechanisms to control calcium concentration, not all RBCs are the same. Kuck observed a heterogenous intracellular calcium concentration which

was thought to be due to the difference in cell ages in the cell suspension [4]. The Piezo1 channel, PMCA and Gardos channel function in tandem to regulate calcium transport, and both result in a loss of intracellular fluid, not only due to supraphysiological shear stresses but also when the cells traverse small capillaries in vivo. This dehydration leads to a loss in cell volume, enhancing the ability of the cell to cross capillaries and splenic slits smaller than the diameter of a resting RBC (~8 μm for an adult human) [26]. As previously stated, although this phenomenon may benefit the cell, it has adverse effects when the stress on the blood exceeds physiologically normal ranges.

Calcium influx not only leads to dehydrated and rigid cells, but it also can lead to the expression of a marker that signals RBC apoptosis. PS normally resides on the interior surface to the lipid bilayer membrane. The appearance of phosphatidylserine (PS) on the outer membrane surface is known to be a marker in cell death [16, 27-30]. Scramblase and flippase are both enzymes regulated by calcium and responsible for the distribution of PS in the red blood cell membrane. As their names suggest, flippase "flips" PS from the outer leaflet back to the inner leaflet of the cell membrane, maintaining membrane asymmetry [31]. Scramblase "scrambles" the phospholipids. Normally, phospholipids like PS are restricted to the inner leaflet of the membrane. Scramblase disrupts this organization by allowing phospholipids to move in both directions, disrupting membrane asymmetry [31]. Calcium inhibits flippase and activates scramblase [16]. This inhibition of flippase, coupled with scramblase activation, results in PS exposure on the outer membrane of the RBC, leading to its clearance by macrophages in the spleen [32] and contributing to hemolytic anemia.

In addition to promoting PS exposure, both elevated intracellular calcium and PS exposure have been linked to microvesicle formation. Studies by Nguyen et al. have seen microvesicle

formation in cells with elevated levels of intracellular calcium and phosphatidylserine on the outer cell membrane leaflet [5]. The formation of microvesicles and the reduction in cell volume are thought to contribute to red blood cell clearance by the spleen, as well as play a role in blood clotting [33, 34]. This is relevant to this study because at high shear rates, microvesicle formation in red blood cells increases with increasing shear exposure time [35]. Thrombosis is dangerous for the patient and compromises the performance of an artificial organ. Overall, the transient dynamics of shear stress-induced changes in intracellular calcium concentrations within RBCs remain a subject requiring further exploration.

To investigate the role of intracellular calcium in mechanically stressed red blood cells, a reliable method is needed to measure calcium levels. Determining intracellular calcium concentrations is challenging due to the very low amounts present. There are myriad calcium probes that have been used to detect changes in calcium within cells. The calcium probes available include, but are not limited to, Fluo-4, AM, Fluo-5N, AM, and Fura-2, AM. Each have their own dissociation constant (K_d) and distinct spectral qualities. The excitation/emission spectra are very important in finding a calcium probe. Most ratiometric probes like Fura-2, AM require UV light excitation [36, 37]. This is unfavorable when applied to red blood cells since hemoglobin has been shown to cause excitation and/or emission quenching in UV conditions [37]. This reaction with hemoglobin crosses Fura-2, AM, and any other ratiometric dye, off the list of possibilities for this experiment. Fluo-4, AM and Fluo-5N, AM have similar excitation/emission values (494/506 nm versus 494/516 nm) [38, 39], so they both do well with a 488 laser. This is when calcium affinity is considered. The dissociation constant is important because it determines the calcium concentration at which the probe responds most effectively. Choosing a dye with a K_d that matches the expected calcium range within a cell ensures accurate

detection of changes. The average calcium content within a red blood cell is 0.015 mM [40], but that number represents the total cell calcium and not just the calcium present in the cytosol. In the cytosol, the calcium content is around 21 nM [41]. High-affinity calcium indicators are best for calcium quantification in the cytosol [42], which is what is needed in this study. The dissociation constant for Fluo-4, AM is ~335 nM [38]. Although this K_d is higher than resting cytosolic calcium, it is ideal for detecting small increases above baseline. A lower K_d might be saturated too quickly, while a much higher K_d might miss subtle responses entirely. Fluo-5N, AM has a dissociation constant of ~90 μM [39]. The K_d value of 335 nM is better than 90 μM because it allows for detection of small increases in calcium. While the precise magnitude of calcium increase under shear stress may vary, a moderate affinity dye like Fluo-4 provides sensitivity to subtle changes. Low-affinity probes like Fluo-5N, AM are typically used in organelles with a high resting calcium concentration like the endoplasmic reticulum [42]. Since red blood cell suspensions are heterogeneous mixtures with cells of different ages, not all cells will experience the same degree of calcium changes. Since the calcium content within the cell is tightly regulated by the PMCA pump, it is likely that most cells will only experience small to moderate increases in intracellular calcium given that the resting calcium concentration inside the RBC cytosol is 21 nM. Using a low-affinity probe like Fluo-5N would cause the cells that experience low/moderate increases in calcium to be missed by the flow cytometer. Fluo-4, AM is better to detect calcium changes across the full population. Another indication to use Fluo-4, AM is the fact that it was ranked best in photostability when compared to Fluo-3, Calcium Green-1, Calcium Orange, Oregon Green 488 BAPTA-1, and Fura-Red [43]. Even though the fluorescent nature of the probe requires darkness when completing experiments, the exposure of shear stress to blood cells is an involved experiment that requires the ability to see. This photostability is

important because it minimizes photobleaching when exposed to the dim lighting that is required to do the experiment. It also minimizes photobleaching when exposed to light of a microscope if one is using a microscope to visualize fluorescence intensity of the probe. Lastly, the use of Fluo-4, AM, in red blood cells is well-documented [4, 27, 30, 44-49]. This is beneficial when developing a method for an experiment.

Due to the reasons described above, Fluo-4, AM was chosen to be the calcium probe in this study. It can be loaded into the cells due to the compound's acetoxymethyl (AM) portion (Figure 1).

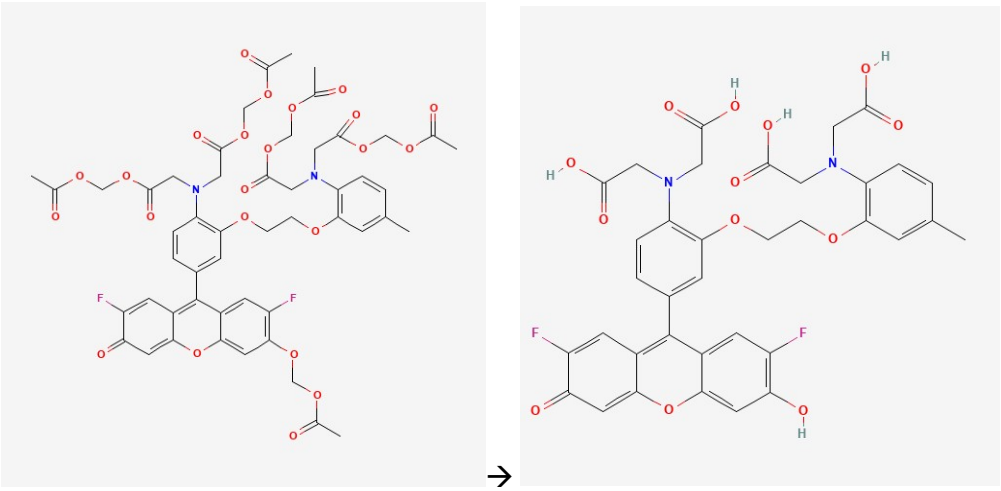

Figure 1: Fluo-4 AM de-esterification [50, 51]

These substituents are hydrophobic so that, when dissolved in dimethyl sulfoxide (DMSO), the compound can integrate into the hydrophobic core of the lipid bilayer. Once inside the cell, esterases hydrolyze the acetoxymethyl portion, releasing free Fluo-4 into the cytoplasm and trapping it in the cell [46]. Since Fluo-4 has the brightest fluorescence among many different calcium indicators, smaller amounts of the fluorescent probe are needed, thus minimizing toxic byproducts like formaldehyde that could damage the cells [52]. To detect the changing amounts

of calcium within the cell, Fluo-4 is used with flow cytometry to detect the median fluorescence of the cells positive for calcium.

The device used to exert shear stress on the red blood cells is just as important as choosing the correct fluorescent indicator. In this study, shear stress was exerted on the cells by microfluidic channels with a rectangular geometry, as shown in Figure 2. In the figure, Region A is the fluid inlet. Region B is the low-shear region: 1500 μm wide, 60 μm tall, and 6800 μm long. Region C is the high-shear region: 45 μm wide and 60 μm tall, varying in length. The length of the constrictions in the 5 ms and 10 ms channels are 4 mm and 8 mm, respectively [23].

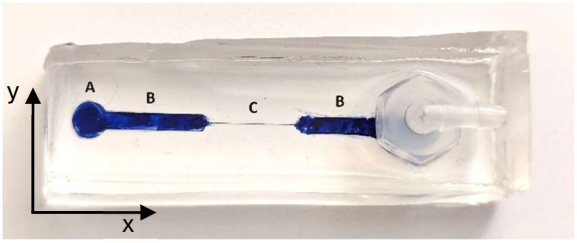

Figure 2: Microfluidic channel: 10 ms exposure time (with blue dye for contrast)

The shear rate within the constricted region was calculated to be approximately 100,000 s^{-1}. Since these devices contain long, straight channels with constant cross sections, the Navier Stokes equation for rectangular channels was used to calculate the theoretical velocity profile and volumetric flow rate, shown in Equations (A.1) and (A.2) in Appendix A, which follows the approach of Buerck et al [29]. The calculated flow rate and cross-sectional dimensions were used to determine shear rate, applying a correction factor (f*) for rectangular channels [53]. Details for this analytical solution can be found in Appendix A. The expressions for the theoretical velocity profile and flow rate were needed to calculate the shear rate. The straight channel, 5 ms channel, and 10 ms channel were used in this experiment to expose the red blood cells to shear stress, varying the exposure time.

The objectives of this study are to investigate the relationship between intracellular calcium and shear stress under conditions similar to mechanical circulatory support (MCS), investigating potential variations over time after exposure. The study also seeks to collect preliminary data on microvesicle formation in relation to shear stress and time. We hypothesize that with increasing shear stress exposure, the higher the calcium concentration within the red blood cell will be. This aligns with trends in existing literature mentioned above. This study aims to fill current gaps in literature since the shear rates used in this study, to the best of our knowledge, have not been considered before in calcium/shear stress studies. Since calcium is linked to microvesicle formation, and prior data from Buerck et al. indicated higher MV levels with increased exposure time [35], we hypothesize a similar outcome in this study.

Materials

Fluo-4, AM was obtained from Invitrogen. As a positive control, 4-bromo-calcium ionophore A23187 was obtained by Millipore Sigma. For the microfluidic channels, Fisherbrand microscope cover glasses (1254G, 35x50-1) were treated with Aquasil (Thermo Fisher Scientific). The microchannels were made from poly-dimethyl siloxane, using the Sylgard ® 184 Silicone Elastomer kit (Dow Corning). Inside the microchannel, a 10-32 UNF Thread elbow with ¼" Hex to 200 series Barb, 1/16" tubing, animal-free natural propylene (Nordson Medical) was placed before curing. To attach the microchannel to the syringe, Silastic laboratory tubing, size 0.062 in. ID x 0.125 in. O.D., was used. Female Luer Lug style to classic series barb, 1/16" ID tubing, clear polycarbonate (Nordson Medical) was used to attach the tubing to the syringe. The syringe for the microfluidic device was a 1 mL Tuberculin syringe without needle (Slip tip) (Becton Dickinson).

Methods

Blood Collection

Venous blood was collected with a 21g needle in the antecubital vein from healthy male and female donors (n = 5) of ages ranging from 20-24, using 3.2% sodium citrate vacutainers (BD). Whole blood was collected from the donor and then aliquoted into a single blood collection tube, then separated at 150 g for 10 minutes. Erythrocytes were isolated with a series of three isotonic saline solution (147.5 mM NaCl) washes, followed by a resuspension in a modified Ringer's solution (147.5 mM NaCl, 4 mM KCl, 2.25 mM CaCl2, and 10 mM glucose, with 0.05 g/L of human serum albumin). With each isotonic wash, supernatant and buffy coat were removed by Pasteur pipette. All blood collection procedures were approved by the University of Oklahoma Institutional Review Board, and all experimental procedures were approved by the Internal Review Board at the University of Oklahoma. Donors were informed of the experiment and research objectives prior to the donation, consent was obtained, and confidentiality was maintained.

Fluo-4, AM

The packed cell volume (PCV) of the cell suspension was measured and adjusted to 1%, consistent with Kuck et al.'s protocol [4]. Fluo-4, AM was added to a final concentration of 5 μM. Fluo-4 labeling was performed at such a low packed cell volume to ensure effective dye loading. After adding Fluo-4, AM, cells were kept in the dark to prevent photobleaching. After a 30-minute incubation at 37°C in a water bath, the cells were washed 3 times with the modified Ringer's solution in the dark. Washing was done by centrifugation at 2500 g for 5 minutes.

4-Bromo-Calcium Ionophore A23187

The stock solution (1 mg/mL in ethanol) was made into 200 µL aliquots and kept frozen. A23187 was added to the samples to a final concentration of 2 µM, consistent with the protocol of Nguyen et al. [5]. The samples were incubated for 12 minutes before being run on the flow cytometer. The analysis of each sample took about 5 minutes. Due to this time constraint, a staggered addition of ionophore was necessary. Instead of adding the ionophore to all of the samples at the same time, ionophore was added to each sample at different times, recording the time the ionophore was added and the time the sample was analyzed on the flow cytometer to ensure that the time elapsed between the time the ionophore was added and the time the sample was analyzed was 12 minutes for all samples.

Microfluidic channels

Microfluidic channels were used to expose the mixture of Fluo-4-loaded cells to the same magnitude of shear stress for different exposure times (0 ms to 10 ms). The channels were prepared using a standard negative photolithography protocol with KMPR 1050 photoresist (MicroChem, Westborough, MA) made for silicon wafers [54, 55]. The devices were made with polydimethylsiloxane (PDMS), the material for the microfluidic channels, and elbow ports were placed in the PDMS before curing. After curing for 1 hour at 80°C, the microchannels were cut out of the molds, and a fluid inlet was created with a biopsy punch. Aquasil was used to treat the coverslips to make them hydrophobic, while a plasma cleaner rendered the microchannel surfaces (PDMS portion) hydrophilic to facilitate bonding and ensure smooth flow of cell suspension during experiments. Once the microchannel and slide were bonded, the fitting, tubing, and syringe were added to complete the device. On the day of the experiment, after the

microfluidic device has been assembled, the microchannel is charged with modified Ringer's solution to ensure the device is compatible with the red blood cells.

Exposing RBCs to shear stress

To promote cell-cell interactions within the microfluidic device during shear exposure, the final suspension was supplemented with RBCs that were not treated with Fluo-4. The 1% packed cell volume (PCV) Fluo-4-labelled RBCs were mixed with RBCs without the probe to a final PCV of 5% to prepare the cells for shear exposure. In each sheared sample and control, there were 2% Fluo-4, AM-treated RBCs. Two syringe pumps were used to expose the loaded red blood cells to shear stress with the microfluidic devices (KD Scientific). The microchannels were set up in the syringe pumps, with the settings shown in Table 1, and a photo of the set-up shown in Figure 3:

Syringe Pump Settings	
Volume	1.00 mL
Mode	Withdraw
Withdrawal Volume	1.00 mL
Withdrawal Rate	125 µL/min
Syringe Diameter	4.70 mm

Table 1: Syringe pump settings for use with microfluidic devices

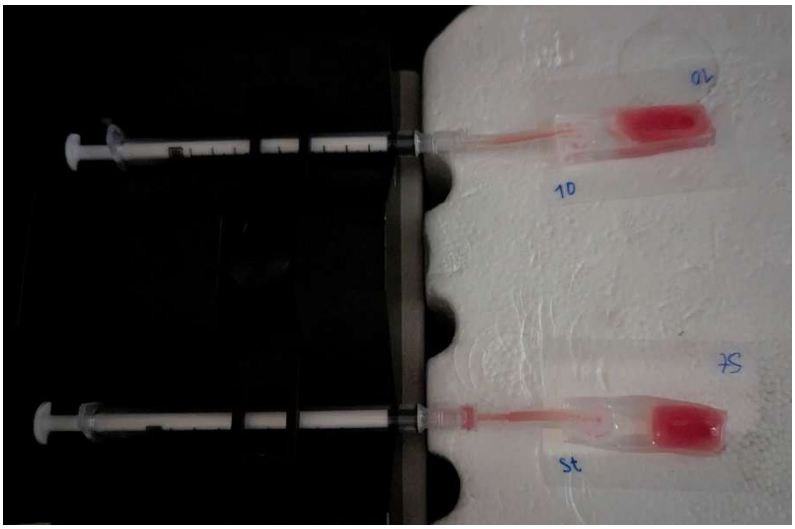

Figure 3: Microfluidic channels (10 ms & straight channel)

Shear exposure took place with the main room light switched off to prevent photobleaching. A small lamp was positioned about 10 feet away from the syringe pumps. After shear exposure, each sample was placed in its respective microcentrifuge tube and on the hematology mixer.

Flow Cytometry

Calcium

The 5% PCV samples were left on the hematology mixer until ready to be analyzed by flow cytometry (at times t=0, t=2.5 hours, t=5 hours). Before being analyzed, dilutions were made in modified Ringers to a final PCV of 0.05%. This concentration allows for optimal loading with the ionophore in the positive control samples. Flow cytometry data were collected using a BD Accuri C6 Flow Cytometer (BD Sciences). The events were gated on the RBC population based on forward scatter and side scatter (FSC-H/SSC-H) characteristics and the Fluo-4 fluorescence. FSC corresponds to cell size, and SSC corresponds to cell complexity. The "H" means "height" and represents the peak of the signal pulse, the maximum intensity of the signal. After selecting the RBC population on the FSC/SSC plot, a secondary plot of FL1-H versus FSC-H was created (Figure 4). FL1 represents the fluorescence intensity in the FL1

channel. Fluo4-H means “FL1-H” – it has been labeled as Fluo4 by the user. The name change does not apply to all samples in the flow cytometry software, so some samples are simply labeled as FL1-H. Fluo-4, AM is excited at 495 nm and fluoresces at 516 nm [56], corresponding to the FL1 channel in the flow cytometer. Gating thresholds were determined using a positive control sample (Figure 6) to identify calcium-positive cells, and the gate was subsequently applied to all samples. The gating for the y-axis (FL1-H) was placed at $4 * 10^3$ and the gating for the x-axis (FSC-H) was placed at $2 * 10^5$. Cells located in the upper right quadrant (Q3-UR) were analyzed for their median fluorescence intensity. Since red blood cells are known to have a very high variation in their ability for calcium accumulation [4], data is not normally distributed. The median was measured instead of the average to minimize the influence of outliers and provide a more robust measure of central tendency. A total of 70,000 events (RBCs) were collected per sample.

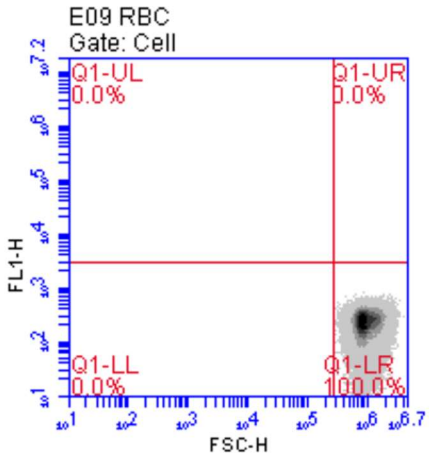

Figure 4: Red blood cells without Fluo-4, AM on FL1-H vs FSC-H Plot

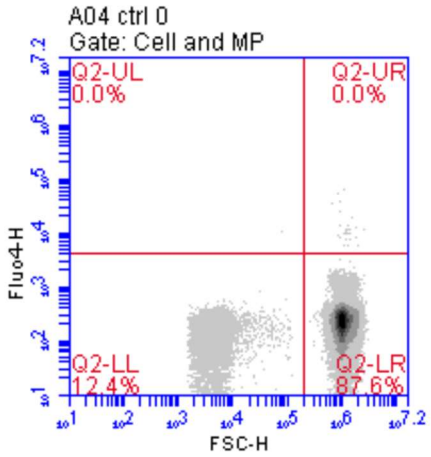

Figure 5: Red blood cell population on FL1-H (Fluo4-H) vs FSC-H plot with Fluo-4, AM, without shear exposure or addition of A23187

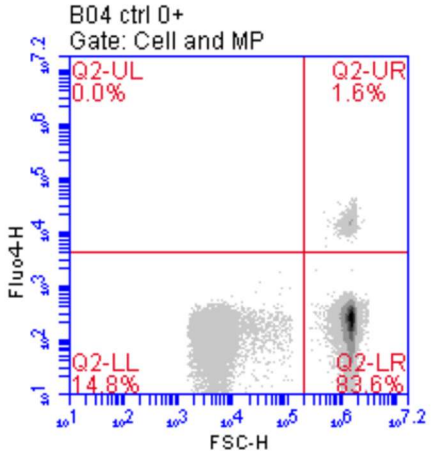

Figure 6: Red blood cell population on FL1-H (Fluo4-H) vs FSC-H plot with Fluo-4, AM, with the addition of A23187, and without shear exposure

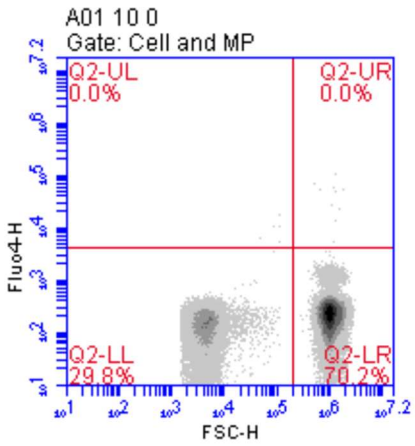

Figure 7: Red blood cell population on FL1-H (Fluo4-H) vs FSC-H plot with Fluo-4, AM and with 10 ms of shear exposure

Microvesicles

Microvesicles were not isolated by centrifugation before analysis. The same sample that was used to analyze calcium was used to analyze the microvesicle count. This means that the microvesicles within the sample were incubating with the cells on the hematology mixer over a period of 5 hours. Once the microvesicle population was selected from the FSC/SSC plot, they appeared in the Q1-LL plot (population shown in Figures 5 through 7). Only the sample microvesicle count was analyzed – not fluorescence intensity. Collection stopped after the 70,000 RBC events were collected, mentioned above.

Statistics

IBM SPSS and Microsoft Excel were used for statistical analysis. A Shapiro-Wilk test was used to confirm that each group had normally distributed data. The Levene Statistic was calculated to confirm the homogeneity of variances based on the mean. After confirming normality and homogeneous variance, a one-way ANOVA was completed for each set of samples, with significance in groups with $p < 0.05$. Following the ANOVA, a Tukey-Kramar test was conducted to determine the statistical significance between each group. Results are reported

as the mean plus or minus the standard deviation. Error bars in all graphs represent the standard deviation of the mean.

Results

Calcium

This study focused on investigating the relationship between shear stress and intracellular calcium in red blood cells. We hypothesized that the longer RBCs are exposed to shear stress at a shear rate of 100,000 s^{-1}, the greater quantity of calcium will be present within the cell. A positive control, using A23187, ensured the cells were loaded adequately with Fluo-4. These cells are shown in Figure 8.

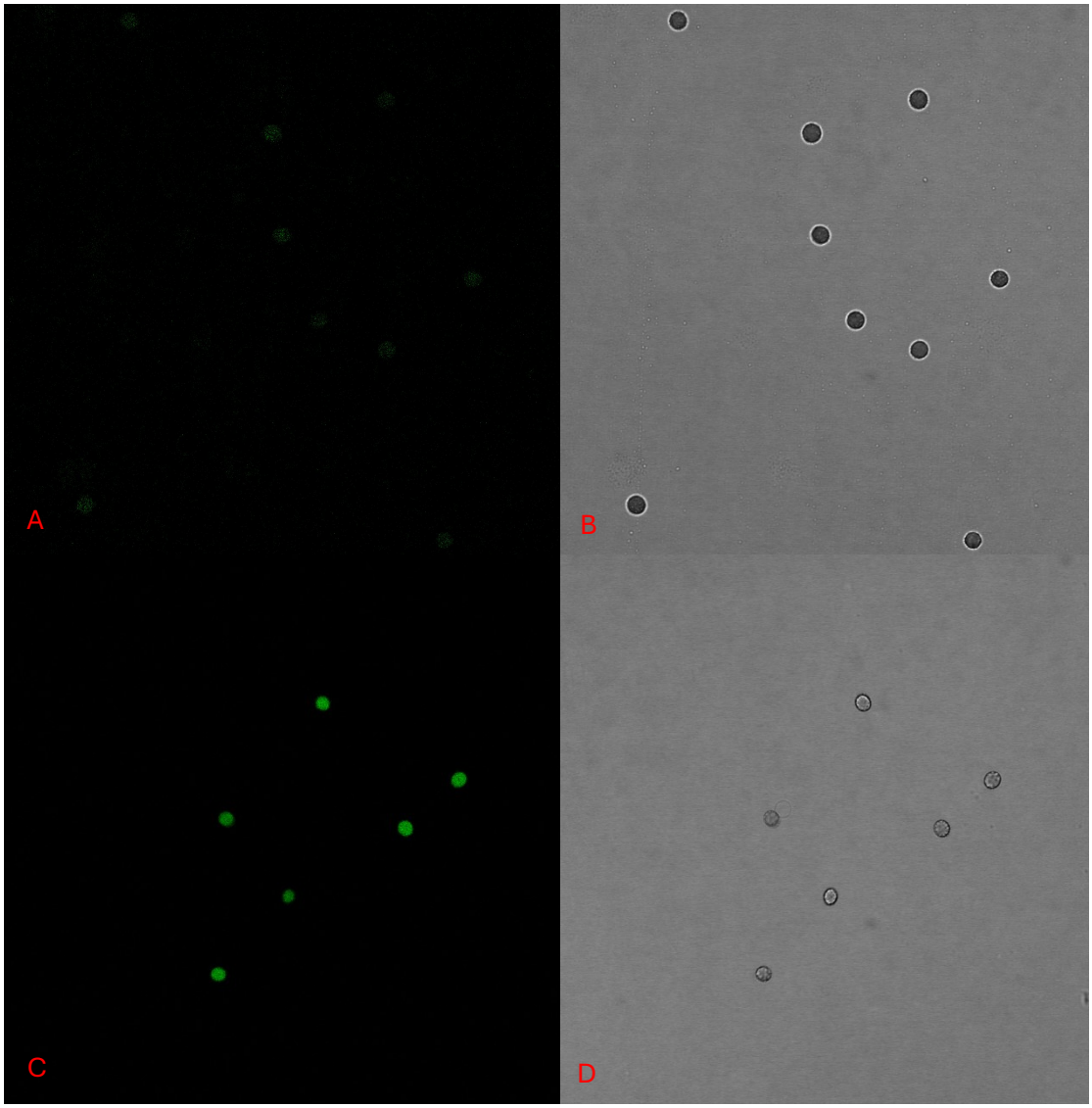

Figure 8: Images A & B: Confocal image (63x/1.40 oil) of red blood cells from the negative control sample, probed with Fluo-4. The average median fluorescence was 11,981 (±1,444). Images B & C: Confocal image (63x/1.40 oil) of red blood cells probed with Fluo-4 and loaded with calcium using 4-Bromo-Calcium Ionophore A23187. The average median fluorescence was 13,065 (±1,367).

It is important to note that shear exposure did not alter the count of cells positive for Fluo-4, and this was observed in the Q2-UR quadrant of Figure 5, compared to that of Figure 7. Shear exposure only altered the fluorescence intensity. Median fluorescence of cells increased

significantly with length of exposure to shear stress ($p = 0.016$) when analyzed immediately after shear exposure. Red blood cells that were run through a 10 ms channel, 5 ms channel, and straight channel had average median fluorescence values of 30,176 (±11,788), 21,974 (±8,893), and 16,450 (±11,220), respectively. The values of the samples run through microfluidic channels were compared to a negative control without shear. Average median fluorescence with 10 ms exposure increased by 160% over the negative control. The average median fluorescence values for the positive and negative control were 13,065 (±1,367) and 11,981 (±1,444), respectively. The negative control was a sample that never encountered a microfluidic device, only probed with Fluo-4, and the positive control was probed with Fluo-4 and stimulated with the 4-bromo-calcium ionophore A23187. There was no statistically significant difference between the negative and positive control. The trend in shear exposure is shown in Figure 9. Figures 10 and 11 show the median fluorescence analyzed 2.5 and 5 hours after shear exposure, and it is visually apparent that a significant difference is not sustained at these time points. Figure 12 shows these results on the same plot to visualize whether the cell successfully attempted to recover optimal calcium concentrations. If this were the case, a lower fluorescence at 5 hours would be expected.

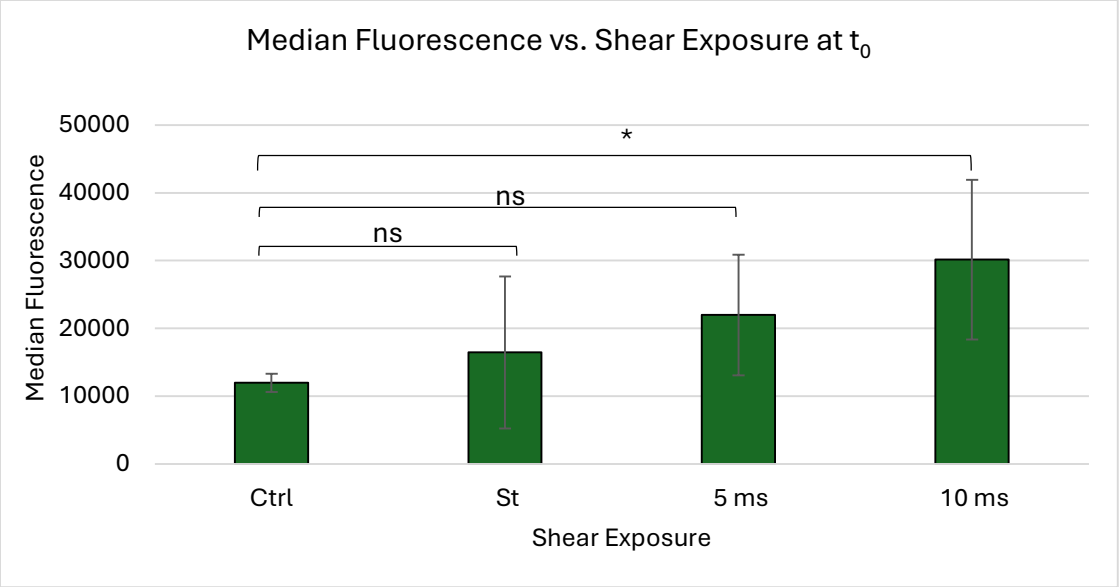

Figure 9: Average median fluorescence versus shear exposure time at high shear rates, analyzed immediately after shear exposure. The control sample (Ctrl) never contacted a microfluidic channel, and the straight sample (St) flowed through a microfluidic channel without a high-shear constriction. "" indicates $p < 0.05$; "ns" indicates "Not Significant".*

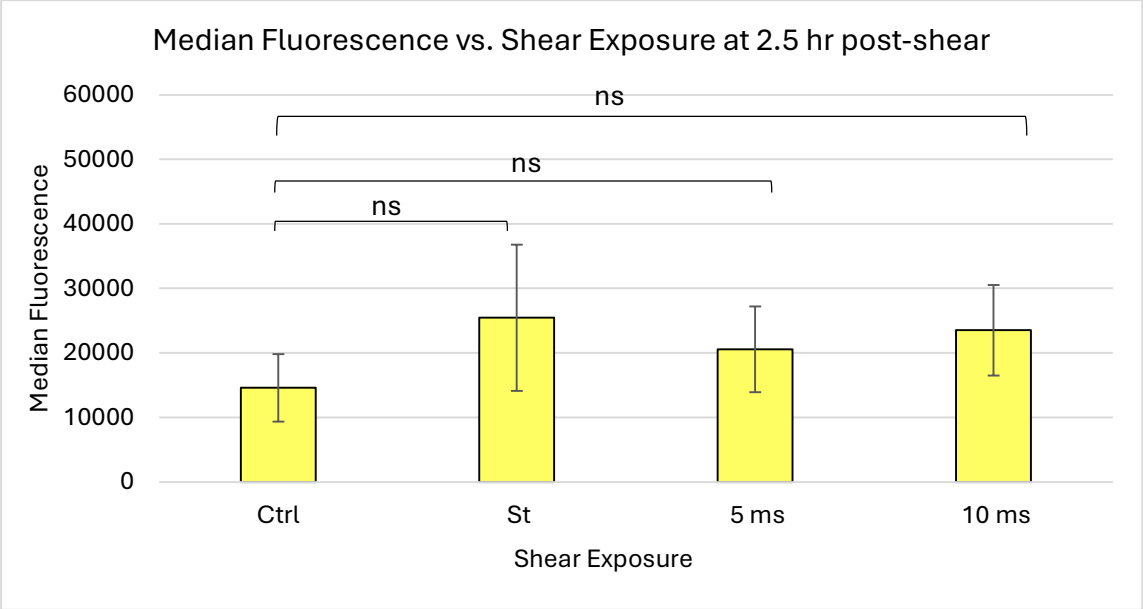

Figure 10: Average median fluorescence versus shear exposure time at high shear rates, analyzed 2.5 hours after shear exposure. "ns" indicates "Not Significant".

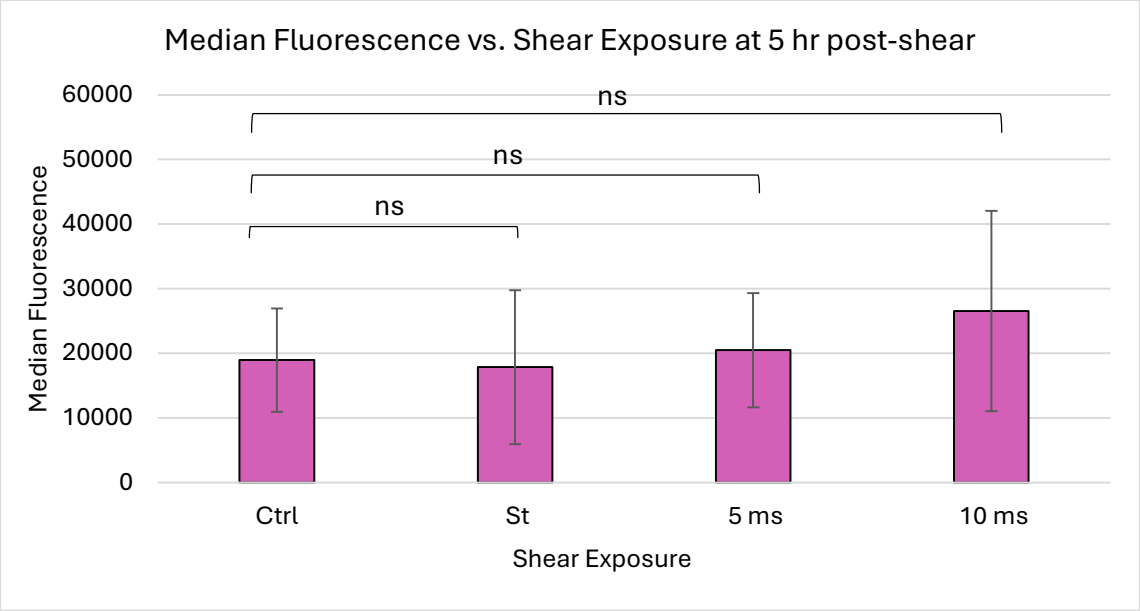

Figure 11: Average median fluorescence versus shear exposure time at high shear rates, analyzed 5 hours after shear exposure. "ns" indicates "Not Significant".

Figure 12: Average median fluorescence versus shear exposure time at high shear rates, analyzed 2.5 and 5 hours after shear exposure, compared on same graph to visualize whether the cells' attempt at recovery of normal calcium levels was successful. "ns" indicates "Not Significant".

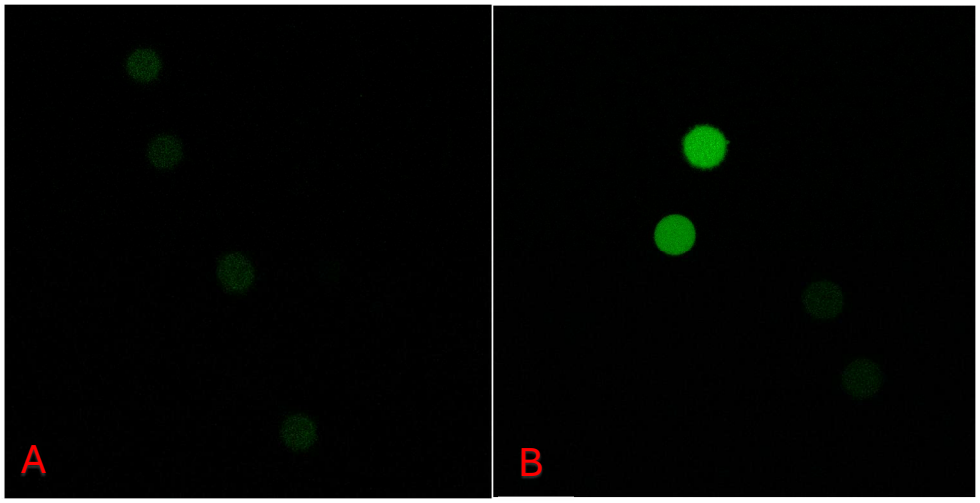

Figure 13: Confocal fluorescence images (63x/1.40 oil, 2.5x zoom). Image A: Fluo-4-probed RBCs sheared in a straight channel. Image B: Fluo-4-probed RBCs sheared in a 10 ms channel.

Th median fluorescence increased significantly with increasing shear exposure ($p = 0.0164$) (Figure 13). A Tukey-Kramer test showed that the only the negative control and 10 ms sheared sample are significantly different from each other ($p = 0.013$). The results of the one-way ANOVA and Tukey-Kramar are shown in Appendix A, Tables 7 and 8.

Microvesicles

The same samples that were analyzed for intracellular calcium response to shear stress were also assessed for microvesicle production, but they failed to show a significant difference in microvesicle production when immediately analyzed after shear or later. Notably, negative control and sheared samples exhibited decreasing MVs with incubation time (Figure 14). The low cell concentration magnified the apparent effect of MV adsorption. When each group was analyzed with respect to time, each group experienced a decrease in microvesicles as time increased, including the negative control.

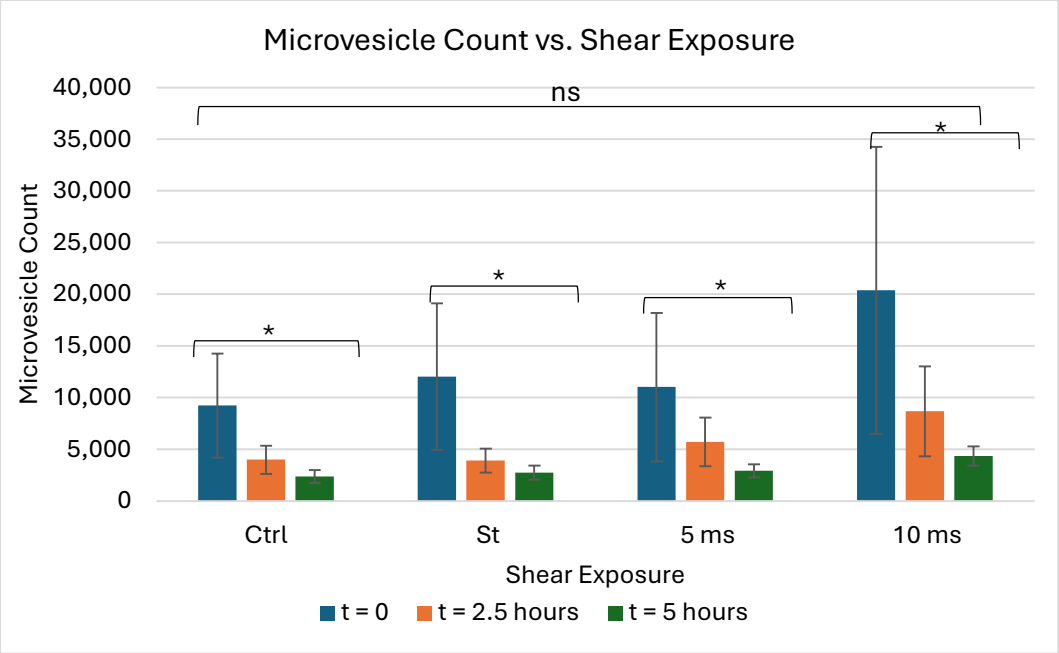

Figure 14: Microvesicle count versus shear exposure for each group with respect to time. "" indicates $p < 0.05$; "ns" indicates "Not significant".*

It is important to note that CD235a, the marker for red blood cells, was not used in this study. The results came from the same sample as the calcium measurements; only the gating was around microvesicles instead of red blood cells and there was no fluorescent marker.

Discussion

Red blood cells showed a significant increase in intracellular calcium when exposed to 100,000 s^{-1} for up to 10 ms. This shear rate and exposure time were selected to reflect the conditions found in medical devices where elevated shear stresses can occur [35, 54]. The exact mechanism of calcium entry is not fully established. One potential pathway involves the mechanosensitive Piezo1 channel, which has been implicated in mediating calcium influx in response to shear stress at physiologic levels [12, 13]. At a supraphysiologic shear stress like that of this study, a plausible mechanism that would explain calcium accumulation would be the formation of transient pores in the cell membrane directly from the mechanical forces [20, 21].

These pores are associated with hemolysis, so they would allow anything below 64 kD (molecular weight of hemoglobin) into the cell, including calcium, which is much smaller than hemoglobin. This, coupled with the fact that the negative charge of PS on the outer leaflet of the membrane may attract calcium ions, might draw more calcium into the cell through the pores. The transient nature of the calcium levels is explained by calmodulin and PMCA's role in regulating intracellular calcium concentrations.

At physiologic shear stress levels, Danielczok et al. saw a transient response to shear stress and that PMCA pumped the calcium out of the RBC in seconds [13]. The momentary increase in calcium that was seen in the study was shown to trigger the Gardos effect, which was observed to increase flexibility. This is because under conditions of low shear stress, the small loss of cell volume coupled with the calcium-calmodulin complex loosening cross-linked spectrin tetramers is enough to assist the cell in deformation [13]. This is not a direct comparison to the conditions of this study, because it has been shown that supraphysiologic shear stresses can lead to significant impairment of deformability [3, 57]. While testing the same phenomenon, we used higher shear stresses and shorter exposure times, and the calcium increase was confirmed to still be present at 10 minutes post-shear. This is very different than Danielczok et al.'s study since they observed that excess calcium from low shear stress exposure can be pumped out in a matter of seconds. However, the decrease seen at 2.5 hours in the 10 ms channel and 5 ms channel supports cell recovery and the transient nature of this phenomenon. While the lack of a significant increase with shear exposure at 2.5 and 5 hours might point to an attempt at recovery, the absence of a decrease in calcium content at 5 hours (compared to 2.5 hours) seems to suggest that recovery was impaired. To our knowledge, there have been no studies concerning the effect of Fluo-4 on red blood cells over extended time periods. One possible explanation for impaired

recovery could be that the calcium binding to the Fluo-4 is so strong that calcium is unable to be eliminated at the same efficiency as an unprobed cell. However, the red blood cells in Danielczok's study also used Fluo-4, AM, and the cells did not appear to have trouble returning to baseline calcium concentration, suggesting that Fluo-4 binding alone is unlikely to explain our findings. It is possible that the elevated intracellular calcium levels induced by extreme shear rates exceeded the ability of Fluo-4-probed cell to restore calcium homeostasis.

Calcium accumulation is not only transient; there is also notable variability between each red blood cell. This is shown in Figure 8, the image of the positive control. Even when A23187 is added to the cell suspension, calcium accumulation varies from cell to cell. The observation of this variation aligns with Kuck et al.'s findings of a heterogenous calcium concentration among many different RBCs [4]. Older RBCs may experience greater and/or longer-lasting calcium accumulation due to decreased ATP levels, as low ATP impairs the function of PMCA, the calcium pump responsible for maintaining calcium homeostasis [9]. However, calcium influx can occur under subhemolytic shear stress without measurable changes in ATP levels [3], suggesting that ATP depletion is not necessary for this response. In addition to energy levels, younger red blood cells have a greater ability to shed more microvesicles due to their greater surface area compared to older cells [58]. As a result, younger cells may exhibit different calcium dynamics due to membrane remodeling associated with vesiculation, which could alter the distribution of calcium channels/pumps and affect calcium uptake or recovery following shear exposure. Shear stress can also reduce deformability without altering cell volume or morphology [3]. Since older RBCs are naturally less deformable [4], this may reduce their sensitivity to mechanical stimuli and thus limit calcium influx. Moreover, in the presence of glucose like the media used in this

study, ATP depletion is not expected to be permanent due to the continued activity of glycolysis, which serves as the primary source of ATP production in RBCs [11].

While the calcium vs. shear exposure trend lost significance with time, the microvesicles decreased with respect to time incubating, which could be explained by their adhering to the red blood cells present in the sample tube, or to the tube walls since low-bind tubes were not used in this experiment. This adsorption happened during the incubation process, while the samples that were sheared were on the hematology mixer for a time period of five hours. This response to incubation time is independent of shear exposure since it was also observed in the negative control. In addition, CD235a was not used in this study, so one cannot say conclusively that the microvesicles detected from the flow cytometer originated from the red blood cells. In the same system, Buerck et al. showed a significant increase in microvesicle formation with increasing shear exposure. Unlike the study by Buerck et al., which used AnnexinV, anti-CD235a, and anti-IgG probes, this study focused primarily on intracellular calcium analysis with Fluo-4, AM. MV detection in this study was incidental, based on side scatter and size gating alone. Additionally, the samples in this study contained only 5% hematocrit during shear exposure, compared to Buerck et al.'s 37%. This difference in hematocrit can drastically influence results due to the differences in the amount of cell-cell interactions. Finally, Buerck et al. isolated microvesicles before analysis, and isolation was not performed in this study.

Future studies should aim to further elucidate the mechanism of calcium influx observed in response to shear stress. One possible approach is the addition of ruthenium red, a widely available, non-competitive Piezo1 inhibitor, to verify whether calcium influx is mediated by Piezo1 activation in these conditions [12, 59]. Furthermore, deformability and mean cell volume testing would allow for investigation of the Gardos effect following Piezo1 stimulation. These

additional experiments could clarify the contribution (or lack thereof) of Piezo1 channels to both calcium homeostasis and mechanical responses in red blood cells under high shear stress conditions.

Conclusion

- The purpose of this study was to investigate whether increasing (short) exposure time to shear stress effects calcium accumulation in red blood cells, and to assess potential microvesicle production in the same samples.
- Median Fluo-4 fluorescence intensity increased with longer shear exposure times (5 ms and 10 ms at 100,000 s^{-1}) when analyzed immediately after shear exposure.
- The increase in median Fluo-4 fluorescence intensity was not sustained at later time points.
- Median Fluo-4 fluorescence intensity did not show a decrease between 2.5 and 5 hours post-shear, potentially answering questions about how Fluo-4 effects the ability of the cell to recover normal calcium levels.
- No significant difference in microvesicle counts with increasing shear exposure was detected when analyzed immediately after shear.
- The hematocrit during shear exposure was 5%, which is lower than that used in previous studies and may have influenced microvesicle production.
- This study helps clarify that mechanical stress alone can cause transient calcium accumulation within RBCs in these conditions.

Chapter 2: Role of calcium in microvesicle formation in a CentriMag mock loop

Abstract

Microvesicle (MV) formation from red blood cells (RBCs) is commonly associated with thrombosis and inflammation in patients receiving mechanical circulatory support. While calcium influx has been implicated in MV production under shear stress, it remains unclear whether calcium is required in the high-shear, short exposure conditions imposed by devices like the CentriMag blood pump. This study examined the role of extracellular calcium in MV formation by circulating bovine RBCs (37%) in a CentriMag mock loop for 6 hours at 4 L/min, 2050 rpm, and 80 mmHg, using media with and without calcium. Samples were collected at multiple time points from both the loop and a stagnant time control, and microvesicle formation was assessed by flow cytometry using CFSE and AnnexinV labeling. CFSE-positive microvesicles increased significantly over 6 hours in the CentriMag loop compared to time controls, indicating that shear stress alone was sufficient to allow MVs to form. However, the presence or absence of extracellular calcium did not significantly affect microvesicle concentrations, and AnnexinV-positive microvesicles showed no consistent trend. Plasma free hemoglobin levels increased over time in both media conditions while mean cell volume remained stable, suggesting that the observed vesiculation was driven primarily by mechanical forces rather than calcium-mediated processes. These findings suggest that calcium influx is unnecessary for MV formation in bovine cells in these conditions.

Introduction

Microvesicles (MVs) are a critical area of study due to their implications in various pathological conditions, including thrombosis, cardiovascular disease, and inflammation [35, 60, 61]. Erythrocyte MVs have been shown to occur in flow with non-physiologic stresses, such as

those found in artificial organs like veno-arterial extracorporeal membrane oxygenation (VA-ECMO) support and left ventricular assist devices (LVADs) [62, 63]. Shear stress has been shown to increase RBC intracellular calcium [3, 4] and has been linked to microvesicle formation in microfluidic studies [35]. An increase in intracellular calcium cannot occur in a system without extracellular calcium. Moreover, understanding the differences between MV formation in systems with and without calcium would help elucidate the actual mechanism responsible for microvesicle formation that occurs with non-physiologic stresses.

Previous studies indicate that calcium plays a major role in microvesicle formation in erythrocytes. Calcium influx at low shear rates is primarily attributed to Piezo1, a mechanically activated channel that permits calcium flow into the cell. In a microfluidic channel to induce shear stress on human erythrocytes, coupled with treatment of a Piezo1 inhibitor (GSMTx4), it was observed that the calcium influx significantly decreased, as did the release of ATP [12]. In another study, shear-conditioned RBCs at 10 Pa and 64 Pa also showed an increase in intracellular calcium [1], and the group hypothesized that Piezo1 might be responsible. In another study focused on understanding the role of shear stress on elevated intracellular calcium, at low shear stresses with long exposure times, the elevated calcium was confirmed to be due to the Piezo1 channel, but the increase was transient [13]. Normal calcium levels were restored once the shear stress ceased.

In contrast, the loss of hemoglobin under conditions of supraphysiologic shear stress is attributed to the formation of transient pores [20]. Pores large enough to allow release of hemoglobin might be expected to allow calcium transport as well. When the mechanical forces cause this much damage to the membrane, PS might also be exposed on the outer leaflet which can draw calcium to the cell due to the electrochemical gradient [22, 23]. O'Rear et al. reported

both calcium and sodium uptake during high shear, along with potassium efflux, at long exposure times (two minutes) [3]. These nonspecific ion fluxes further support the theory that it is pore formation, not Piezo1 activation, that causes observable changes in calcium dynamics when RBCs are exposed to high shear stress. Since hemolysis occurs at high shear stresses, this points away from Piezo1 since Piezo1 cannot transport hemoglobin. Although the shear stresses in O'Rear et al.'s study were supraphysiologic and the exposure time (two minutes) exceeds that of this study (milliseconds), their findings still support the idea that high shear stress can lead to elevated intracellular calcium, and calcium is a well-known contributor to MV formation. When cells were treated with 4-bromo-A23187, a calcium ionophore, the resulting increase in calcium levels was correlated with MV formation and phosphatidylserine expression [5]. It is unknown whether mechanical stress at high shear rates stimulates the biochemical mechanisms of MV formation.

Intracellular calcium overload co-occurs with changes in erythrocyte dynamics. Elevated intracellular calcium levels disrupt erythrocyte membrane integrity by activating enzymes that redistribute phospholipids and promote membrane blebbing, leading to microvesicle formation [5]. Using calcium ionophore A23187 to induce elevated intracellular calcium, Nguyen et al. observed scramblase activation and flippase inhibition, leading to phosphatidylserine exposure on the outer leaflet of the red blood cell membrane. Microvesicles were subsequently observed [30]. This indicates that phosphatidylserine plays a role in one mechanism of calcium-induced microvesicle formation. Calcium activates ion channels, such as the Gardos channel, causing potassium and water efflux, which alters erythrocyte volume and flexibility, making the cell more prone to fragmentation and MV shedding.

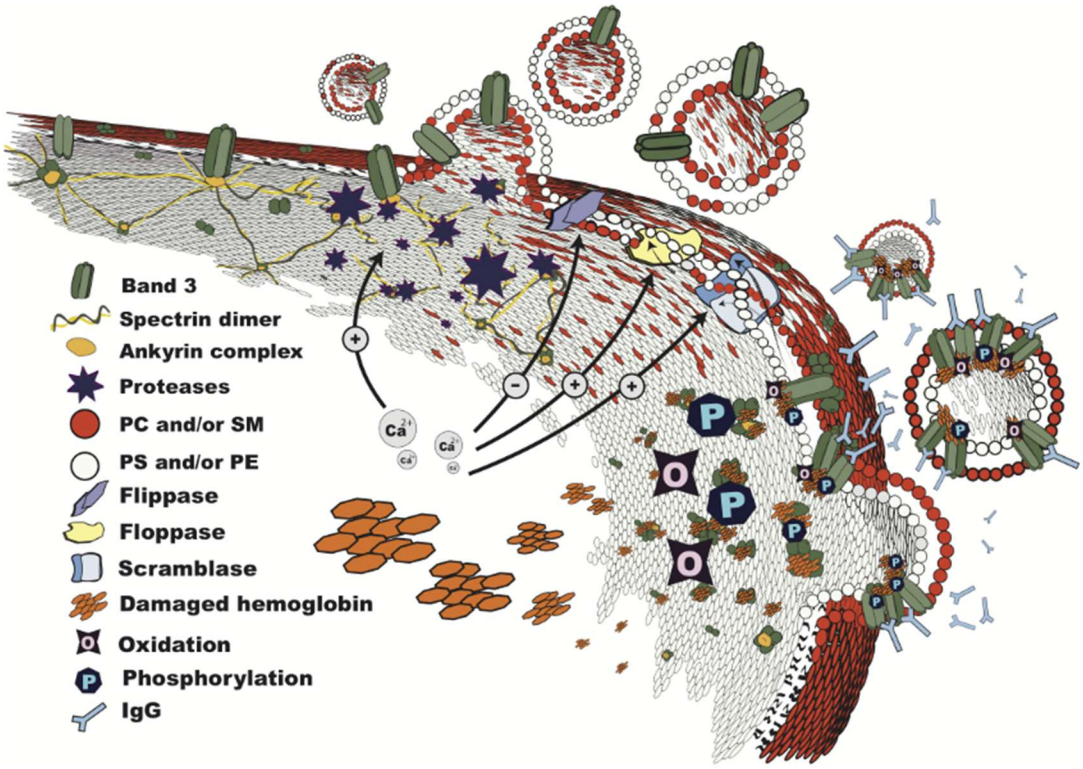

Figure 15: Process of microvesiculation in erythrocytes [64]

In addition to altering membrane composition, calcium also contributes to membrane destabilization by activating proteases that cleave the bond between Band 3 and ankyrin, disrupting its connection to the cytoskeleton (Figure 15) [64]. If Band 3 (and therefore the membrane) separates from the cytoskeleton before vesiculation, then the vesicles bud off without cytoskeletal components, potentially explaining why MVs might lack cytoskeletal proteins. Increased calcium weakens the cytoskeletal structure and decreases erythrocyte deformability under shear stress, contributing to fragmentation and MV release in response to shear [65]. As flexibility within the cell declines, cells are more likely to respond to the deformation with fragmentation, increasing MV release.

The CentriMag blood pump (Abbott) is used in hospitals for acute mechanical circulatory support (MCS). The CentriMag is favored by many hospitals due to its lower levels of

hemolysis, most likely due to its magnetically levitated design with no bearings or seals, minimizing heat generation and shear stress [66, 67]. Even though it is more gentle than other pumps, it is known to expose blood to non-physiological shear stresses [68]. According to the ASTM standard, the maximum run-time for flow loop experiments is 6 hours to ensure that blood viability remains intact while providing enough samples for statistics [69]. To our knowledge, no mock loop studies simulating MCS conditions have been conducted to investigate the role of calcium. The available literature on the impact of calcium on red blood cells focuses more on lower shear stresses [4, 12, 13]. The CentriMag pump imposes high shear stresses on the red blood cells for short exposure times [70]. Running sets of mock loop experiments using the CentriMag with and without calcium-containing media could help fill the knowledge gap that is currently present.

Without understanding the role of calcium in microvesicle formation in these conditions, experimental outcomes may be misinterpreted, leading to ineffective applications in related research. This study aims to clarify the role of extracellular calcium in microvesicle formation within the CentriMag blood pump, which is used in mechanical circulatory support with low levels of hemolysis. The media without calcium makes it unlikely to increase intracellular calcium within the erythrocyte, allowing us to compare microvesicle formation in the presence or absence of calcium. Even though the media was made without calcium, it may be difficult to eliminate all calcium within the system. We hypothesize that calcium-containing media will result in more microvesicles forming, increasing with time in the loop. The goal is to determine whether microvesicle formation might result from calcium influx or another mechanism.

Materials and Methods

Blood Acquisition and Red Blood Cell Isolation

One liter of whole bovine blood was collected (12-gauge needle, jugular vein) from healthy female cattle (n = 8) by Animal Technologies in Tyler, Texas. The blood was shipped the day of collection and received the following day. After blood retrieval (on ice), whole blood was aliquoted into 50 mL conical centrifuge tubes and placed in a water bath at 37°C for around 20 minutes. To isolate red blood cells, the whole blood was centrifuged at 1100 g for 15 minutes with the brake set to "Slow" at 25°C. Buffy coat and plasma were removed by Pasteur pipette, followed by isotonic saline resuspension. This process was repeated two more times, followed by a final resuspension with a modified Ringer's solution after a fourth centrifugation. Packed cell volume (PCV) was taken, and the cell suspension was adjusted to 37%.

Media and Reagents

Isotonic saline (154 mM NaCl) was prepared, along with a modified Ringer's solution with and without calcium (147.5 mM NaCl, 4 mM KCl, 2.25 mM $CaCl_2$ 10 mM glucose, 0.05 g/L BSA and 151 mM NaCl, 4 mM KCl, 2.25 mM $CaCl_2$ 10 mM glucose, 0.05 g/L BSA, respectively). A modified Ringer's solution with no protein (147.5 mM NaCl, 4 mM KCl, 2.25 mM $CaCl_2$ 10 mM glucose) was made because it was required for the protocol of microvesicle analysis. Media was filtered through a 0.2 µm filter to sterilize. Osmolarity of both media was confirmed to be about 285 mOsm/kg (Osmette S Automatic Osmometer).

The antibody Annexin V was used to measure phosphatidylserine exposure on the outer leaflet of the cell membrane. It was conjugated with the Fluorescent Protein Labeling Kit-AlexaFluor 647 by Thermo Fisher/Invitrogen. Carboxyfluorescein diacetate succinimidyl ester

(CFSE) was used to mark cell-derived particles. CFSE was obtained by Thermo Fisher (Molecular Probes) and reconstituted in DMSO for a stock solution of 5 mM.

In Vitro Circulation Loop

The effect of the CentriMag centrifugal blood pump (Abbott) was tested by an in vitro circulation loop. The loop consisted of polyvinylchloride tubing (3/8-inch ID), a port for sampling, two ports for loading and de-airing the loop, and two ports for pressure measurements. The two ports for loading and de-airing the loop were attached to the blood reservoir (Medtronic, R-38). The ports for pressure measurements were located at the inlet and outlet of the CentriMag, with a Hoffman clamp to apply a load pressure drop of 80 mmHg. The pressure was monitored by the Living Systems PM-4 Pressure Monitor. The 3/8" Flow Probe (Abbott) was placed to measure the flow following the Hoffman clamp. The CentriMag and Flow Probe was connected to the 2nd Generation CentriMag Primary Console (Abbott). This setup is shown in Figure 16.

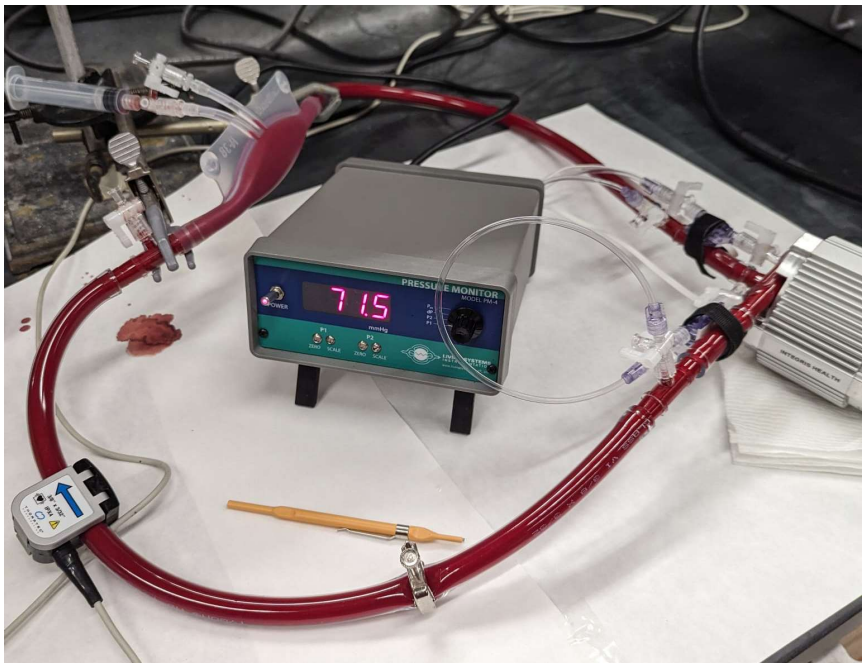

Figure 16: Mock loop set-up

In addition to the 80 mmHg pressure drop, the flow rate of the loop was set to 4 L/min, which leads to a rotational speed of 2050 rpm. After red blood cell isolation and PCV adjustment to 37%, the loop was loaded to a final volume of 150 mL. Two 50 mL conical tubes were filled, one to serve as a time control and one to serve as the Bulk that was used to replace volume lost by sampling. Next, care was taken to eliminate all air bubbles before turning on the CentriMag Support System. The timer started once the first sample was taken.

Experimental Procedure

Sampling took place at the beginning of the experiment, as well as hours 1, 2, 3, and 6. A baseline sample was also taken from the Bulk conical tube at the start of the experiment. One milliliter was taken from the loop and time control tube (and bulk at t = 0 hour) for microvesicle analysis and the same process for the PFH analysis. From these aliquots, PCV and cell count were taken for hours 0, 1, 3, and 6. Cell count was carried out with the Moxi Z Cell Counter (Orflo Technologies), with Type S Moxi Z cassettes, in Small Particle Mode, after cells were diluted 10,000x in isotonic saline. After sampling, the lost volume was replaced, and the sample port was flushed with isotonic to prevent contamination of subsequent samples. At the beginning of the experiment, another 1-milliliter aliquot was taken from the Bulk tube for the Total Plasma Free Hemoglobin (tPFH) measurement, and 10 µL were placed into five microcentrifuge tubes, each already containing 88.8 µL of the modified Ringer's solution containing calcium for the positive control. After the experiment, all parts of the mock loop are rinsed and left to soak overnight in a mixture of water and Tergazyme (Alconox), a powder, enzyme-active detergent.

Mean Cell Volume Calculation

To calculate MCV, cell count and PCV values are necessary. The "curve" value of cell concentration is used for this calculation since the Moxi Z cell counter user manual states that

this value is most accurate, as opposed to "gated" [71]. The cell counter yields concentrations in units of cells/mL. Since the samples used for cell counting are diluted 10,000x, the cell count obtained from the Moxi Z Counter is multiplied by 10,000, then divided by 1,000 to convert to units of cells/µL. Then, the MCV equation, equation 1 [72], can be used to yield the MCV value in μm^3. In the MCV equation, "Hct%" refers to hematocrit. In this work, packed cell volume is substituted for hematocrit.

$$MCV = \frac{Hct\% * 10}{RBC\ count\ (\frac{millions}{mm^3})} \text{ (Equation 1)}$$

Microvesicle Isolation

The time control and loop samples (along with Bulk for t = 0 hours) were centrifuged at 500 g for 5 minutes. The supernatant was collected into a new microcentrifuge tube and then centrifuged at 1500 g for 5 minutes. The supernatant was collected into a Lo-Bind Tube (Eppendorf) and stored at 4°C for future flow cytometry analysis.

Plasma Free Hemoglobin Assay Preparation

The second one-milliliter aliquot taken from the time control and loop (along with Bulk and Total Plasma Free Hemoglobin sample for t = 0 hours) was centrifuged at 2000 g for 15 minutes. The Bulk, time control, and loop supernatants were collected into a new microcentrifuge tube. In contrast, for the tPFH sample, the supernatant was removed, and the volume was replaced with Nanopure water. The sample was left on the hematology mixer for at least 30 minutes. For all samples except tPFH, the supernatant was centrifuged at 13,000 g for 15 minutes, then collected into a labeled microcentrifuge tube, and placed in the freezer at -20°C for analysis at a later date. After the ≥ 30-minute incubation of the tPFH sample, the sample was centrifuged at 13,000 g for 30 minutes. The stroma (about the top half milliliter of the sample)

was collected into a labeled microcentrifuge tube. This was also placed in the freezer at -20°C for later analysis.

Plasma Free Hemoglobin Assay

The Harboe method was used for the PFH assay [73]. Samples were taken out of the freezer and left to thaw. While samples were thawing, diluent was prepared (0.94 mM sodium carbonate in Nanopure water) and filtered with a 0.2 µm filter. Samples were diluted 11x, except for the total PFH sample, which was diluted 501x. Diluted samples were plated in triplicate on a Corning Costar 96-well plate (polystyrene, clear, flat bottom, no lid). A Synergy H1 Plate Reader was used to measure the absorbance at 380 nm, 415 nm, and 450 nm wavelengths with a read speed of normal, 100 msec delay, and eight measurements/data point.

Plasma Free Hemoglobin Assay Analysis

Microsoft Excel is used to analyze absorbance readings according to the Harboe method and ASTM standard. Reporting donor source, volume, flow rate, and experiment time is essential to the analysis, as well as calculating NIH and MIH (Equations 3 and 4) [69].

$$fHb\ \left(\frac{mg}{dL}\right) = 83.6(2 * A_{415\ nm} - A_{380\ nm} - A_{450\ nm})^{9} \text{ (Equation 2)}$$

$$NIH\ \left(\frac{g}{100\ L}\right) = \frac{\Delta Pf\ \ * V * \frac{(100 - Hct)}{100}}{Q * \Delta T * 1000} \text{ (Equation 3)}$$

$$MIH = \frac{\Delta PfH * V * \frac{(100 - Hct)}{100}}{Q * \Delta T * tHgb} \text{ (Equation 4)}$$

After factoring in dilutions, Equation 2 can be used to obtain PFH values [74]. The NIH and MIH can be calculated using volume, flow rate, experiment times, total hemoglobin concentration, and PCV.

Positive Control

The positive control was created using 4-Bromo-Calcium Ionophore A23187 (Sigma Aldrich). A stock solution (1 mg/mL in ethanol) was added to a final concentration of 10^{-3} mg/mL to the five aliquots mentioned above. The aliquots were placed in an oven to incubate at 37°C for two hours, mixing every hour. After incubation, the aliquots were consolidated into one tube, and the MV isolation protocol mentioned above was completed.

Annexin V and CFSE staining

The samples taken at each time point were all analyzed at the end of the 6-hour experiment. To prepare for analysis, 10 µL of the microvesicle supernatant was added to 37 µL of modified Ringer's containing calcium since Annexin V requires calcium to bind. Annexin V Alexa Fluor 647 was added to the suspension. Next, an 8 µM CFSE solution was made with Ringer's solution (no protein) as the diluent. Fifty microliters of this solution were immediately added to the sample tube containing MVs, Ringer's, and Annexin V to a final CFSE concentration of 4 µM. Samples were incubated on the hematology mixer at room temperature for 30 minutes in the dark to prevent photobleaching. Immediately before imaging, 400 µL of Ringer's without protein was added to the sample tube. Diluting the sample before imaging reduces non-specific binding by lowering the concentration of loosely bound molecules, minimizing their interaction with surfaces. The positive control sample was analyzed with the same preparation except, due to the different concentration than the loop and time control samples, 1 µL of the MV supernatant was added to 93 µL of Ringer's. Then, 6 µL Annexin V was added. The CFSE protocol was the same for all samples.

Flow Cytometry

The Accuri C6 Flow Cytometer (BD Biosciences) was used to analyze CFSE and Annexin V expression in microvesicle samples. Samples were run in random order to reduce the likelihood of a trend due to how long each sample stayed at 4°C before analysis. The flow rate was set to a custom flow rate of 10 µL/min and a core size of 5 µm. Ten microliters were collected.

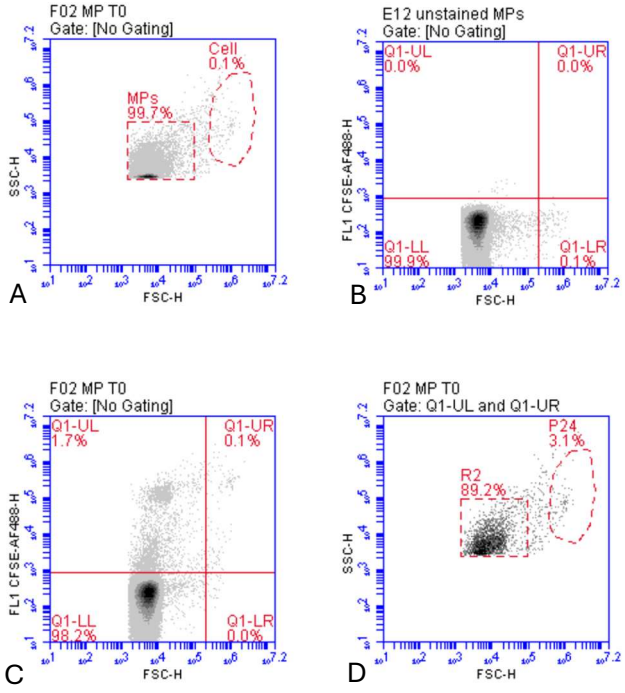

Figure 17: Plot A: SSC-H vs FSC-H for MP population. Plot B: FL1-H vs FSC-H for unstained MPs. Plot C: FL1-H vs FSC-H for sample. Plot D: SSC-H vs FSC-H gated on positive events in the sample.

The first step was to create a SSC-H vs FSC-H plot and select the population of microvesicles (1×10^3 to 1×10^5 for FSC-H and 3×10^3 to $1 * 10^5$ for SSC-H) with the lasso tool (MPs in Figure 17.A). Next, a FL1-H vs FSC-H plot was created to visualize the unstained MVs (Figure 17.B). The y-axis gating was placed on top of the unstained population. The x-axis gating was placed to the right of this population, ensuring it was positioned to the left of where the RBC

population is typically observed. To analyze a sample, the gating from the unstained MP sample was placed such that the events in Q1-UL and Q1-UR were positive for CFSE (Figure 17.C). From these regions, another plot (SSC-H vs FSC-H) was created, gated by size on the events in Q1-UL and Q1-UR in Figure C (Figure 17.D). Concentration values from the "R2" region were analyzed. Due to sample preparation, the samples were diluted 50x and the positive control was diluted 500x. For accurate concentration values, values were multiplied by their respective dilution factors before analysis took place. This process was repeated for AnnexinV-positive concentrations and AnnexinV & CFSE-positive concentrations.

Statistical Analysis

IBM SPSS Statistics software was used for statistical analysis. A Shapiro-Wilk test was used to confirm normality in all groups. The change in microvesicle concentration, PFH, and MCV with time were analyzed with a One-Way ANOVA. Differences of samples taken from the CentriMag loop with the stagnant time control were analyzed with a paired t-test. The Pearson correlation coefficient was also computed to evaluate the degree of association between the two measurements, providing insight into the consistency of individual differences across conditions, indicating whether samples that had a higher concentration of microvesicles or higher PFH in the loop tended to also have the same tendency in the time control. A repeated-measures ANOVA was run on P_0 and PFH as well [75]. Mauchly's sphericity test was run to ensure sphericity was not violated. If sphericity was violated, a Greenhouse-Geisser correction was applied. Significance was reached if $p < 0.05$. Partial eta squared values were recorded with the p-value to determine effect size. Post-hoc pairwise comparisons (with Bonferroni correction) were performed in significant groups with the repeated-measures ANOVA. Error bars in all graphs

represent the standard deviation of the mean. Concentration values are reported as the mean ± standard deviation.

Results

Over six hours, the concentration of CFSE-positive microvesicles in the CentriMag loop (4 L/min, 80 mmHg, 2050 rpm) showed a clear increasing trend (214% increase in calcium media, 172% increase in no-calcium media), while levels in the time control remained stable (Figure 18). There was minimal difference between calcium and no-calcium media, although the no-calcium group exhibited a statistically significant increase over time (Appendix B, Table 21), with the concentration of CFSE+ MVs rising from a concentration of 9,386 particles/µL (± 825) at 0 hours to a value of 25,867 particles/µL (± 8,371) at 6 hours where it seemed to plateau.

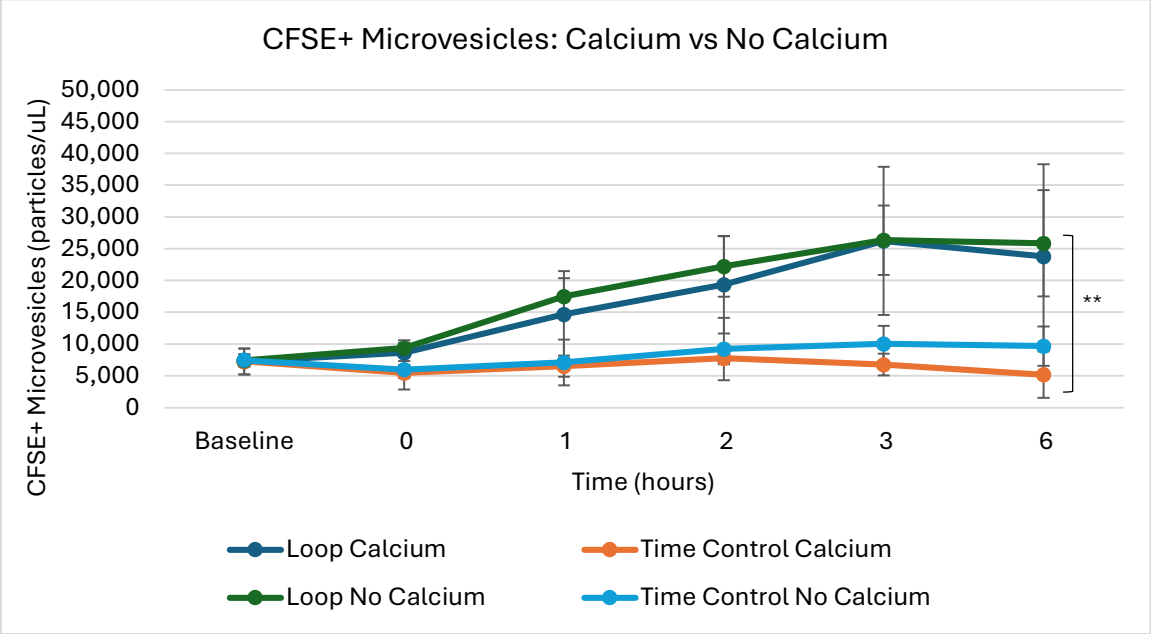

*Figure 18: CFSE-positive microvesicle concentration with respect to time in the loop. "**" indicates $p < 0.01$.*

When focusing on the first three hours, both the calcium and no-calcium groups demonstrated significant increases in CFSE-positive microvesicle concentrations in the CentriMag condition

(Appendix B, Table 22). Repeated-measures ANOVA confirmed that the effect of condition was significant, indicating greater microvesicle formation in the CentriMag loop compared to the time control, while media type and time did not have significant effects (Appendix B, Table 25). Paired t-tests revealed significant differences between the CentriMag loop and time control at several time points in the no-calcium media (Appendix B, Table 27).

Microvesicles positive for AnnexinV alone remained stable over time across all conditions and media types (Figure 19). Statistical analysis showed no significant effects or interactions, and there were no clear correlations (Appendix B, Tables 31 and 32). Paired t-tests identified isolated significant differences between the CentriMag loop and time control, but these findings were not part of an overall trend (Appendix B, Table 33).

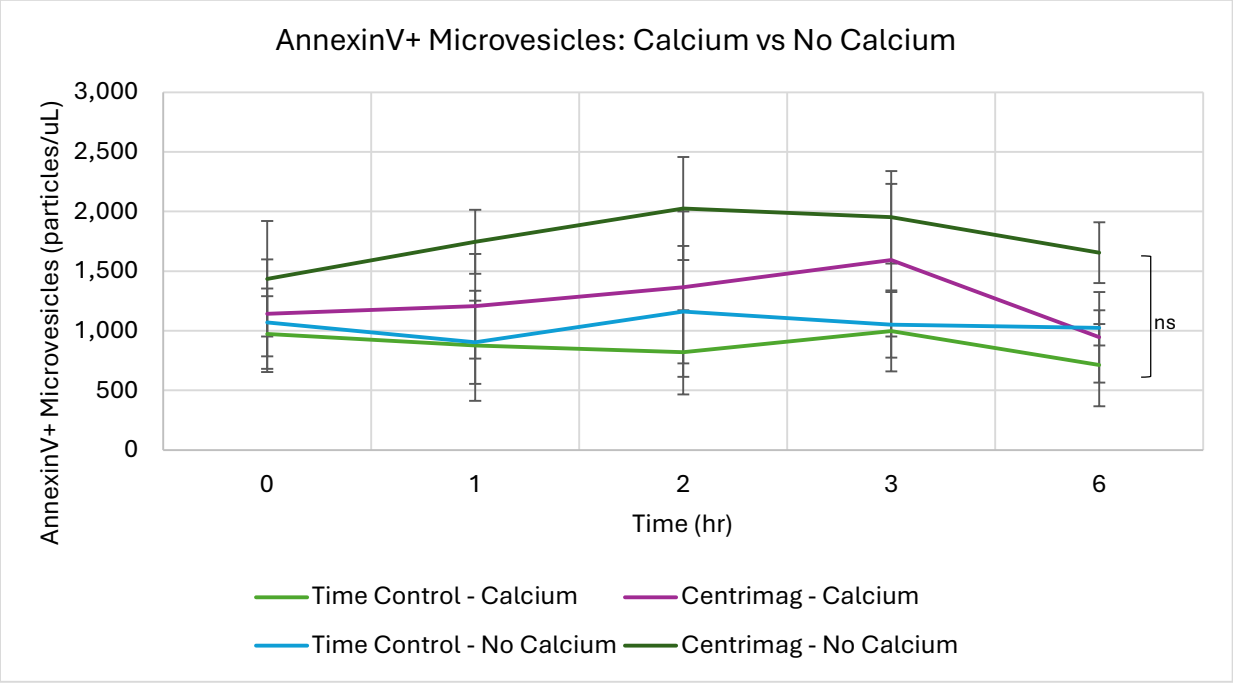

Figure 19: AnnexinV-positive microvesicle concentration with respect to time in the loop. "ns" indicates "Not Significant".

Following the same trend, or lack thereof, microvesicles positive for AnnexinV, microvesicles positive for both CFSE and Annexin V remained relatively stable with time (Figure 20), with no significant changes in concentrations over time (Appendix B, Table 34). Although the effect of condition was significant (Appendix B, Table 37), indicating higher microvesicle concentrations in the CentriMag loop compared to the time control, other factors such as media, time, and interactions were not significant.

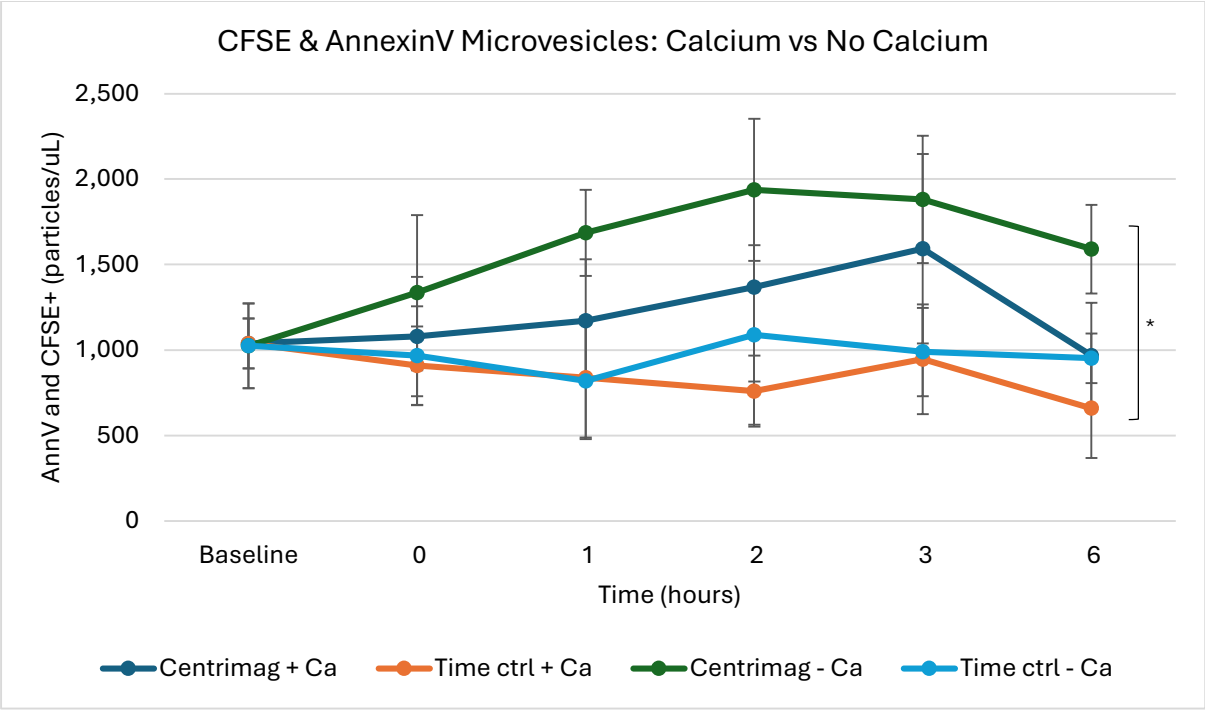

Figure 20: CFSE-positive and AnnexinV-positive microvesicle concentration with respect to time in the loop. "" indicates $p < 0.05$.*

Correlation analyses revealed weak or inconsistent relationships over time, while paired t-tests showed significant differences at isolated time points in both calcium and no-calcium media (Appendix B, Table 38 and 39).

Plasma free hemoglobin concentrations increased over time in the CentriMag loop for both media types, while the time control remained stable (Figure 21). This increase reached statistical significance for both media types (Appendix B, Table 40).

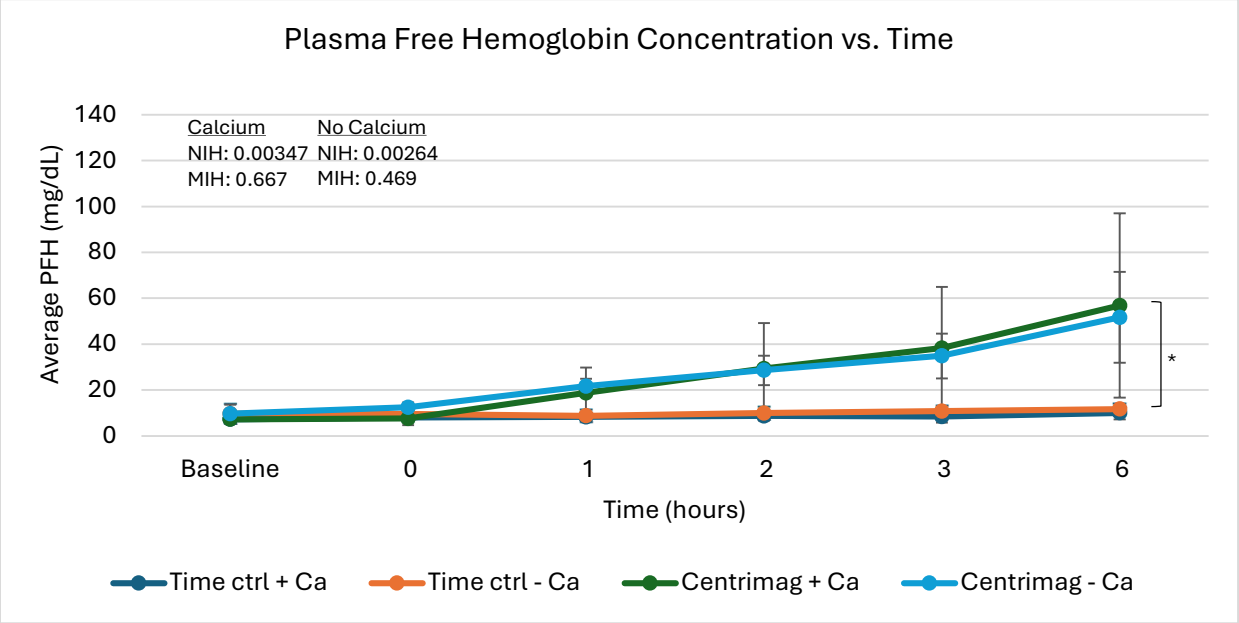

Figure 21: Plasma free hemoglobin concentration at each time point from the loop and the corresponding time controls. "" indicates $p < 0.05$.*

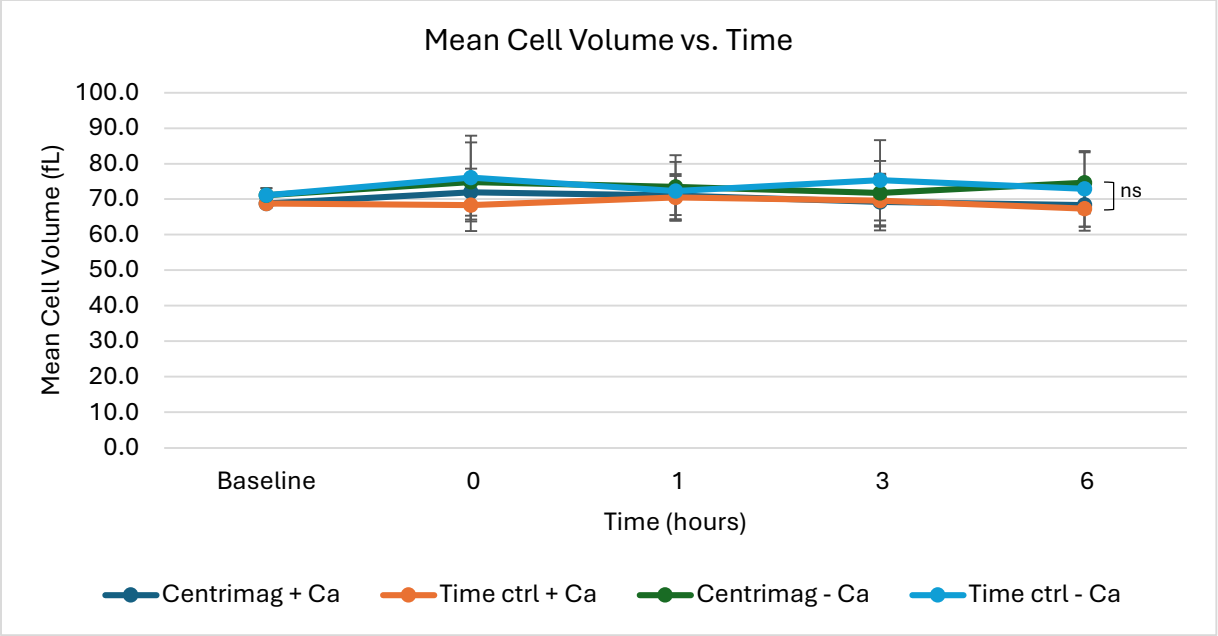

Figure 22: Mean cell volume at time points 0, 1, 3, and 6 hours within the loop and corresponding time controls. "ns" indicates "Not Significant".

Repeated-measures ANOVA confirmed significant effects of both time and condition, as well as their interaction, indicating that PFH levels rose more prominently in the CentriMag loop than in the time control (Appendix B, Table 43). Post-hoc Bonferroni adjustments reaffirmed significant differences between conditions and the condition/time interaction across both media types (Appendix B, Table 44 and 45). Paired t-tests showed a significant increase in the no-calcium media, reinforcing the results of the repeated-measures ANOVA (Appendix B, Table 47).

Mean cell volume did not show any clear trend over time in either condition (Figure 22), confirmed by one-way ANOVA (Appendix B, Table 48).

Discussion

Under the flow conditions used in this study, the presence or absence of extracellular calcium did not significantly affect microvesicle (MV) formation in isolated red blood cells (RBCs) subjected to six hours of flow at 4 L/min, 80 mmHg and 2050 rpm. This finding leads to

the rejection of our hypothesis that calcium-containing media would result in greater MV formation. Instead, the positive trend observed in CFSE-only positive microvesicles over time suggests that MV formation was primarily driven by mechanical forces rather than mechanical stimulation of biochemical mechanisms effected by calcium [65].

The plateau in CFSE-positive microvesicle counts observed between three and six hours may indicate that the population of cells capable of shedding MVs (e.g., younger or less damaged cells) had reached a threshold beyond which further vesiculation was limited. Another possible explanation is that RBC membranes stabilize or become progressively less deformable over time, reducing their capacity for continued MV shedding. These findings suggest that while extracellular calcium may modulate MV formation under certain conditions [5], vesiculation is not strictly required under the high-shear, short exposure time conditions present in the CentriMag blood pump. While many of our statistical tests did not show significant p-values, it is essential to note that the main effect of time and condition/time interaction demonstrated large effect sizes (η^2 values > 0.7). These large effect sizes indicate that experimental conditions may explain a substantial portion of the variability in these outcomes despite the lack of statistical significance. The high η^2 values suggest that the effect may have reached significance if the sample size was larger. This highlights the need for future experiments with larger sample sizes to confirm these findings and better characterize the relationship between shear stress, calcium availability, and microvesicle production. In addition, the Pearson correlation coefficients for CFSE-positive microvesicles indicated strong correlations between the CentriMag loop and time control samples, particularly in the no-calcium group at several time points (values approaching or exceeding ± 0.8), though not all correlations reached statistical significance. The correlations observed between the CentriMag and time control suggest that factors beyond shear stress, such

as the effect of experiment time itself, or sample handling may also influence microvesicle counts.

Overall, our results indicate that mechanical stress alone is sufficient to trigger significant MV formation in erythrocytes. In addition, the increased variability in the microvesicle production observed in the calcium-containing media suggests that extracellular calcium might influence the rate of microvesicle production or the properties of microvesicles produced from the shear stress. Nevertheless, in our study, calcium was not a major determinant of MV generation, which aligns with the theory that at higher shear stresses, physical disruption of the membrane may play a more dominant role in vesiculation than calcium-mediated processes [76]. The lack of any clear trend in AnnexinV-positive microvesicles and those positive for CFSE and AnnexinV further reinforces the conclusion that mechanical factors outweigh calcium-dependent biochemical mechanisms under the experimental conditions tested. Prior studies have demonstrated that calcium influx, whether via Piezo1 channels at lower shear stresses or via pores formed under extreme mechanical stress, can activate scramblase and expose PS on the outer leaflet of the RBC membrane—a key marker of MV formation [4, 30, 76, 77]. However, in this study, PS-positive MVs did not increase significantly over time in either media condition, nor was there a substantial difference between loop samples and time controls. These findings indicate that PS exposure is not the primary modulator of MV release in the CentriMag loop model and that mechanical shear stress may induce membrane shedding without calcium-driven enzymatic activation. Future studies using a flow cytometer with a broader size range could help determine whether small, PS-exposing microvesicles were missed. Even if we did not observe an apparent, consistent increase in AnnexinV-positive microvesicles, extracellular calcium could create more opportunities for subtle, variable calcium influx events across the population of

cells, consistent with the calcium group having the highest variability. Some cells might take in more calcium than others or react more strongly to small increases, depending on factors like membrane condition, age, or prior stress.

Plasma free hemoglobin (PFH) levels followed a similar trend to CFSE-positive microvesicles, significantly increasing in calcium-containing and calcium-free media over time. This suggests prolonged exposure to high shear stress compromises RBC membrane integrity and leads to hemolysis, regardless of calcium availability. The observed hemolysis may reflect the same mechanical forces that drive MV shedding, supporting the conclusion that mechanical damage is the dominant factor in these conditions.

In calcium-mediated vesiculation, MCV typically decreases due to cell dehydration via activation of the Gardos channel, which allows potassium and water efflux [65]. The absence of change in MCV in both systems (with and without calcium) suggests that Gardos channel activity and calcium-induced volume regulation were not major contributors to the observed MV formation. This finding supports the hypothesis that, under the conditions of this study, MV production in bovine red blood cells is driven by direct mechanical forces, resulting in small-scale membrane damage rather than changes in water content.

There are limitations to this study. First, although calcium-free media were used to prevent extracellular calcium influx, they do not eliminate the possibility of residual calcium activity. Intracellular calcium levels are very low and difficult to measure, and intracellular calcium concentrations were not assessed in this experiment. Therefore, it is possible that some calcium signaling may have still contributed to MV formation, despite the absence of added extracellular calcium. A direct assessment of intracellular calcium, like in the work of O'Rear et al. using atomic absorption spectrometry [2], would provide more insight into its role under these

conditions. This would clarify whether transient calcium influx or intracellular calcium release plays a role, even in the absence of extracellular calcium. In addition, employing specific inhibitors, such as GsMTx4 or ruthenium red, to block Piezo1 channels could further elucidate whether mechanosensitive channels contribute to microvesicle formation under varying shear stresses, particularly in high shear, low exposure time systems like the CentriMag loop.

In addition to the calcium within the cells, the human serum albumin used in the experiment may have introduced trace calcium due to its natural calcium-binding capacity. Prior studies have shown that albumin binds calcium at multiple binding sites [78]. These interactions are dependent on both the concentration of albumin and concentration of ultrafilterable calcium, making it difficult to eliminate bound calcium entirely from the albumin-containing media. Another limitation of this study is the small sample size, which likely reduced the power to detect statistically significant differences, despite large effect sizes observed in several analyses. Additionally, the markers used to identify microvesicles (CFSE and AnnexinV) offer only a partial view of the MV population, especially given the limited size detection range of the flow cytometer. Further studies incorporating additional markers and characterizing vesicle size, content, and functional activity would provide a more comprehensive understanding of MVs in this system.

Deformability testing of erythrocytes pre- and post-shear exposure should be incorporated into future studies. Techniques such as constant flow-rate filtration could assess whether changes in RBC deformability correlate with MV formation. Reduced deformability results from cytoskeletal weakening, which can precede or accompany vesiculation. In this context, evaluating whether mechanical stress leads to detectable changes in cell deformability would help clarify whether vesiculation is associated with sublethal injury or irreversible cellular

damage. If deformability decreases while PCV remains constant, sublethal injury would be likely. In contrast, decreases in both PCV and deformability would indicate irreversible cellular damage/cell loss. This is particularly relevant because sublethal injury can weaken membrane integrity, leaving cells more susceptible to MV release. These insights could also indicate whether the remaining RBC population is more prone to fragmentation, which may further exacerbate microvesicle release or hemolysis over time.

Conclusion

- This study's purpose was to investigate whether extracellular calcium influences MV formation in RBCs exposed to prolonged circulation in the CentriMag mock loop set-up, and to assess how the mechanical stress and calcium differences might affect PFH and MCV as well.
- CFSE-positive microvesicle concentration increased over time in the CentriMag loop (4 L/min, 80 mmHg, 2050 rpm) and remained stable in the time control.
- AnnexinV-positive, CFSE & AnnexinV-positive microvesicle concentrations, and MCV values remained stable over time in the CentriMag loop and time control.
- Plasma free hemoglobin concentration increased over time in the CentriMag loop for both media types and remained stable in the time control.
- This study indicates that mechanical forces alone can drive MV formation in CentriMag blood pump conditions.

Acknowledgments

Kylie Foster shared experiments and data containing calcium, assisted in developing the experimental protocol, and assisted with the flow cytometry gating strategy. Unconjugated

Annexin V was generously provided by the lab of Dr. Roger Harrison in the Chemical Engineering Department at the University of Oklahoma.

Chapter 3: Deformability in human and bovine red blood cells in CentriMag mock flow loop

Abstract

Red blood cell (RBC) deformability is essential in ensuring efficient blood flow, especially through the smallest blood vessels, allowing for adequate oxygen delivery. However, mechanical circulatory support devices like centrifugal blood pumps can place stress on RBCs, potentially leading to damage over time. Prolonged circulation through the CentriMag blood pump and its effect on RBC deformability, plasma free hemoglobin (PFH), and mean cell volume (MCV) in both bovine and human RBCs was investigated. An RBC suspension (37%) circulated in a mock loop system for up to 4.5 hours at 4 L/min, 2050 rpm, and 80 mmHg in the bovine group and for up to 6 hours at 5 L/min, 2300 rpm, and 100 mmHg in the human group, simulating clinical conditions. We found that RBC deformability, measured by filtration, stayed mostly stable at first but showed a significant decrease after extended time in the loop, particularly at the final time points. At the same time, PFH levels steadily increased, indicating more hemolysis the longer the RBCs circulated. Mean cell volume stayed consistent in the bovine samples but decreased in human RBCs, which might suggest cell dehydration from calcium influx and activation of the Gardos channel. Although the two blood types were tested under slightly different conditions, both showed similar overall trends. Interestingly, bovine RBCs seemed to handle mechanical stress better than human RBCs. These results highlight the need to carefully monitor red blood cell health during prolonged use of mechanical circulatory devices and point to deformability and PFH as valuable markers of RBC damage over time.

Introduction

The RBC's ability to deform allows them to traverse capillaries narrower than their resting diameter and is essential for oxygen transport and efficient blood circulation. Without

adequate deformability, red blood cells are unable to make it through the small slits within the spleen. As a result, they are sequestered and removed from circulation, which can potentially lead to hemolytic anemia [79]. Deformability is primarily governed by cellular geometry, membrane elasticity, and internal viscosity [80-82]. This suggests that changes in these properties could impact RBC function and overall circulatory health. Shear stress has been shown to be a significant factor influencing RBC deformability. When cells are exposed to shear stress within the physiological range, the deformability of the red cell is enhanced [1]. Still, exposure to supraphysiological shear stresses found in artificial organs can lead to negative changes in their mechanical properties. Studies have shown that exposure to subhemolytic shear stress can result in reversible and or only partially reversible alterations in RBC deformability [1, 83]. This indicates that shear forces encountered in circulation, particularly in medical devices, could have lasting effects on RBC integrity. The implications of these findings extend to conditions where mechanical stress is heightened, such as during extracorporeal circulation in blood pumps.

In conjunction with shear stress, increased intracellular calcium has been linked to decreased deformability [3], possibly due to altered membrane viscoelastic properties. Beyond shear-induced calcium accumulation, elevated intracellular calcium has also been shown to reduce deformability by forming a calcium-calmodulin complex that interacts with cytoskeletal proteins, increasing membrane stiffness [84]. The decreased deformability of cells loaded with calcium (ATP, volume, and morphology restored) was reversed with calmodulin inhibitors. In addition to these mechanisms, other pathways may also contribute to calcium-induced deformability impairment.

Another mechanism linking calcium to deformability impairment centers around an enzyme primarily located in the cytoplasm – protein kinase C (PKC). Ugurel et al. observed evidence to suggest that calcium decreases cellular deformability regardless of shear stress and that PKC is a likely contributor [19]. Additionally, phosphatase activity appears to help recovery of deformability after shear stress by counteracting kinases like PKC. Furthermore, Kuck et al. demonstrated that calcium entry through mechanically activated Piezo1 channels impairs deformability, contributing to RBC damage under shear stress [4]. Beyond direct effects on cytoskeletal organization, calcium can also indirectly impair deformability via the Gardos effect. The Gardos effect occurs when increased calcium levels within the cell cause the efflux of potassium and water, thereby regaining optimal ion concentrations. The dehydrated cell is inherently less deformable due to increased viscosity and lower surface area-to-volume ratio [18]. These studies suggest that calcium regulation is essential in maintaining RBC flexibility. Disruptions in normal calcium levels could exacerbate mechanical trauma to RBCs in high-shear environments.

Various experimental techniques have assessed RBC deformability, each offering advantages and limitations. Ektacytometry, first introduced by Bessis and Mohandas [85] and based on the rheoscope of Schmid-Schönbein et al. [86], has been employed by researchers such as Renoux and Chunyi to assess RBC deformability. This technique uses laser diffraction, applies shear stress to RBC suspensions, and measures the degree of cell elongation [81, 87]. It provides a deformability measurement under varying shear conditions, making it a good method for detecting subtle changes in mechanical properties. Ektacytometry may be more appropriate for assessing changes in internal viscosity since RBC elongation under shear is influenced by intracellular hemoglobin concentration and membrane elasticity [81]. However, ektacytometry

does not directly measure RBC traversal through microcapillary-like structures, limiting its applicability for assessing flow resistance. Another method to determine deformability is micropipette aspiration. It evaluates deformability at the single-cell level by applying suction to an individual RBC and observing its entry into a small glass capillary [26, 88]. This technique offers precise measurements of membrane elasticity and cortical tension. Still, it is labor-intensive and does account for how RBCs collectively move through capillary-like structures under bulk flow conditions. Additionally, it lacks the throughput required for large-scale deformability assessments.

This study employs a constant flow rate filtration device to better simulate physiological conditions. At a constant flow rate, one can evaluate the pressure drop across the microporous membrane through which the cell suspension is infused [89-92]. When there is more resistance to flow across the membrane, it is correlated to less deformable cells. Unlike ektacytometry, since filtration assays primarily assess RBC traversal through a constricted path, these assays are particularly sensitive to the surface-area-to-volume ratio (SA:V) [80, 93]. However, recent findings suggest that filtration assays may not be the most effective tool for measuring intracellular viscosity, as Namvar et al. demonstrated that SA:V ratio has a more significant impact on RBC passage through microchannels than viscosity alone [93]. Constant flow rate filtration provides a robust approach for detecting mechanical stress-induced changes in RBC deformability.

Using animal blood products for in-vitro studies of mechanical circulatory support devices is beneficial due to its low cost and availability. However, one must consider the differences between human red blood cells and other animals. Morphometric parameters like diameter, circumference, and surface area of erythrocytes, as well as molecular composition,

differ between species, and these will affect the deformability of the red blood cell [94-97]. For this reason, the use of animal blood products in RBC deformability studies has been debated. McNamee et al. and Chan et al. compared bovine and human RBCs under similar shear conditions and found that bovine RBCs exhibited greater resilience to mechanical stress than human RBCs [95, 98].

Available literature values for the surface area of a typical bovine red blood cell are limited. It is necessary to obtain an accurate value for this since the critical diameter of the red blood cell is needed when determining what size pore diameter filters to use for the filtration assays. The critical diameter is important because if the pore diameter is less than the critical diameter, the cell cannot pass through the membrane [99]. Care must be taken when searching for this value since some reports list projected surface area rather than the actual surface area that considers the biconcave shape of the cell. Gruber and Deuticke report actual surface area and volume values for multiple species, including bovine [100]. The mean cell volume for bovine red blood cells is reported to be 58 μm^3. Gruber and Deuticke used the method by W.F. Emmons [101], with equations 5 and 6 below, to calculate the surface area. The 'Y' term is the distance from the cell's axis and center of gravity, and the 'P' term is the perimeter (length) of the segment of the cell. Gruber and Deuticke did not determine these values experimentally – they calculated surface area values from cell diameter [102] and MCV [103] data in existing literature. They noted that since there are assumptions in Emmons' formula, there is an error of 10-20% [100].

$$2\pi YP = Area \text{ (Equation 5)}$$

The surface area values for bovine red blood cells are reported to be 95 μm^2 [100].

For human red blood cells, a more advanced measurement method was used by Fung and Evans. They applied microscopic holography with an interference microscope to capture the phase distribution of the cells and reconstruct their three-dimensional geometry [104]. Unlike methods relying on geometric approximations, this approach directly accounts for the biconcave shape and internal structure of the cell. The surface area and volume were calculated from the reconstructed phase distribution of individual cells, using an optimization algorithm to minimize the differences between measured and modeled diffraction patterns. From their measurements, the surface area for human RBCs was found to be approximately 135 μm^2, with an average volume of 94 μm^3 (300 mOsm) [104]. This larger surface area-to-volume ratio indicates higher deformability in human RBCs compared to bovine [105]. Since the surface area and volume are known, the critical diameter can be calculated with the simplification that the cell is cylindrical [99, 101]. The relation of area to volume by Equation 6 will allow the calculation of the critical diameter.

$$A = \left(\frac{\pi D^2}{2}\right) + \left(\frac{4V}{D}\right) \text{ (Equation 6)}$$

Solving for the critical diameter yields 2.70 μm for human RBCs and 2.64 μm for bovine RBCs (Appendix C, Figure 32 and 33). Even though the surface area-to-volume ratio is different between bovine and human cells, the critical diameters are similar, so the same pore size filters (3 μm) can be used in filtration assays. The differences between species could be attributed to variations in cytoskeletal composition and intracellular viscosity [26, 105]. These findings highlight the need for caution when extrapolating results from animal models to human applications, particularly in the context of evaluating mechanical circulatory support devices.

Just as cell geometry is essential when testing deformability, plasma free hemoglobin is also crucial to measure. The Harboe method is used to quantify free hemoglobin, as shown below in Equation 7 [74].

$$fHb\ \left(\frac{mg}{dL}\right) = 83.6(2 * A_{415\,nm} - A_{380\,nm} - A_{450\,nm})^9 \text{ (Equation 7)}$$

Not only is free hemoglobin essential to quantify, but so are the Normalized Index of Hemolysis (NIH) and Modified Index of Hemolysis (MIH) (Equations 8 and 9) for flow loop systems [69]. The NIH has historically been reported in blood pump tests, but it does not account for the total hemoglobin concentration of the blood, so MIH can be used to supplement since it includes the hematocrit (also known as PCV) and total hemoglobin concentration (g/dL) [69]. Both quantities factor in the flow rate (Q), hematocrit, change in time, and blood volume in the loop.

$$NIH\ \left(\frac{g}{100\,L}\right) = \frac{\Delta PfH * V * \frac{(100-Hct)}{100}}{Q * \Delta T * 1000} \text{ (Equation 8)}$$

$$MIH = \frac{\Delta PfH * V * \frac{(100-Hct)}{100}}{Q * \Delta T * tHgb} \text{ (Equation 9)}$$

ASTM standards suggest that both are reported when performing experiments with blood pumps since they provide a well-rounded quantification of hemolysis in a blood pump. Hemolysis can affect the deformability of a cell due to changes in intracellular viscosity. Hemolysis occurs when RBCs experience excessive mechanical stress, leading to the cell membrane rupture, pore formation, and subsequent hemoglobin release [20, 95, 106]. This is particularly relevant in mechanical circulatory support devices where there is prolonged exposure to supraphysiological shear stress. Elevated plasma free hemoglobin levels can affect deformability measurements by potentially reducing cell count and altering intracellular viscosity. In addition, the free hemoglobin itself can affect the intact red blood cells because it has been shown to play a role in

oxidizing membrane proteins and forming senescent cell antigens, both of which are avenues for RBC removal by the spleen [107]. Therefore, measuring free hemoglobin alongside deformability provides a more complete understanding of hemolysis and its effect on red blood cell integrity in MCS conditions.

Given the significance of RBC deformability in the rheological properties of blood and its subsequent clinical implication in mechanical circulatory support patients, this study aims to investigate the effects of prolonged exposure to shear stress in a mock loop system using the CentriMag blood pump. By studying bovine and human RBC suspensions subjected to conditions of intermittent shear stress found in the CentriMag and similar devices, the goal is to understand the interaction between intermittent mechanical forces, RBC deformability, and species differences.

Materials and Methods

Blood Acquisition

Bovine Blood

Animal Technologies collected one liter of whole bovine blood (12-gauge needle, jugular vein) from healthy female cattle (n = 8) in Tyler, Texas. The blood was shipped on the day of collection and received the following day.

Human Blood

Our Blood Institute (OBI) in Oklahoma City, Oklahoma, collected one unit (450 mL) of whole human blood (16-gauge needle, median cubital vein) from healthy human subjects (n = 3). OBI provides human blood products for life-saving medical use and research purposes. The units received are fully de-identified. Human subjects research, according to 45 CFR 46, section

§46.102(e), requires there to be the obtaining of specimens through interaction with the individual and the obtaining of private information/identifiable biospecimens [108]. Since the blood units are fully de-identified and no donor interaction is needed on our part, the use of these products does not constitute human subjects research under federal regulations. Therefore, Institutional Review Board approval is not required. There was one 77-year-old Caucasian male, one 57-year-old Caucasian female, and one 18-year-old Caucasian male. The blood was drawn the day before it was available for pick-up. Blood was picked up, transported back to the University of Oklahoma on ice, and used upon arrival. Donor demographics and screening test results were provided. The screening test results contained the total plasma cholesterol concentrations of each donor.

Media

Isotonic saline (154 mM NaCl) and a modified Ringer's solution (147.5 mM NaCl, 4 mM KCl, 2.25 mM $CaCl_2$, 10 mM glucose, 0.05 g/L HSA or BSA), adjusted to a pH of 7.40 with sodium bicarbonate, were prepared days in advance of the experiment. Media was filtered through a 0.2 µm filter to sterilize. Osmolarity was confirmed to be about 285 mOsm/kg (Osmette S Automatic Osmometer).

Red Blood Cell Isolation

The isolation protocol was identical for bovine and human experiments. After blood retrieval (on ice), whole blood was aliquoted into 50 mL conical centrifuge tubes and placed in a water bath at 37°C for around 20 minutes. The whole blood was centrifuged at 1100 g for 15 minutes to isolate red blood cells with the brake set to "Slow" at 25°C. Buffy coat and plasma were removed by Pasteur pipette, followed by isotonic saline resuspension. This process was repeated twice, followed by a final resuspension with a modified Ringer's solution after a fourth

centrifugation. Packed cell volume (PCV) was taken, and the cell suspension was adjusted to 37%.

In Vitro Circulation Loop

Set-Up

The effect of the CentriMag centrifugal blood pump (Abbott) is tested by an in vitro circulation loop. The loop consisted of polyvinylchloride tubing (3/8-inch ID), a port for sampling, two ports for loading and de-airing the loop, and two ports for pressure measurements. The two ports for loading and de-airing the loop are attached to the blood reservoir (Medtronic, R-38). The ports for pressure measurements are located at the inlet and outlet of the CentriMag, with a Hoffman clamp to apply a load pressure of 80 mmHg for bovine experiments and 100 mmHg for human experiments. The pressure was monitored by the Living Systems PM-4 Pressure Monitor. The 3/8" Flow Probe (Abbott) is placed to measure the flow following the Hoffman clamp. The CentriMag and Flow Probe is connected to the 2nd Generation CentriMag Primary Console (Abbott). This setup is shown in Figure 23.

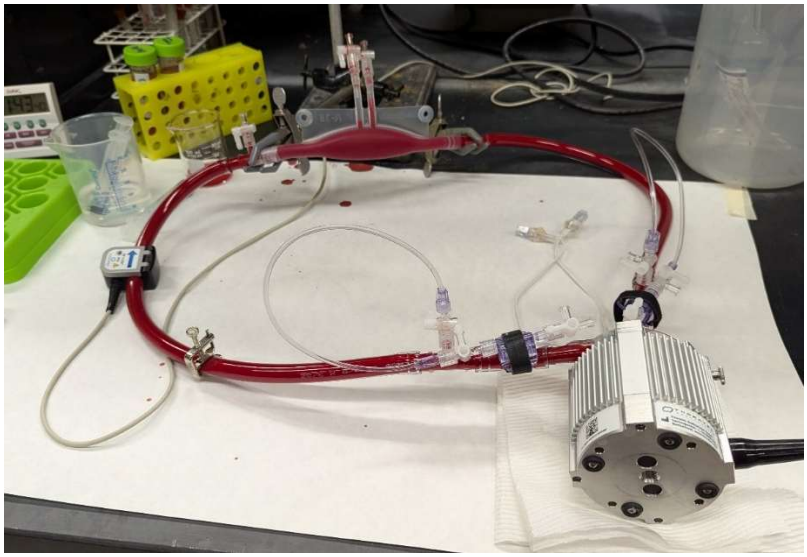

Figure 23: In vitro circulation loop

The flow rate was set to 4 L/min and 5 L/min for the bovine and human experiments, respectively, which led to a rotational speed of 2050 rpm and 200 rpm. After red blood cell isolation and PCV adjustment to 37%, the loop was loaded to a final volume of 150 mL. Two 50 mL conical tubes were filled, one to serve as a time control and one to serve as the Bulk that is used to replace volume lost by sampling. Next, care was taken to eliminate all air bubbles before turning on the CentriMag Support System. The timer started once the first sample was taken.

Sampling Procedure

Sampling took place at the beginning of the experiment, as well as hours 1.5, 3, and 4.5 for the bovine experiments and 1, 3, and 6 for the human experiments. For the deformability assays, 1 mL of RBC suspension was taken from the loop and time control pool at each time point and placed in a plastic sample tube containing Ringer's solution for a 15x dilution. One milliliter was taken from the loop and time control tube and placed in a microcentrifuge tube for PFH analysis. From the microcentrifuge tube, PCV and cell count were taken for each time point. Cell count was carried out with the Moxi Z Cell Counter (Orflo Technologies, small

particle mode for bovine, normal mode for human) after cells were diluted 10,000x in isotonic saline. After sampling, the lost volume was replaced, and the sample port was flushed with isotonic solution to prevent RBCs from drying in the port and avoid contamination of subsequent samples. At the beginning of the experiment, another 1 milliliter aliquot was taken from the Bulk tube for the Total Plasma Free Hemoglobin (tPFH) measurement. After the experiment, all parts of the mock loop are rinsed with water and left to soak overnight in a mixture of water and Tergazyme (Alconox), a powder, enzyme-active detergent. They are rinsed with water the next day and left out to dry.

Mean Cell Volume Calculation

To calculate MCV, cell count and PCV values are necessary. The "curve" value of cell concentration is used for this calculation since the Moxi Z cell counter user manual states that this value is most accurate, as opposed to "gated" [71]. The cell counter yields concentrations in units of cells/mL. Since the samples used for cell counting are diluted 10,000x, the cell count obtained from the Moxi Z Counter is multiplied by 10,000, then divided by 1,000 to convert to units of cells/µL. Then, the MCV equation, equation 10 [72], was used to yield the MCV value (μm^3). In the MCV equation, "Hct%" refers to hematocrit. In this work, packed cell volume is substituted for hematocrit.

$$MCV = \frac{Hct\% * 10}{RBC\ count\ (\frac{millions}{mm^3})} \quad \text{(Equation 10)}$$

DAQ and LabView VI for Pressure Monitoring During Cell Filtrations

The specifications of the pressure monitor were used to choose the data acquisition device (DAQ). The PM-4 Perfusion Pressure Monitor measured pressure using a 10 mV/mmHg

analog voltage output signal ranging from 0 to 2 VDC (0 to 200 mmHg). The LabJack U3-LV was chosen to be the DAQ for this experiment due to its compatibility with the pressure monitor's voltage output range. A USB-USB cable was used to connect the DAQ to the USB. A female BNC socket to wire lead test lead was used for each pressure input. Two male-to-male BNC cables connected these to the output channels on the pressure monitor. A LabView VI (code in Appendix C, Figure 34) was used to record and save the pressure-time curve.

Filtration Apparatus for Deformability Measurements

The plunger was removed from a 50 mL luer-lock syringe (BD). After mixing, the 15x-diluted sample was poured into the 50 mL syringe with a finger over the outlet to keep the sample contained. After pouring, the plunger was inserted into the syringe while the syringe was moved to an upward orientation. All gas was removed from the syringe. Next, the syringe was placed into a syringe pump (KD Scientific), which was set to infuse at 1.5 mL/min. A three-way female luer/female luer/male luer with luer lock ring stopcock (Nordson Medical) was modified to allow for the opening of all three channels. The syringe plunger was pushed so the sample filled the three-way stopcock, taking care not to form any bubbles. Once the barrel of the stopcock was filled with cell suspension, the pressure transducer was attached to the Luer-lock connector on the stopcock and connected to the “P1” input in the pressure monitor. Once the stopcock was filled, the syringe pump lock was set so the plunger could not be manually manipulated anymore. Since the pressure on the outlet side of the filter is atmospheric, a second pressure transducer was attached to the “P2” input in the pressure monitor and taped on the platform at the same height as the filter holder.

The Whatman Nuclepore filter holder (pop-top, polypropylene, 13 mm diameter, 3.7 cm height) was submerged in saline, immediately removed and placed on a paper towel. Whatman

Nuclepore Polycarbonate Track Etched Membranes (13 mm diameter, hydrophilic, 3 µm pore size, circle, hydrophilic) were used for each sample. It was important to keep the lot consistent for all experiments to minimize variability since each lot has slightly different specifications. The lot used in this study was A29594143, so the pore diameter ranged from 2.5 to 2.9 µm and the pore density was $2.1 \times 10^6/cm^2$. The filter was obtained from its container with small forceps and placed on the filter holder. The filter holder was firmly tapped on the table to allow the membrane to settle, and the forceps were used to gently push around the perimeter to ensure the membrane was secure. The pop-top was pushed onto the base of the filter holder with the O-ring attached. The entire filter holder was submerged in saline and inverted, allowing the bubbles to escape, tapping onto the side of the beaker if the bubbles did not naturally come to the surface. Once there was no more air in the filter holder, a finger was placed on the tip of the outlet to keep the liquid inside, raised out of the water, and placed on the stopcock. A beaker was placed underneath to catch the cell suspension (Figure 24).

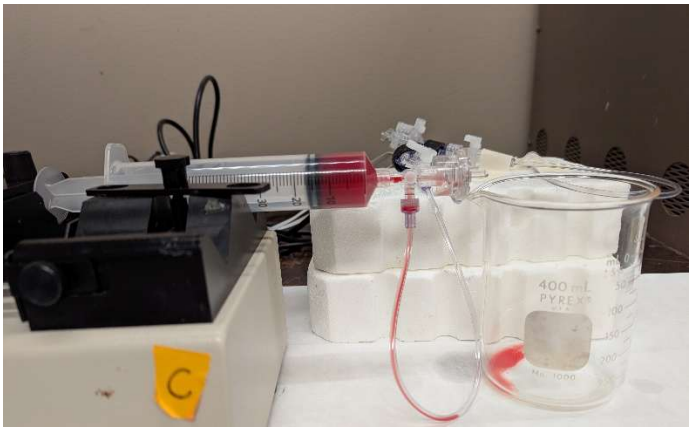

Figure 24: Filtration apparatus for deformability measurement

The "Start" button was pushed on the LabView VI interface connected to the Living Systems PM-4 Pressure Monitor, recording the pressure curves. Immediately afterward, the "Start" button on the syringe pump was pressed to initiate flow and commence the deformability experiment.

The recording and syringe pump were stopped immediately after 10 mL had been infused. The syringe and membrane were discarded after each sample. The stopcock and filter holder were washed with DI water and saline in between samples. After the experiment, all non-disposable parts of the filtration apparatus are rinsed with water and left to soak overnight in a mixture of water and Tergazyme (Alconox), a powdered enzyme-active detergent. They were rinsed with water the next day and left out to dry.

Determination of Initial Pressure Drop

The pressure vs syringe pump infusion time curve was recorded with the LabView VI, which was programmed to save as a text file. The text file was imported into Excel. The pressure drop across the filter membrane was calculated ($P_2 - P_1$) and plotted against time. P_1 was the pressure (mmHg) just before the filter and P_2 was atmospheric pressure since the outlet of the filter was open to the atmosphere. The region where the curve became linear (steady state) was identified. The initial pressure drop was determined from this line by extrapolating backward to zero time [89, 91]. Appendix C (Figures 35 to 63) contains the plots of pressure vs time for each experiment.

Plasma Free Hemoglobin Assay

Preparation

The second one-milliliter aliquot taken from the time control and loop (along with Bulk and Total Plasma Free Hemoglobin sample for t = 0 hours) was centrifuged at 2000 g for 15 minutes. The bulk, time control, and loop supernatants were collected into a new microcentrifuge tube. In contrast, the supernatant was removed for the tPFH sample, and the volume was replaced with nanopure water. The sample was left on the hematology mixer for at least 30 minutes. For all samples except tPFH, the supernatant was centrifuged at 13,000 g for 15

minutes, then collected into a labeled microcentrifuge tube and placed in the freezer at -20°C for analysis at a later date. After the ≥ 30-minute incubation of the tPFH sample, the sample was centrifuged at 13,000 g for 30 minutes. The stroma (about the top half milliliter of the sample) was collected into a labeled microcentrifuge tube. This was also placed in the freezer at -20°C for later analysis.

Assay

The Harboe method was used for the PFH assay [73]. Samples were taken out of the freezer and left to thaw. While samples were thawing, diluent was prepared (0.94 mM sodium carbonate in Nanopure water) and filtered with a 0.2 µm filter. Samples were diluted 11x, except for the total PFH sample, which was diluted 501x. Diluted samples were plated in triplicate on a Corning Costar 96-well plate (polystyrene, clear, flat bottom, no lid). A Synergy H1 Plate Reader was used to measure the absorbance at 380 nm, 415 nm, and 450 nm wavelengths with a read speed of normal, 100 msec delay, and eight measurements/data point.

Analysis

Microsoft Excel is used to analyze absorbance readings according to the Harboe method and ASTM standard. It is important to the analysis to report donor source, volume, flow rate, and experiment time to calculate NIH and MIH. After factoring in dilutions, Equation 7 can be used to obtain PFH values. Using volume, flow rate, experiment times, total hemoglobin concentration, and hematocrit, the NIH and MIH can be calculated using Equations 8 and 9.

Statistics

IBM SPSS Statistics software was used for statistical analysis. A Shapiro-Wilk test was used to confirm normality in all groups. The change in initial pressure drop (P_0), PFH, and MCV

with time were analyzed with a One-Way ANOVA. Differences in samples from the CentriMag loop with the stagnant time control were analyzed with a paired t-test. The Pearson correlation coefficient was also computed to evaluate the degree of association between the two measurements, providing insight into the consistency of individual differences across conditions, indicating whether samples that had a high P_0, high PFH, or high MCV in the loop tended to also have the same tendency in the time control. A repeated-measures ANOVA was run on these dependent variables as well [75]. Mauchly's sphericity test was run to ensure sphericity was not violated. If sphericity was violated, a Greenhouse-Geisser correction was applied. Significance was reached if $p < 0.05$. Partial eta squared values were recorded with the p-value to determine effect size. Post-hoc pairwise comparisons (with Bonferroni correction) were performed in significant groups with the repeated-measures ANOVA. Pearson correlation coefficients were calculated and analyzed to determine the correlation between deformability and human donor plasma cholesterol levels. Error bars in all figures represent the standard deviation of the mean.

Results

Bovine

Deformability, measured by P_0, remained stable over time in both the CentriMag loop (4 L/min, 80 mmHg, and 2050 rpm) and time control. Although no significant changes were detected across time points (Appendix C, Table 49), the CentriMag sample at the final time point exhibited the highest P_0 value observed during the experiment, seen in Figure 25, translating to a 10% impairment in deformability. This difference was statistically significant when comparing the CentriMag sample to the time control at 4.5 hours.

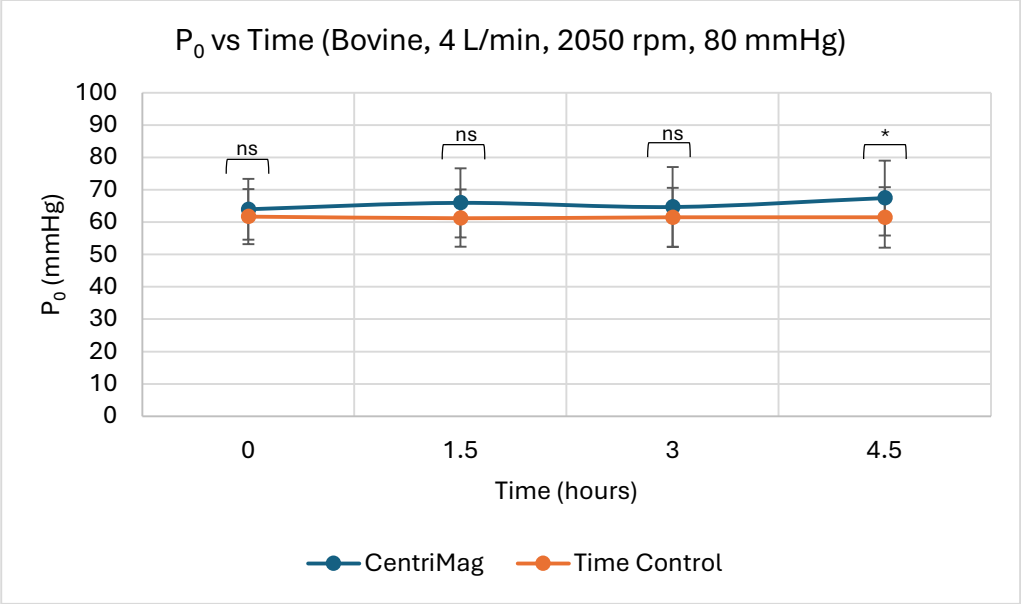

Figure 25: Initial pressure drop vs time in the in vitro circulation loop compared to time control with bovine RBCs. "" indicates $p < 0.05$; "ns" indicates "Not Significant".*

Repeated-measures ANOVA confirmed these findings, indicating no significant effect of time or interaction between time and condition. However, the effect of condition approached significance, suggesting a trend toward increased P_0 in the CentriMag loop (Appendix C, Table 52). Correlation analyses showed moderate to strong correlations between CentriMag and time control samples over time (Appendix C, Table 53). Paired t-tests further confirmed a significant difference at 4.5 hours, with high P_0 values in the CentriMag samples compared to the time control (Appendix C, Table 54).

Plasma free hemoglobin (PFH) steadily increased over time in the CentriMag loop, while remaining relatively stable in the time control (Figure 26). Statistical analysis revealed a significant increase in PFH in the CentriMag condition, consistent with visual trends (Appendix C, Table 55). Repeated-measures ANOVA could not confirm a significant effect of time (Appendix C, Table 58). Paired t-tests showed significant differences at 1.5 hours, 3 hours, and

4.5 hours, with higher PFH levels in the CentriMag loop compared to the time control (Appendix C, Table 60).

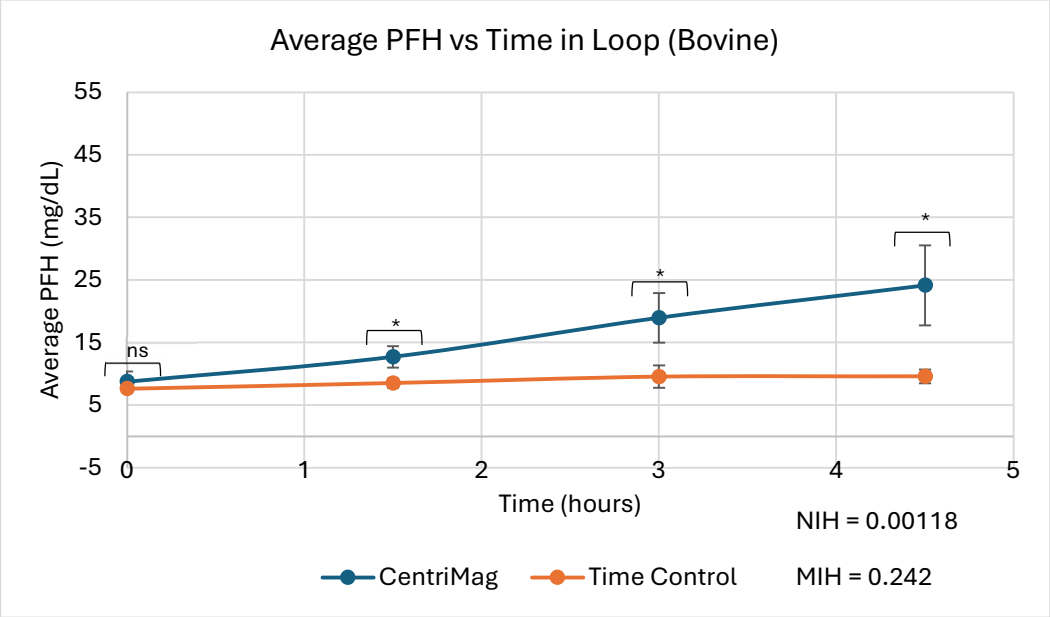

Figure 26: Average plasma free hemoglobin vs time in the in vitro circulation loop compared with time control for bovine RBCs. "" indicates $p < 0.05$; "ns" indicates "Not Significant".*

Percent hemoglobin release exceeded the 0.2% threshold for notable cell membrane damage [109] at all time points in the CentriMag samples after the initial measurement (Table 2).

Sample (Bovine)	% Hemoglobin Release
CentriMag 0 hours	0.17
CentriMag 1.5 hours	0.25
CentriMag 3 hours	0.37
CentriMag 4.5 hours	0.47
Time Control 0 hours	0.15
Time Control 1.5 hours	0.17
Time Control 3 hours	0.19

Time Control 4.5 hours	0.19

Table 2: Percent hemoglobin release for each bovine sample

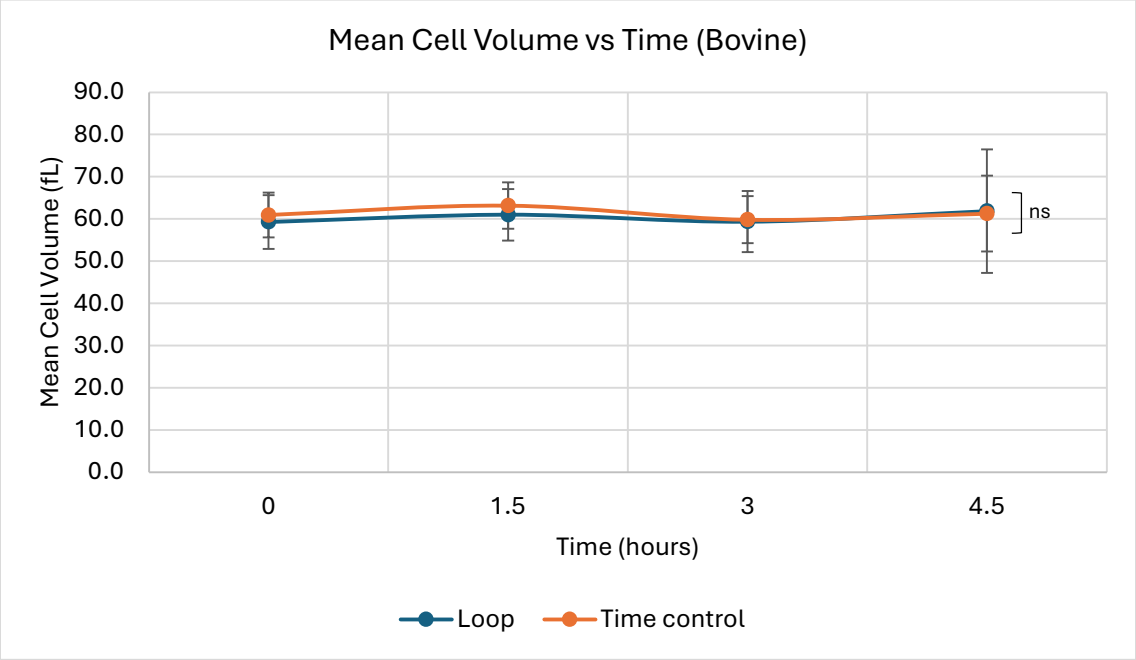

Figure 27: Average mean cell volume vs time in the in vitro circulation loop compared with time control for bovine RBCs. "ns" indicates "Not Significant".

Mean cell volume (MCV) remained stable over time in both conditions, with no significant changes detected (Figure 27). Although there was a slight decrease in MCV in the CentriMag condition at 1.5 hours, this difference was not sustained at later time points. Paired t-tests indicated no significant overall effects (Appendix C, Table 62).

Human

P_0 values in human RBCs remained relatively stable over time in both the CentriMag loop (5 L/min, 100 mmHg, 2300 rpm) and time control conditions, with a slight increase observed (Figure 28). No significant changes were detected across time in either condition (Appendix C, Table 63). However, at 6 hours, the CentriMag loop showed the highest P_0 value recorded, translating to a 9% impairment in deformability. A paired t-test identified this

difference as significant (Appendix C, Table 68). The deformability in the CentriMag was also significantly decreased compared to the time control at 1 hour.

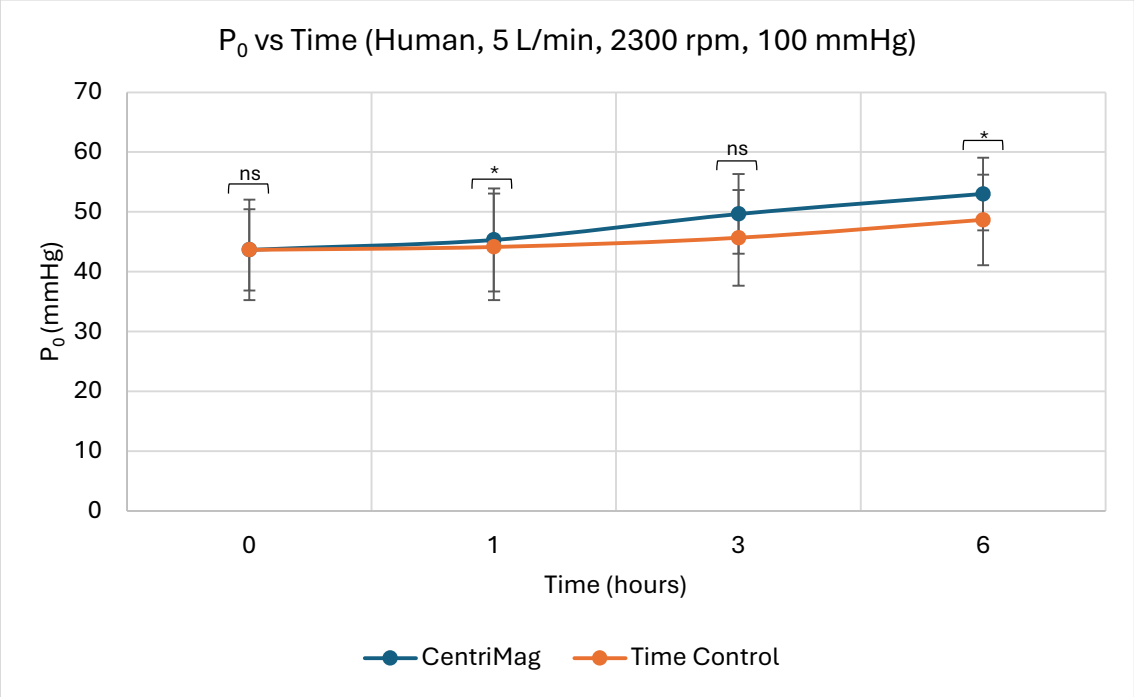

Figure 28: Initial pressure drop vs time in the in vitro circulation loop compared to time control with human RBCs. "" indicates $p < 0.05$; "ns" indicates "Not Significant".*

Repeated-measures ANOVA confirmed no significant effects of time, condition, or their interaction on P_0 values (Appendix C, Table 66). Correlation analyses between the CentriMag and time control samples demonstrated strong relationships across time points (Appendix C, Table 67).

Plasma free hemoglobin levels in human RBCs showed an increasing trend over time in the CentriMag loop, while remaining relatively stable in the time control condition (Figure 29). Statistical analysis indicated a significant increase in PFH over time within the CentriMag samples (Appendix C, Table 69).

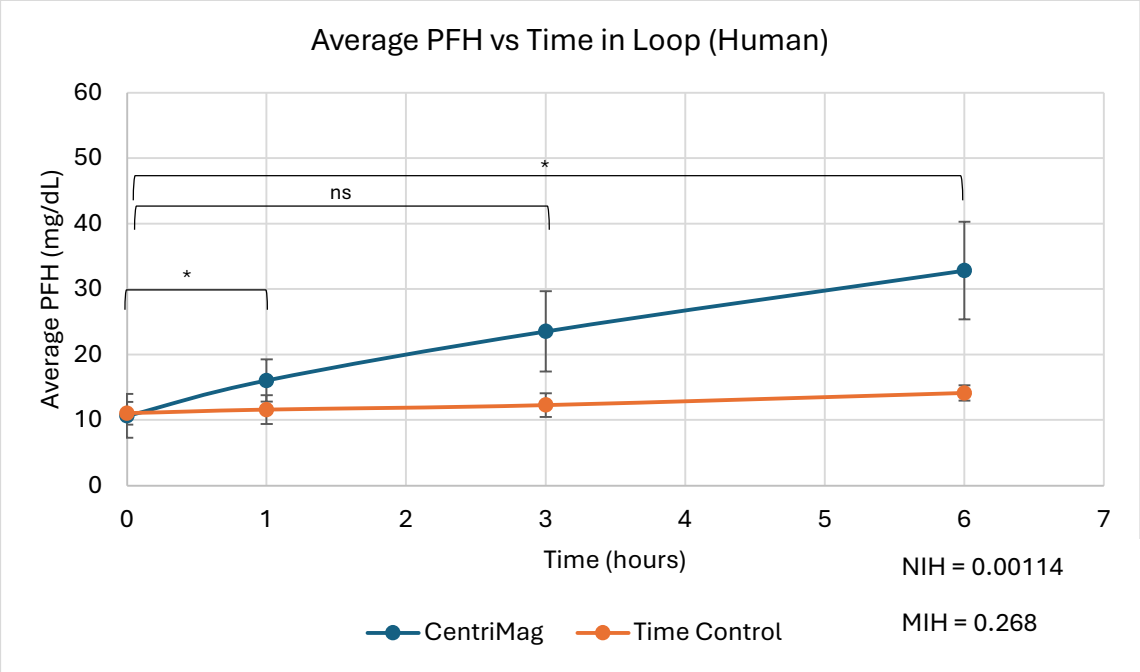

Figure 29: Average plasma free hemoglobin vs time in the in vitro circulation loop compared with time control for human RBCs. "" indicates $p < 0.05$; "ns" indicates "Not Significant".*

Repeated-measures ANOVA confirmed a significant effect of time, with trends suggesting an interaction between time and condition (Appendix C, Table 72). Post-hoc Bonferroni adjustments confirmed these effects (Appendix C, Table 73). Paired t-tests identified significant differences between conditions at 1 hour, 3 hours, and 6 hours, with higher PFH levels in the CentriMag loop (Appendix C, Table 75). Percent hemoglobin release in the CentriMag condition exceeded the 0.2% threshold for notable cell membrane damage [109] at all time points (Table 3).

Sample (Human)	% Hemoglobin Release
CentriMag 0 hours	0.25
CentriMag 1 hour	0.38
CentriMag 3 hours	0.56
CentriMag 6 hours	0.77

Time Control 0 hours	0.26
Time Control 1 hour	0.27
Time Control 3 hours	0.29
Time Control 6 hours	0.33

Table 3: Percent hemoglobin release for each human sample

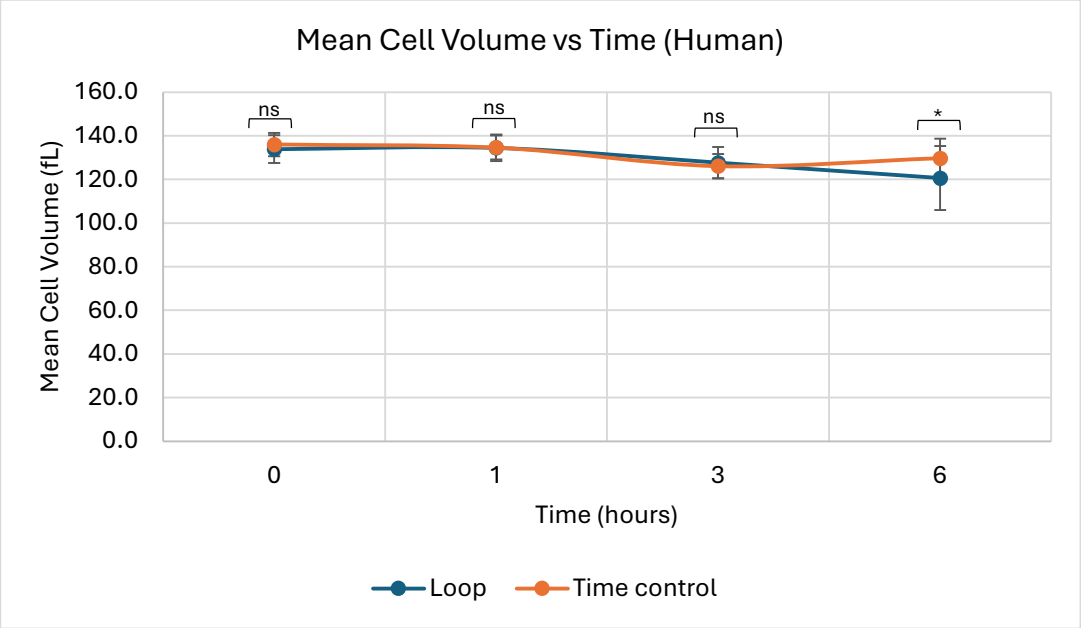

Figure 30: Average mean cell volume vs time in the in vitro circulation loop compared with time control for human RBCs. "" indicates $p < 0.05$; "ns" indicates "Not Significant".*

MCV in human samples remained largely unchanged over time (Figure 30), with no differences detected between the CentriMag loop and time control. Paired t-tests revealed a significant decrease in MCV in the CentriMag condition at 6 hours (Appendix C, Table 77). Correlation analyses indicated moderate to strong relationships between conditions at select time points (Appendix C, Table 78). The packed cell volume remained intact over the course of the experiment.

Finally, total whole blood cholesterol levels in the three human donors were 133, 232, and 200 mg/dL. Correlation analysis between cholesterol levels and average P_0 showed strong,

though not statistically significant, positive relationships in both the CentriMag and time control conditions (Appendix C, Table 79).

Discussion

This study evaluated prolonged CentriMag circulation and its effect on bovine RBCs (4 L/min, 2050 rpm, 80 mmHg) and human RBCs (5 L/min, 2300 rpm, 100 mmHg). Early measurements showed negligible differences between the CentriMag and time control P_0 values, but a significant difference emerged at 4.5 hours in bovine samples and 6 hours in human samples. This suggests that extended circulation may be required to observe measurable changes in RBC deformability. The large effect sizes observed for the Condition independent variable (loop vs time control) indicate that the CentriMag may substantially influence deformability despite the lack of statistical significance, likely due to the small sample size (n = 4 for bovine and n = 3 for human.

In bovine RBCs, deformability remained relatively stable during the first three time points but showed a significant difference from the time control at 4.5 hours. This observation aligns with prior work concerning cumulative trauma from prolonged mechanical shear. Lee et al. reported that repeated or continuous exposure to shear stress in a capillary tube flow loop progressively stiffens the RBC membrane, leading to reduced deformability over time. In their study, bovine RBC deformability decreased by 73% under high shear conditions of 300 Pa [110]. Although shear stresses in the CentriMag are much lower, computational fluid dynamics by Chen et al. showed that wall shear stresses on the impeller surface can still be substantial. At an operating condition of 4.5 L/min, 75 mmHg, and 2100 rpm, the area-weighted average wall shear stress was 36.5 Pa, and 3.3% of the surface area experienced wall shear stress above 125 Pa [68]. The volume-weighted average scalar shear stress in the bulk flow was lower, at 5.7 Pa, but that

may not fully capture the impact of localized shear spikes. These wall stresses may contribute more meaningfully to cumulative RBC trauma than bulk flow shear alone. It's important to note that in Lee et al.'s capillary flow loop study, they observed slight deformability reductions at 216 seconds and 288 seconds of exposure to 90 Pa and negligible deformability reductions before those time-points. While the exact number of times a single red blood cell is exposed to the shear stress from the CentriMag pump is unknown, it can be inferred that it is around the timeframe that Chen tested in the computational fluid dynamics simulation. However, Lee et al.'s study provided controlled exposure times and well-defined shear conditions, whereas the exact exposure conditions of individual RBCs in the CentriMag loop, like the number of passes through high-shear regions and the duration of each exposure, is not known. As a result, comparisons between the two systems should be interpreted cautiously.

Lee et al. also tested the time it took for the red blood cells to regain deformability after impairment by shear stress. While deformability changes were irreversible at 300 Pa, bovine cells were observed to have the ability to regain deformability after being subjected to lower shear stress, with a recovery time of 0.15 seconds after being exposed to 90 Pa for 288 seconds. It takes significantly longer than 0.15 seconds to measure deformability in a filtration-based experimental setup. While one sample is being measured, the other sits in its sample tube for up to 30 minutes. This amount of time might be long enough for the cells to regain some deformability that was impaired by the shear stress of the CentriMag blood pump. This might explain why the differences between the loop and time controls were, at least visually, subtle for all time points. The nature of shear stress exposure in the device is also important to consider. In devices like the CentriMag, RBCs cycle through regions of high shear stress for milliseconds

before returning to lower-shear environments [68], potentially extending the time required for cumulative trauma to result in measurable deformability loss.

In human RBCs, the deformability trends mirrored those observed in bovine cells. Both the time control and CentriMag groups remained stable until a significant difference emerged at the last time point. This suggests that prolonged exposure to supraphysiological shear stress may eventually alter mechanical properties. At 1 hour in the human experiment, a paired t-test revealed an unexpected significant difference in deformability between conditions, with the CentriMag group displaying a slightly higher P_0 but a statistically significant paired difference in the opposite direction. This may be attributed to within-subject variability, which is exacerbated by a small sample size. Factors such as donor oxidative stress levels, RBC age distribution, and sex differences could contribute to these variations. For instance, oxidative stress levels can vary substantially based on age, sex, plasma cholesterol levels, and BMI [111]. The bovine samples, in contrast, were obtained from animals of the same sex, in the same location, with controlled diets and conditions, potentially reducing variability. Additionally, while the literature reports an inverse correlation between total plasma cholesterol levels and RBC deformability in humans, our study found an insignificant positive correlation [112]. Kohno et al's study might help explain any variability of P_0 between donors. In our study, correlation analyses in both human and bovine showed that in samples with a high P_0 value in the CentriMag, time control values appeared to be slightly elevated too. Studies concerning factors (oxidative stress) that cause this donor-to-donor variability are needed. This study should not be compared with cholesterol content in the RBC membrane. Although cholesterol content in the RBC membrane may influence mechanical properties, plasma cholesterol levels may not directly reflect membrane composition.

Unlike deformability, plasma free hemoglobin (PFH) levels in both bovine and human samples increased progressively in the CentriMag group while remaining stable in the time controls. In bovine RBCs, significant differences in PFH were observed as early as 1.5 hours, whereas deformability differences only appeared at 4.5 hours. Similarly, in human RBCs, significant increases in PFH occurred earlier (1 hour, 3 hours, and 6 hours) than in deformability changes. These results indicate that hemolysis can precede detectable changes in deformability. Early PFH release may be due to the mechanical rupture of more fragile or older RBCs, or from flow through regions of higher stress, while remaining RBCs maintain deformability until further cumulative trauma. Together, the increase in PFH, the stable hematocrit, and the delayed changes in deformability suggest that the RBCs in this study predominantly experience sublethal injury, with membrane compromise occurring before significant loss of cells that were circulating in the mock loop. Svenmarker et al. previously observed increased PFH without concurrent changes in deformability during cardiopulmonary bypass procedures using human blood [109]. Watanabe et al. also reported stable porcine RBC deformability for up to eight hours in a rotary pump, despite rising PFH [113]. Bovine RBCs are comparable to porcine RBCs in this context because they have the same surface area-to-volume ratio [100]. Our findings align with those prior studies mentioned above and further support the idea that RBC deformability may remain stable while hemolysis increases. Notably, in our study, hemoglobin release in bovine RBCs ranged from 0.17% to 0.47% in the CentriMag group, exceeding the 0.2% threshold associated with significant membrane damage [109]. However, these levels did not coincide with early measurable deformability impairments, indicating that PFH is a more sensitive early marker of RBC trauma than P_0.

When comparing human and bovine RBCs, our results suggest that bovine cells are more resistant to mechanical damage. Bovine RBCs demonstrated less deformability loss and lower PFH increases compared to human RBCs under similar conditions. These findings are consistent with prior studies by McNamee et al. and Chan et al. which found bovine RBCs to be more resilient to shear-induced damage than human RBCs [95, 98]. The morphological and structural differences between species likely contribute to these disparities. Bovine RBCs have a lower surface area-to-volume ratio and greater membrane stability than human RBCs [96, 100]. Smith et al. found that bovine RBCs deformed less than human cells at high shear stress (590 dyn/cm^2), with minimum cell diameters of 2.5 μm for bovine cells compared to 2.9 μm for human cells [96]. These differences highlight the importance of species selection in hemocompatibility testing for medical devices.

In addition to assessing deformability and PFH, mean cell volume was evaluated. In both bovine and human RBCs, MCV remained relatively stable over time in the time control groups. However, there was a slight, but insignificant, decline in MCV observed in the CentriMag loop conditions for human samples, with a statistically significant decrease at 6 hours in the paired t-test. However, this isolated finding did not correspond to a significant overall effect of condition and given the overall stability of MCV across other time points and moderate correlations between conditions, it is likely that this decrease reflects biological variability, sample size limitations, or measurement variability rather than a true physiological response.

Calcium influx plays an important role in regulating RBC volume via Gardos channel. While it is theoretically possible that mechanical stress could induce intracellular calcium influx and activate the Gardos channel, this interpretation remains highly speculative in the context of our data. Calcium accumulation can promote potassium efflux and water loss via the Gardos

channel, decreasing cell volume and reducing deformability due to cell dehydration [3, 4, 18]. Prior studies by Murakami et al. and Kuck et al. demonstrated that calcium entry through mechanosensitive channels compromises RBC deformability due to a decrease in volume [4, 84]. However, our study did not measure intracellular calcium. O'Rear et al. reported reductions in deformability associated with elevated intracellular calcium in patients with prosthetic heart valves, even without significant MCV changes. The conditions of prosthetic heart valves are comparable to CentriMag conditions due to high shear stress and short exposure times. This observation points to the need for further studies that concurrently assess deformability, intracellular calcium levels, and MCV in cells exposed to the CentriMap mock loop setup.

The divergence in trends between PFH, deformability, and MCV trends raises questions about underlying mechanisms. One possibility is that oxidative stress or intracellular calcium levels may vary among donors, influencing susceptibility to shear-induced damage. Muravyov et al. suggested that elevated intracellular calcium and oxidative stress can impair RBC deformability [57]. O'Rear et al. observed reduced hematocrit and elevated serum lactate dehydrogenase levels, markers of hemolysis, in patients with prosthetic heart valves and inferred that increased intracellular calcium may have contributed to the observed reductions in deformability [2]. These findings highlight potential mechanisms for shear-induced deformability loss, even in the absence of early MCV changes. That being said, future studies should incorporate measurements of oxidative stress markers (e.g., malondialdehyde) and intracellular calcium testing to clarify their roles in RBC trauma in blood pumps [114]. In addition, due to the unexpected correlation between cholesterol and deformability, further studies with larger sample sizes are needed to elucidate donor-specific factors affecting RBC deformability when exposed to shear stress. Due to the differences in the mock loop settings for

bovine and human experiments, the ability to draw definite conclusions on comparisons between the two is limited.

Conclusion

- The purpose of this study was to evaluate the effects of prolonged circulation in the CentriMag blood pump on RBC deformability, hemolysis, and cell volume and both human and bovine blood.
- In the bovine mock loop (4 L/min, 80 mmHg, 2050 rpm), deformability (P_0) remained stable during early time points, but it showed a significant increase at 4.5 hours in the CentriMag loop compared to the time control.
- In the human mock loop (5 L/min, 100 mmHg, 2300 rpm), deformability remained stable until 6 hours when a significant increase in P_0 was observed, compared to the time control.
- In both species, PFH increased in the CentriMag loop and was significantly higher than the time controls at multiple time points.
- PFH increases occurred earlier than deformability changes, indicating that hemolysis preceded measurable impairments in deformability.
- MCV remained generally stable in both species, with an isolated significant decrease observed at 6 hours in human RBCs.
- These findings suggest that in conditions mock loop set-up, using the CentriMag blood pump, hemolysis is an earlier indicator of RBC trauma than deformability loss.

Acknowledgments

Andrew D'Amico developed the LabView VI code and assisted in choosing the Data Acquisition Device.

References

[1] L. Kuck, M. Grau, and M. J. Simmonds, "Recovery time course of erythrocyte deformability following exposure to shear is dependent upon conditioning shear stress," *Biorheology,* vol. 54, no. 5-6, pp. 141-152, 2018, doi: 10.3233/bir-17151.

[2] E. O'Rear, et al., "Increased Intracellular Calcium and Decreased Deformability of Erythrocytes from Prosthetic Heart Valve Patients," *Clinical Hemorheology,* vol. 4, pp. 461-471, 1984.

[3] E. O'Rear, et al., "Reduced erythrocyte deformability associated with calcium accumulation," *Biochemica et biophysica acta,* vol. 691, no. 2, pp. 274-280, 1982.

[4] P. J. Kuck L, Simmonds M, "Calcium dynamically alters erythrocyte mechanical response to shear," *Biochimica et biophys acta,* vol. 1867, no. 11, p. 118802, 2020.

[5] D. B. Nguyen *et al.*, "Characterization of Microvesicles Released from Human Red Blood Cells," *Cellular Physiology and Biochemistry,* vol. 38, no. 3, pp. 1085-1099, 2016, doi: 10.1159/000443059.

[6] F. L. Larsen, S. Katz, B. D. Roufogalis, and D. E. Brooks, "Physiological shear stresses enhance the Ca2+ permeability of human erythrocytes," *Nature,* vol. 294, no. 5842, pp. 667-668, 1981, doi: 10.1038/294667a0.

[7] J. Wan, W. D. Ristenpart, and H. A. Stone, "Dynamics of shear-induced ATP release from red blood cells," *Proceedings of the National Academy of Sciences,* vol. 105, no. 43, pp. 16432-16437, 2008, doi: 10.1073/pnas.0805779105.

[8] K. De Jong and F. A. Kuypers, "Flow cytometric determination of PMCA-mediated Ca²⁺-extrusion in individual red blood cells," *Cytometry Part A,* vol. 71A, no. 9, pp. 693-699, 2007, doi: 10.1002/cyto.a.20429.

[9] T. Shiga, M. Sekiya, N. Maeda, K. Kon, and M. Okazaki, "Cell age-dependent changes in deformability and calcium accumulation of human erythrocytes," *Biochemica et biophysica acta,* vol. 814, no. 2, pp. 289-299, 1985, doi: 10.1016/0005-2736(85)90447-X.

[10] R. I. Weed, P. L. Lacelle, and E. W. Merrill, "Metabolic dependence of red cell deformability," *Journal of Clinical Investigation,* vol. 48, no. 5, pp. 795-809, 1969, doi: 10.1172/jci106038.

[11] D. Darghouth *et al.*, "Alterations of red blood cell metabolome in overhydrated hereditary stomatocytosis," *Haematologica,* vol. 96, no. 12, pp. 1861-1865, 2011, doi: 10.3324/haematol.2011.045179.

[12] E. Cinar, S. Zhou, J. Decourcey, Y. Wang, R. E. Waugh, and J. Wan, "Piezo1 regulates mechanotransductive release of ATP from human RBCs," *Proceedings of the National Academy of Sciences,* vol. 112, no. 38, pp. 11783-11788, 2015, doi: 10.1073/pnas.1507309112.

[13] J. G. Danielczok *et al.*, "Red Blood Cell Passage of Small Capillaries Is Associated with Transient Ca2+-mediated Adaptations," *Frontiers in Physiology,* vol. 8, 2017, doi: 10.3389/fphys.2017.00979.
[14] L. B. Leverett, J. D. Hellums, C. P. Alfrey, and E. C. Lynch, "Red Blood Cell Damage by Shear Stress," *Biophysical Journal,* vol. 12, no. 3, pp. 257-73, 1972, doi: 10.1016/S0006-3495(72)86085-5.
[15] A. Dyrda *et al.*, "Local Membrane Deformations Activate Ca2+-Dependent K+ and Anionic Currents in Intact Human Red Blood Cells," *PLoS ONE,* vol. 5, no. 2, p. e9447, 2010, doi: 10.1371/journal.pone.0009447.
[16] M. Föller and F. Lang, "Ion Transport in Eryptosis, the Suicidal Death of Erythrocytes," *Frontiers in Cell and Developmental Biology,* vol. 8, 2020, doi: 10.3389/fcell.2020.00597.
[17] R. S. Franco *et al.*, "Changes in the properties of normal human red blood cells during in vivo aging," *American Journal of Hematology,* vol. 88, no. 1, pp. 44-51, 2013, doi: 10.1002/ajh.23344.
[18] G. Gardos, "The function of calcium in the potassium permeability of human erythrocytes," *Biochemica et biophysica acta* vol. 30, no. 3, pp. 653-4, 1958.
[19] K. Z. Ugurel E, Aksu Y, Goksel E, Cilek N, Yalcin O, "Calcium/protein kinase C signaling mechanisms in shear-induced

mechanical responses of red blood cells " *Microvascular Research,* vol. 135, p. 104124, 2021.
[20] P. Blackshear and G. Blackshear, "Mechanical Hemolysis," in *Handbook of Bioengineering*: McGraw-Hill, Inc., 1987, ch. 15.
[21] M. Lokhandwalla, J. A. McAteer, J. C. Williams, and B. Sturtevant, "Mechanical haemolysis in shock wave lithotripsy (SWL): II.In vitrocell lysis due to shear," *Physics in Medicine and Biology,* vol. 46, no. 4, pp. 1245-1264, 2001, doi: 10.1088/0031-9155/46/4/323.
[22] T. Yeung, G. E. Gilbert, J. Shi, J. Silvius, A. Kapus, and S. Grinstein, "Membrane Phosphatidylserine Regulates Surface Charge and Protein Localization," *Science,* vol. 319, no. 5860, pp. 210-213, 2008, doi: 10.1126/science.1152066.
[23] C. Sinn, M. Antonietti, and R. Dimova, "Binding of calcium to phosphatidylcholine–phosphatidylserine membranes," *Colloids and Surfaces A: Physicochemical and Engineering Aspects,* vol. 282-283, pp. 410-419, 2006, doi: 10.1016/j.colsurfa.2005.10.014.
[24] J. Tait and D. Gibson, "Phospholipid Binding of Annexin V: Effects of Calcium

and Membrane Phosphatidylserine Content," *Archives of Biochemistry and Biophysics,* vol. 298, no. 1, pp. 187-191, 1992, doi: 10.1016/0003-9861(92)90111-9.
[25] E. Bevers and P. Williamson, "Getting to the Outer Leaflet: Physiology of Phosphatidylserine Exposure at the Plasma Membrane," *Physiological Reviews,* vol. 92, no. 2, pp. 605-645, 2016, doi: doi: 10.1152/physrev.00020.2015.
[26] O. Linderkamp, P. Y. K. Wu, and H. J. Meiselman, "Geometry of Neonatal and Adult Red Blood Cells," *Pediatric Research,* vol. 17, no. 4, pp. 250-253, 1983, doi: 10.1203/00006450-198304000-00003.
[27] M. C. Wesseling *et al.*, "Measurements of Intracellular Ca2+ Content and Phosphatidylserine Exposure in Human Red Blood Cells: Methodological Issues,"

Cellular Physiology and Biochemistry, vol. 38, no. 6, pp. 2414-2425, 2016, doi: 10.1159/000445593.
[28] M. Avcı, E. A. O'Rear, K. M. Foster, and D. V. Papavassiliou, "Sublethal Damage to Erythrocytes during Blood Flow," *Fluids,* vol. 7, no. 2, p. 66, 2022, doi: 10.3390/fluids7020066.
[29] J. P. Buerck, D. K. Burke, D. W. Schmidtke, T. A. Snyder, D. Papavassiliou, and E. A. O'Rear, "A Flow Induced Autoimmune Response and Accelerated Senescence of Red Blood Cells in Cardiovascular Devices," *Scientific Reports,* vol. 9, no. 1, 2019, doi: 10.1038/s41598-019-55924-y.
[30] D. B. Nguyen *et al.*, "Regulation of Phosphatidylserine Exposure in Red Blood Cells," *Cellular Physiology and Biochemistry,* vol. 28, no. 5, pp. 847-856, 2011, doi: 10.1159/000335798.
[31] S. Nagata, T. Sakuragi, and K. Segawa, "Flippase and scramblase for phosphatidylserine exposure," *Current Opinion in Immunology,* vol. 62, pp. 31-38, 2020, doi: 10.1016/j.coi.2019.11.009.
[32] I. Bernhardt, D. B. Nguyen, M. C. Wesseling, and L. Kaestner, "Intracellular Ca2+ Concentration and Phosphatidylserine Exposure in Healthy Human Erythrocytes in Dependence on in vivo Cell Age," *Frontiers in Physiology,* vol. 10, 2020, doi: 10.3389/fphys.2019.01629.
[33] G. Barshtein, R. Ben-Ami, and S. Yedgar, "Role of red blood cell flow behavior in hemodynamics and hemostasis," *Expert Review of Cardiovascular Therapy,* vol. 5, no. 4, pp. 743-752, 2014, doi: 10.1586/14779072.5.4.743.
[34] R. L. Koshiar, S. Somajo, E. Norström, and B. Dahlbäck, "Erythrocyte-Derived Microparticles Supporting Activated Protein C-Mediated Regulation of Blood Coagulation," *PLoS ONE,* vol. 9, no. 8, p. e104200, 2014, doi: 10.1371/journal.pone.0104200.
[35] J. P. Buerck, D. K. Burke, D. W. Schmidtke, T. A. Snyder, D. V. Papavassiliou, and E. A. O'Rear, "Production of erythrocyte microparticles in a sub-hemolytic environment," *Journal of Artificial Organs,* vol. 24, no. 2, pp. 135-145, 2021, doi: 10.1007/s10047-020-01231-7.
[36] Invitrogen, "Fura and Indo Ratiometric Calcium Indicators," Molecular Probes, Product Information 2011. Accessed: April 25, 2025.
[37] T. W. Kaestner L, Weiss E, Bernhardt I, Lipp P, "Calcium imaging of individual erythrocytes: problems and approaches," *Cell Calcium,* vol. 39, pp. 13-19, 2006.
[38] Invitrogen. "Fluo-4, AM, cell permeant." Thermo Fisher Scientific. https://www.thermofisher.com/order/catalog/product/F14201 (accessed April 25, 2025).
[39] Invitrogen. "Fluo-5N, AM, cell permeant - Special Packaging." Thermo Fisher Scientific. https://www.thermofisher.com/order/catalog/product/F14204?SID=srch-srp-F14204 (accessed April 25, 2025.
[40] E. O'Rear, et al., "Problems in measurement of erythrocyte calcium," *American Journal of Hematology,* vol. 11, no. 3, pp. 283-292, 1981, doi: 10.1002/ajh.2830110309.
[41] E. Murphy, L. Berkowitz, E. Orringer, L. Levy, S. Gabel, and R. London, "Cytosolic free calcium levels in sickle red blood cells," *Blood,* vol. 69, no. 5, pp. 1469-1474, 1987, doi: 10.1182/blood.v69.5.1469.1469.

[42] R. M. Paredes, J. C. Etzler, L. T. Watts, W. Zheng, and J. D. Lechleiter, "Chemical calcium indicators," *Methods,* vol. 46, no. 3, pp. 143-151, 2008, doi: 10.1016/j.ymeth.2008.09.025.
[43] T. S. Thomas D, Collins T, Bootman M, "A comparison of fluorescent Ca2+ indicator properties and their use in measuring elementary and global Ca2+ signals," *Cell Calcium,* vol. 28, no. 4, pp. 213-23, 2000.
[44] A. Hatem, G. Poussereau, M. Gachenot, L. Pérès, G. Bouyer, and S. Egée, "Dual action of Dooku1 on PIEZO1 channel in human red blood cells," *Frontiers in Physiology,* vol. 14, 2023, doi: 10.3389/fphys.2023.1222983.
[45] L. Hertz *et al.*, "Is Increased Intracellular Calcium in Red Blood Cells a Common Component in the Molecular Mechanism Causing Anemia?," *Frontiers in Physiology,* vol. 8, 2017, doi: 10.3389/fphys.2017.00673.
[46] V. Introini *et al.*, "Evidence against a Role of Elevated Intracellular Ca2+ during Plasmodium falciparum Preinvasion," *Biophysical Journal,* vol. 114, no. 7, pp. 1695-1706, 2018, doi: 10.1016/j.bpj.2018.02.023.
[47] L. Kuck *et al.*, "Lysis of human erythrocytes due to Piezo1-dependent cytosolic calcium overload as a mechanism of circulatory removal," *Proceedings of the National Academy of Sciences,* vol. 121, no. 36, 2024, doi: 10.1073/pnas.2407765121.
[48] L. Kuck, J. N. Peart, and M. J. Simmonds, "Piezo1 regulates shear-dependent nitric oxide production in human erythrocytes," *American Journal of Physiology-Heart and Circulatory Physiology,* vol. 323, no. 1, pp. H24-H37, 2022, doi: 10.1152/ajpheart.00185.2022.
[49] J. Wang *et al.*, "Morphologically Homogeneous Red Blood Cells Present a Heterogeneous Response to Hormonal Stimulation," *PLoS ONE,* vol. 8, no. 6, p. e67697, 2013, doi: 10.1371/journal.pone.0067697.
[50] "PubChem Compound Summary for CID 25058176, Fluo-4." National Center for Biotechnology Information. https://pubchem.ncbi.nlm.nih.gov/compound/Fluo-4 (accessed March 23, 2025.
[51] "PubChem Compound Summary for CID 4060965, Fluo-4 AM." National Center for Biotechnology Information. https://pubchem.ncbi.nlm.nih.gov/compound/Fluo-4-AM (accessed March 23, 2025.
[52] G.-S. J. Tiffert T, Lew V, "Irreversible ATP depletion caused by low concentrations of formaldehyde and of calcium-chelator esters in intact human red cells," *Biochemica et biophysica acta,* vol. 773, pp. 143-156, 1984.
[53] Y. Son, "Determination of shear viscosity and shear rate from pressure drop and flow rate relationship in a rectangular channel," *Polymer,* vol. 48, pp. 632-637, 2007.
[54] N. Z. Alsmadi, S. J. Shapiro, C. S. Lewis, V. M. Sheth, T. A. Snyder, and D. W. Schmidtke, "Constricted microfluidic devices to study the effects of transient high shear exposure on platelets," *Biomicrofluidics,* vol. 11, no. 6, p. 064105, 2017, doi: 10.1063/1.4989386.
[55] E. A. Shimp, N. Z. Alsmadi, T. Cheng, K. H. Lam, C. S. Lewis, and D. W. Schmidtke, "Effects of shear on P-selectin deposition in microfluidic channels," *Biomicrofluidics,* vol. 10, no. 2, p. 024128, 2016, doi: 10.1063/1.4944823.
[56] K. Gee, K. Brown, W.-N. Chen, J. Bishop-Stewart, and G. Johnson, "Chemical and physiological characterization of fluo-4 Ca2+-indicator dyes," *Cell Calcium,* vol. 27, no. 2, pp. 97-106, 2000.

[57] J. T. Horobin, S. Sabapathy, and M. J. Simmonds, "Repetitive Supra-Physiological Shear Stress Impairs Red Blood Cell Deformability and Induces Hemolysis," *Artificial Organs,* vol. 41, no. 11, pp. 1017-1025, 2017.
[58] R. Waugh, M. Narla, C. Jackson, T. Mueller, T. Suzuki, and G. Dale, "Rheologic properties of senescent erythrocytes: loss of surface area and volume with red blood cell age," *Blood,* vol. 79, no. 5, pp. 1351-1358, 1992, doi: 10.1182/blood.v79.5.1351.1351.
[59] N. D. Thien, N. Hai-Nam, D. T. Anh, and D. Baecker, "Piezo1 and its inhibitors: Overview and perspectives," *European journal of Medicinal Chemistry,* vol. 273, p. 116502, 2024, doi: 10.1016/j.ejmech.2024.116502.
[60] F. L. A. Willekens, J. M. Werre, Y. A. M. Groenen-Döpp, B. Roerdinkholder-Stoelwinder, B. De Pauw, and G. J. C. G. M. Bosman, "Erythrocyte vesiculation: a self-protective mechanism?," *British Journal of Haematology,* vol. 141, no. 4, pp. 549-556, 2008, doi: 10.1111/j.1365-2141.2008.07055.x.
[61] A. Nascimbene *et al.*, "Association between cell-derived microparticles and adverse events in patients with nonpulsatile left ventricular assist devices," *The Journal of Heart and Lung Transplantation,* vol. 33, no. 5, pp. 470-477, 2014, doi: 10.1016/j.healun.2014.01.004.
[62] R. Sansone *et al.*, "Macrovascular and microvascular function after implantation of left ventricular assist devices in

end-stage heart failure: role of microparticles," *The Journal of heart and lung transplantation,* vol. 34, no. 7, pp. 921-32, 2015.
[63] P. M. Siegel *et al.*, "Extracellular Vesicles Are Associated With Outcome in Veno-Arterial Extracorporeal Membrane Oxygenation and Myocardial Infarction," *Frontiers in Cardiovascular Medicine,* vol. 8, 2021, doi: 10.3389/fcvm.2021.747453.
[64] F. Leal, J. Kauffimann, M. Adjobo-Hermans, and G. Bosman, "Red Blood Cell Homeostasis: Mechanisms and Effects of Microvesicle Generation in Health and Disease," *Frontiers in Physiology,* vol. 9, 2018, doi: 10.3389/fphys.2018.00703.
[65] L. Kuck, J. N. Peart, and M. J. Simmonds, "Active modulation of human erythrocyte mechanics," *American Journal of Physiology-Cell Physiology,* vol. 319, no. 2, pp. C250-C257, 2020, doi: 10.1152/ajpcell.00210.2020.
[66] M. A. Sobieski, G. A. Giridharan, M. Ising, S. C. Koenig, and M. S. Slaughter, "Blood Trauma Testing of CentriMag and RotaFlow Centrifugal Flow Devices: A Pilot Study," *Artificial Organs,* vol. 36, no. 8, pp. 677-682, 2012, doi: 10.1111/j.1525-1594.2012.01514.x.
[67] P. Li *et al.*, "A comprehensive comparison of the in vitro hemocompatibility of extracorporeal centrifugal blood pumps," *Frontiers in Physiology,* vol. 14, 2023, doi: 10.3389/fphys.2023.1136545.
[68] Z. Chen, J. Zheng, T. Li, D. Tran, B. Griffith, and Z. Wu, "The impact of shear stress of device-induced platelet hemostatis dysfunction relevant to thrombosis and bleeding in mechanically assisted circulation," *Artificial Organs,* vol. 44, no. 5, pp. E201-E213, 2020.
[69] *Standard Practice for Assessment of Hemolysis in Continuous Flow Blood Pumps*, ASTM International, 2021.
[70] S. Wang, W. Sun, D. Han, K. P. Clark, B. P. Griffith, and Z. J. Wu, "In vitro study on device-induced damage to blood cellular components and degradation of von Willebrand

factor in a <scp>CentriMag</scp> pump-assisted circulation," *Artificial Organs,* vol. 48, no. 9, pp. 988-996, 2024, doi: 10.1111/aor.14766.
[71] ORFLO Technologies, *Moxi Z: The Mini Automated Cell Counter User Manual OS 4.3*. 2012.
[72] B. S. Maner, R. B. Killeen, and L. Moosavi, *Mean Corpuscular Volume*. Treasure Island, FL: StatPearls, 2024.
[73] M. Harboe, "A method for determination of hemoglobin in plasma by near-ultraviolet spectrophotometry," *Scandinavian Journal of Clinical and Laboratory Investigation,* vol. 11, no. 1, pp. 66-70, 1959, doi: 10.3109/00365515909060410.
[74] H. J. Chung *et al.*, "Automation of Harboe method for the measurement of plasma free hemoglobin," *Journal of Clinical Laboratory Analysis,* vol. 34, no. 6, 2020, doi: 10.1002/jcla.23242.
[75] L. M. Sullivan, "Repeated Measures," *Circulation,* vol. 117, no. 9, pp. 1238-1243, 2008, doi: 10.1161/circulationaha.107.654350.
[76] Y. Chen and M. K. Sharp, "A Strain-Based Flow-Induced Hemolysis Prediction Model Calibrated by In Vitro Erythrocyte Deformation Measurements," *Artificial Organs,* vol. 35, no. 2, pp. 145-156, 2011, doi: 10.1111/j.1525-1594.2010.01050.x.
[77] M. Lokhandwalla, "Damage Mechanisms in Shock Wave Lithotripsy (SWL)," Doctor of Philosophy, California Institute of Technology, 2001.
[78] A. Besarab, A. Deguzman, and J. W. Swanson, "Effect of albumin and free calcium concentrations on calcium binding in vitro," *Journal of Clinical Pathology,* vol. 34, no. 12, pp. 1361-1367, 1981, doi: 10.1136/jcp.34.12.1361.
[79] W. Tillman and W. Schroter, "Deformability of red cells and splenectomy in hemolytic anemias," *Clinical Hemorheology,* vol. 3, pp. 409-428, 1983.
[80] W. Reinhart and S. Chien, "Roles of cell geometry and cellular viscosity in red cell passage through narrow pores," *The American Journal of Physiology* vol. 248, pp. C473-C479, 1985.
[81] C. Renoux *et al.*, "Impact of surface-area-to-volume ratio, internal viscosity and membrane viscoelasticity on red blood cell deformability measured in isotonic condition," *Scientific Reports,* vol. 9, no. 1, 2019, doi: 10.1038/s41598-019-43200-y.
[82] N. Mohandas, M. R. Clark, M. S. Jacobs, and S. B. Shohet, "Analysis of factors regulating erythrocyte deformability," *Journal of Clinical Investigation,* vol. 66, no. 3, pp. 563-573, 1980, doi: 10.1172/jci109888.
[83] M. Simmonds, N. Atac, and O. Baskurt, "Erythrocyte deformability responses to intermittent and continuous subhemolytic shear stress," *Biorheology,* vol. 51, no. 2-3, pp. 171-85, 2014.
[84] J. Murakami, N. Maeda, K. Kon, and T. Shiga, "A contribution of calmodulin to cellular deformability of calcium-loaded human erythrocytes," *Biochemica et biophysica acta,* vol. 863, pp. 23-32, 1986.
[85] M. Bessis and N. Mohandas, "A diffractometric method for the measurement of cellular deformability," *Blood Cells,* vol. 1, p. 307, 1975.
[86] H. Schmid-Schonbein and R. Wells, "Fluid Drop-Like Transition of Erythrocytes under Shear," *Science,* vol. 165, no. 3890, pp. 288-291, 1969, doi: 10.1126/science.165.3890.288.

[87] Y. Z. Chunyi W, Wiebo K, "The influence of calcium ions and ionophore A23187 on microrheological characteristics of erythrocytes by new model ektacytometry," *Clinical Hemorheology and Microcirculation,* vol. 24, no. 1, pp. 19-23, 2001.
[88] D. K. Kuettner J, Rao G, "Influence of the ionophore A23187 on the plastic behavior of normal erythrocytes," *The American Journal of Pathology,* vol. 88, no. 1, pp. 81-94, 1977.
[89] E. A. O'Rear, L. V. McIntire, B. O. Shah, and E. C. Lynch, "Use of Rheological Technique to Evaluate Erythrocyte Membrane Alterations," in *Journal of Rheology*, 1979, vol. 23, no. 6, pp. 721-733.
[90] J. A. Velker, L. V. McIntire, and E. C. Lynch, "Alteration of erythrocyte deformability due to shear stress assessed by nuclepore filters," *American Society for Artificial Internal Organs,* vol. 23, no. 1, 1977.
[91] T.-W. Chung and E. A. O'Rear, "Assessing Erythrocyte Filterability with 3 um pore size polycarbonate membranes at constant cell flux," *Clinical Hemorheology,* vol. 10, pp. 505-514, 1990.
[92] K. G. Engström, "New red blood cell filtration device with improved time resolution and its application to the impaired RBC deformability in the diabetic ob/ob mouse," *Biorheology,* vol. 26, no. 4, pp. 711-721, 1989, doi: 10.3233/bir-1989-26404.
[93] A. Namvar *et al.*, "Surface area-to-volume ratio, not cellular rigidity, determines red blood cell traversal through small capillaries," Cold Spring Harbor Laboratory, 2020.
[94] N. Adili, M. Melizi, and H. Belabbas, "Species determination using the red blood cells morphometry in domestic animals," *Veterinary World,* vol. 9, no. 9, pp. 960-963, 2016, doi: 10.14202/vetworld.2016.960-963.
[95] A. McNamee, L. Kuck, and M. Simmonds, "Bovine erythrocytes are poor surrogates for human when exposed to sublethal shear stress," *The International Journal of Artificial Organs,* vol. 45, 6, pp. 580-587, 2022.
[96] J. E. Smith, N. Mohandas, and S. B. Shohet, "Variability in erythrocyte deformability among various mammals," *American Journal of Physiology-Heart and Circulatory Physiology,* vol. 236, no. 5, pp. H665-H786, 1979.
[97] S. M. Farooqui, R. K. Wali, R. F. Baker, and V. K. Kalra, "Effect of cell shape, membrane deformability and phospholipid organization on phosphate-calcium-induced fusion of erythrocytes," *Biochemica et Biophysica Acta (BBA) - Biomembranes,* vol. 904, no. 2, pp. 239-250, 1987.
[98] C. H. H. Chan, I. L. Pieper, C. R. Robinson, Y. Friedmann, V. Kanamarlapudi, and C. A. Thornton, "Shear Stress-Induced Total Blood Trauma in Multiple Species," *Artificial Organs,* vol. 41, no. 10, pp. 934-947, 2017, doi: 10.1111/aor.12932.
[99] E. A. Evans and P. L. La Celle, "Intrinsic material properties of the erythrocyte membrane indicated by mechanical analysis of deformation," *Blood,* vol. 45, no. 1, pp. 29-43, 1975.
[100] W. Gruber and B. Deuticke, "Comparative aspects of phosphate transfer across mammalian erythrocyte membranes," *The Journal of Membrane Biology,* vol. 13, no. 1, pp. 19-36, 1973, doi: 10.1007/bf01868218.
[101] W. F. Emmons, "The interrelation of number, volume, diameter and area of mammalian erythrocytes," *The Journal of Physiology,* vol. 64, no. 3, pp. 215-228, 1927, doi: 10.1113/jphysiol.1927.sp002431.
[102] E. Ponder, *Hemolysis and Related Phenomena*. New York: Grune and Stratton, 1948.

[103] G. T. Rich, R. I. Sha'afi, T. G. Barton, and A. K. Solomon, "Permeability studies on red cell membranes of dog, cat and beef," *Journal of General Physiology,* vol. 50, no. 10, pp. 2391-405, 1967, doi: 10.1085/jgp.50.10.2391.
[104] E. Evans and F. Yuan-Cheng, "Improved Measurements of Erythrocyte Geometry," *Microvascular Research,* vol. 4, pp. 335-347, 1972, doi: 10.1016/0026-2862(72)90069-6.
[105] A. Namvar *et al.*, "Surface area-to-volume ratio, not cellular viscoelasticity, is the major determinant of red blood cell traversal through small channels," *Cellular Microbiology,* vol. 23, no. 1, 2021, doi: 10.1111/cmi.13270.
[106] K. H. Fraser, T. Zhang, M. E. Taskin, B. P. Griffith, and Z. J. Wu, "A Quantitative Comparison of Mechanical Blood Damage Parameters in Rotary Ventricular Assist Devices: Shear Stress, Exposure Time and Hemolysis Index," *Journal of Biomechanical Engineering,* vol. 134, no. 8, p. 081002, 2012, doi: 10.1115/1.4007092.
[107] M. Comporti, C. Signorini, G. Buonocore, and L. Ciccoli, "Iron release, oxidative stress and erythrocyte ageing," *Free Radical Biology and Medicine,* vol. 32, no. 7, pp. 568-576, 2002.
[108] *Federal Policy for the Protection of Human Subjects*. [Online] Available: https://www.ecfr.gov/current/title-45/subtitle-A/subchapter-A/part-46/subpart-A/section-46.102
[109] S. Svenmarker, E. Jansson, H. Stenlund, and K. G. Engstrom, "Red blood cell trauma during cardiopulmonary bypass: narrow pore filterability versus free haemoglobin," *Perfusion,* vol. 15, no. 1, pp. 33-40, 2000, doi: 10.1177/026765910001500106.
[110] S. S. Lee *et al.*, "Strain hardening of red blood cells by accumulated cyclic supraphysiological stress," *Artificial Organs,* vol. 31, no. 1, pp. 80-86, 2007, doi: 10.1111/j.1525-1594.2007.00344.x.
[111] G. Block, "Factors Associated with Oxidative Stress in Human Populations," *American Journal of Epidemiology,* vol. 156, no. 3, pp. 274-285, 2002, doi: 10.1093/aje/kwf029.
[112] M. Kohno *et al.*, "Improvement of erythrocyte deformability by cholesterol-lowering therapy with pravastatin in hypercholesterolemic patients," *Metabolism,* vol. 46, no. 3, pp. 287-291, 1997, doi: 10.1016/S0026-0495(97)90255-9.
[113] N. Watanabe, D. Sakota, K. Ohuchi, and S. Takatani, "Deformability of Red Blood Cells and Its Relation to Blood

Trauma in Rotary Blood Pumps," *Artificial Organs,* vol. 31, no. 5, pp. 352-358, 2007.
[114] A. H. Sawas and S. N. Pentyala, "Evaluation of lipid peroxidation in red blood cells by monitoring the uptake of sucrose and phenol red," *Journal of applied toxicology,* vol. 24, no. 3, pp. 223-229, 2004.
[115] S. P. Timoshenko, *Theory of Elasticity*, Third ed. 1970.
[116] N.-T. W. Nguyen, Steven T., "Fundamentals and Applications of Microfluidics," Second ed., 2006, pp. 30-31.

Appendices

Appendix A

Raw Data (Flow Cytometry)

Calcium						
t = 0	Median FL1-H					StDev
Ctrl	12041	14341	11090	11850.5	10581	1444.308727
St	12843.5		20882	17005.5	15069	3409.06671
5	11166	12718.5	29387	24816	31784.5	9509.897301
10	17141	26465	30505	27490	49282.5	11790.50384
t = 1	Median FL1-H					Stdev
Ctrl	9252.5	13674.5	16499.5	10200	23294	5656.959844
St	15296		31879	40265	14361	12739.5173
5	8857.5	24910	27491.5	23575	17960	7412.268821
10	23791	19407	29977.5	12941	31478	7647.458977
t = 2	Median FL1-H					StDev
Ctrl	7389.5	11594	27496.5	25519.5	22745	8921.307467
St	8755		38127	10224	14382	13711.99861
5	9475.5	27771	10234	24719	30196	9894.543827
10	10063	28111	30367	12924	51299	16484.90383
Microparticles						
t = 0	count					StDev
Ctrl	10974	4168	4712	16487	9879	5053.760333
St	6065		5806	20039	16210	7209.620471
5	6179	4218	7320	20287	17139	7188.733637
10	5477	8125	20680	37884	29719	13838.18382
t = 1	count					Stdev
Ctrl	2156	6243	3845	3977	3778	1458.185756
St	2032		4150	4771	4707	1285.938568
5	2551	5481	5317	8926	6350	2287.864834
10	5687	5673	7117	16655	8270	4588.349137
t = 2	count					StDev
Ctrl	2924	1731	2616	2088	2555	471.3498701
St	2262		2673	2580	3503	529.1190792
5	2535	2038	3456	3374	3222	614.5404787
10	3254	4053	4722	4719	5072	721.8507463

Pos Ctrl					
Median FL1-H				Avg	StDev
13,490.00	15,099.00	12,100.00	11,572.00	13,065.25	1367.301608

Table 4: Chapter 1 Calcium Raw Data (Flow Cytometry)

Statistics

Calcium

Sample	**Shapiro-Wilk**

		Statistic	df	Sig.
Fluorescence	Ctrl	.892	5	.369
	St	.980	4	.905
	5 ms	.869	5	.261
	10 ms	.897	5	.395

Table 5: Tests of normality for Fluo-4-positive red blood cells (Ctrl, St, 5 ms, 10 ms)

Tests of Homogeneity of Variances

		Levene Statistic	df1	df2	Sig.
Fluorescence	Based on Mean	3.101	3	15	.059

Table 6: Tests of homogeneity of variances for Fluo-4-positive red blood cells (Ctrl, St, 5 ms, 10 ms)

ANOVA

Fluorescence

	Sum of Squares	df	Mean Square	F	Sig.
Between Groups	907077533.647	3	302359177.882	4.719	.016
Within Groups	961025827.800	15	64068388.520		
Total	1868103361.447	18			

Table 7: One-way ANOVA for the effect of shear exposure time on median fluorescence intensity (Fluo-4, AM) of red blood cells, analyzed immediately after shear exposure

Multiple Comparisons

Dependent Variable: Fluorescence

Tukey HSD

(I) Sample	(J) Sample	Mean Difference (I-J)	Std. Error	Sig.	95% Confidence Interval	
					Lower Bound	Upper Bound
Ctrl	St	-4469.30000	5369.42966	.838	-19944.7945	11006.1945
	5 ms	-9993.70000	5062.34683	.241	-24584.1362	4596.7362
	10 ms	-18196.00000*	5062.34683	.013	-32786.4362	-3605.5638
St	Ctrl	4469.30000	5369.42966	.838	-11006.1945	19944.7945

	5 ms	-5524.40000	5369.42966	.736	-20999.8945	9951.0945
	10 ms	-13726.70000	5369.42966	.091	-29202.1945	1748.7945
5 ms	Ctrl	9993.70000	5062.34683	.241	-4596.7362	24584.1362
	St	5524.40000	5369.42966	.736	-9951.0945	20999.8945
	10 ms	-8202.30000	5062.34683	.397	-22792.7362	6388.1362
10 ms	Ctrl	18196.00000*	5062.34683	.013	3605.5638	32786.4362
	St	13726.70000	5369.42966	.091	-1748.7945	29202.1945
	10 ms	8202.30000	5062.34683	.397	-6388.1362	22792.7362

*. The mean difference is significant at the 0.05 level.

Table 8: Post-hoc Tukey Kramer test for the median fluorescence intensity (Fluo-4,AM) of red blood cells, analyzed immediately after shear exposure

Anova: Single Factor						
t = 1 median calcium FL1H						
SUMMARY						
Groups	*Count*	*Sum*	*Average*	*Variance*		
ctrl	5	72920.5	14584.1	32001194.68		
st	4	101801	25450.25	162295300.9		
5	5	102794	20558.8	54941729.08		
10	5	117594.5	23518.9	58483628.8		
ANOVA						
Source of Variation	*SS*	*df*	*MS*	*F*	*P-value*	*F crit*
Between Groups	316938911.2	3	105646303.7	1.482974221	0.259345	3.287382
Within Groups	1068592113	15	71239474.2			
Total	1385531024	18				

Table 9: One-way ANOVA for the effect of shear exposure time on median fluorescence intensity (Fluo-4, AM) of red blood cells, analyzed 2.5 hours after shear exposure

Anova: Single Factor						
t = 2 median calcium FL1H						
SUMMARY						
Groups	*Count*	*Sum*	*Average*	*Variance*		
ctrl	5	94744.5	18948.9	79589726.93		
st	4	71488	17872	188018906		
5	5	102395.5	20479.1	97901997.55		
10	5	132764	26552.8	271752054.2		
ANOVA						
Source of Variation	*SS*	*df*	*MS*	*F*	*P-value*	*F crit*
Between Groups	215396075.1	3	71798691.7	0.456148181	0.716885	3.287382
Within Groups	2361031833	15	157402122.2			
Total	2576427908	18				

Table 10: One-way ANOVA for the effect of shear exposure time on median fluorescence intensity (Fluo-4, AM) of red blood cells, analyzed 5 hours after shear exposure

Microvesicle

Anova: Single Factor						
t = 0 Microparticle count						
SUMMARY						
Groups	*Count*	*Sum*	*Average*	*Variance*		
ctrl	5	46220	9,244.00	25540493.5		
st	4	48120	12,030.00	51978627.3		
5	5	55143	11,028.60	51677891.3		
10	5	101885	20,377.00	191495332		
ANOVA						
Source of Variation	*SS*	*df*	*MS*	*F*	*P-value*	*F crit*
Between Groups	364829834.6	3	121609944.9	1.48209529	0.2595694	3.287382
Within Groups	1230790747	15	82052716.48			
Total	1595620582	18				

Table 11: One-way ANOVA for the effect of shear exposure time on microvesicle count, analyzed immediately after shear exposure

Anova: Single Factor						
t = 1 Microparticle count						
SUMMARY						
Groups	*Count*	*Sum*	*Average*	*Variance*		
ctrl	5	19999	3,999.80	2126305.7		
st	4	15660	3,915.00	1653638		
5	5	28625	5,725.00	5234325.5		
10	5	43402	8,680.40	21052947.8		
ANOVA						
Source of Variation	*SS*	*df*	*MS*	*F*	*P-value*	*F crit*
Between Groups	71595504.11	3	23865168.04	3.01797265	0.062807171	3.287382
Within Groups	118615230	15	7907682			
Total	190210734.1	18				

Table 12: One-way ANOVA for the effect of shear exposure time on microvesicle count, analyzed 2.5 hours after shear exposure

Anova: Single Factor						
t = 2 Microparticle count						
SUMMARY						
Groups	*Count*	*Sum*	*Average*	*Variance*		
ctrl	5	11914	2,382.80	222170.7		
st	4	11018	2,754.50	279967		
5	5	14625	2,925.00	377660		
10	5	21820	4,364.00	521068.5		
ANOVA						
Source of Variation	*SS*	*df*	*MS*	*F*	*P-value*	*F crit*
Between Groups	11178989.99	3	3726329.996	10.4996662	0.00056596	3.287382
Within Groups	5323497.8	15	354899.8533			
Total	16502487.79	18				

Table 13: One-way ANOVA for the effect of shear exposure time on microvesicle count, analyzed 5 hours after shear exposure

Anova: Single Factor						
Ctrl Microparticle Count						
SUMMARY						
Groups	*Count*	*Sum*	*Average*	*Variance*		
Time 0	5	46220	9,244.00	25540493.5		
Time 2.5	5	19999	3,999.80	2126305.7		
Time 5	5	11914	2,382.80	222170.7		
ANOVA						
Source of Variation	*SS*	*df*	*MS*	*F*	*P-value*	*F crit*
Between Groups	128653980.1	2	64326990.07	6.91961628	0.010033	3.885294
Within Groups	111555879.6	12	9296323.3			
Total	240209859.7	14				

Table 14: One-way ANOVA for the effect of incubation time on microvesicle count, analyzed in the negative control sample

Anova: Single Factor						
St Microparticle Count						
SUMMARY						
Groups	*Count*	*Sum*	*Average*	*Variance*		
Time 0	4	48120	12,030.00	51978627.3		
Time 2.5	4	15660	3,915.00	1653638		
Time 5	4	11018	2,754.50	279967		
ANOVA						
Source of Variation	*SS*	*df*	*MS*	*F*	*P-value*	*F crit*
Between Groups	204313180.7	2	102156590.3	5.68460547	0.025334	4.256495
Within Groups	161736697	9	17970744.11			
Total	366049877.7	11				

Table 15: One-way ANOVA for the effect of incubation time on microvesicle count, analyzed in the straight channel sample

Anova: Single Factor						
5 ms Microparticle Count						
SUMMARY						
Groups	*Count*	*Sum*	*Average*	*Variance*		
Time 0	5	55143	11,028.60	51677891.3		
Time 2.5	5	28625	5,725.00	5234325.5		
Time 5	5	14625	2,925.00	377660		
ANOVA						
Source of Variation	*SS*	*df*	*MS*	*F*	*P-value*	*F crit*
Between Groups	169394176.5	2	84697088.27	4.43518609	0.036133	3.885294
Within Groups	229159507.2	12	19096625.6			
Total	398553683.7	14				

Table 16: One-way ANOVA for the effect of incubation time on microvesicle count, analyzed in the 5 ms sample

Anova: Single Factor						
10 ms Microparticle Count						
SUMMARY						
Groups	*Count*	*Sum*	*Average*	*Variance*		
Time 0	5	101885	20,377.00	191495332		
Time 2.5	5	43402	8,680.40	21052947.8		
Time 5	5	21820	4,364.00	521068.5		
ANOVA						
Source of Variation	*SS*	*df*	*MS*	*F*	*P-value*	*F crit*
Between Groups	686429882.5	2	343214941.3	4.83243993	0.028877	3.885294
Within Groups	852277391.2	12	71023115.93			
Total	1538707274	14				

Table 17: One-way ANOVA for the effect of incubation time on microvesicle count, analyzed in the 10 ms sample

Shear Stress Calculations

The velocity distribution must be known before continuing with shear stress calculations.

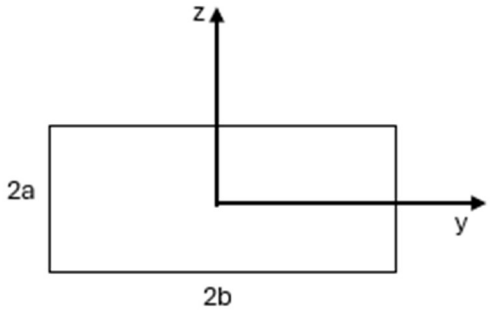

Figure 31: Coordinate system for velocity distribution in the microchannel [67]

Assuming that the RBC suspension is laminar and Newtonian, the Navier Stokes equation (A.3) can be used to describe the flow of the RBC suspension. Since flow is in the x-direction, the Navier Stokes equation for the x-component is chosen.

Beginning with the equation of continuity,

$$\frac{\partial \rho}{\partial t} + \frac{\partial}{\partial x}\rho v_x + \frac{\partial}{\partial y}\rho v_y + \frac{\partial}{\partial z}\rho v_z = 0 \qquad \text{(A.1)}$$

Since flow is only in the x-direction and the fluid is incompressible, the simplified continuity equation becomes:

$$\frac{\partial}{\partial x}\rho v_x = 0 \qquad \text{(A.2)}$$

$$\rho\left(\frac{\partial v_x}{\partial t} + v_x\frac{\partial v_x}{\partial x} + v_y\frac{\partial v_x}{\partial y} + v_z\frac{\partial v_x}{\partial z}\right) = -\frac{\partial p}{\partial x} + \mu\left[\frac{\partial^2 v_x}{\partial x^2} + \frac{\partial^2 v_x}{\partial y^2} + \frac{\partial^2 v_x}{\partial z^2}\right] + \rho g_x \qquad \text{(A.3)}$$

The flow is steady state, so the transient term is omitted. There is no velocity in the y or z direction, so any term concerning those quantities can be omitted. By the equation of continuity, the variation of v_x with respect to x can be omitted. Gravity is not in the x-direction, so that term can be omitted. We are left with (A.4).

$$\frac{\partial^2 v_x}{\partial y^2} + \frac{\partial^2 v_x}{\partial z^2} = \frac{-\Delta P}{\mu L} \tag{A.4}$$

Symmetry along the y-axis and the no-slip boundary conditions at z = ±a can be satisfied by expressing v_x in series form.

$$v_x = \sum_{n=1,2,3,5,\ldots}^{\infty} b_n \cos\left(\frac{n\pi z}{2a}\right) Y_n \tag{A.5}$$

The pressure term along -a < z < a can be expressed by the Fourier series.

$$-\frac{\Delta P}{\mu L} = -\sum_{n=1,3,5,\ldots}^{\infty} \frac{\Delta P}{\mu L} * \frac{4}{n\pi} (-1)^{\frac{n-1}{2}} \cos\left(\frac{n\pi z}{2a}\right) \tag{A.6}$$

$$Y_n'' - \frac{n^2\pi^2}{4a^2} Y_n = -\frac{\Delta P}{\mu L} * \frac{4}{n\pi b_n} (-1)^{\frac{n-1}{2}} \tag{A.7}$$

$$Y_n = A \sinh\left(\frac{n\pi y}{2a}\right) + B \cosh\left(\frac{n\pi y}{2a}\right) + \frac{16\Delta P * a^2}{\mu L n^3 \pi^3 b_n} (-1)^{\frac{n-1}{2}} \tag{A.8}$$

Since flow is symmetrical along the z-axis, the hyperbolic sine term can go to zero (A = 0).

Constant B is determined that for y = ±b, $Y_n = 0$.

$$Y_n = \frac{16\Delta P * a^2}{\mu L n^3 \pi^3 b_n} (-1)^{\frac{n-1}{2}} \left[1 - \frac{\cosh\left(\frac{n\pi y}{2a}\right)}{\cosh\left(\frac{n\pi b}{2a}\right)}\right] \tag{A.9}$$

$$v_x = \frac{16\Delta P * a^2}{\mu L^3} \sum_{n=1,3,5,\ldots}^{\infty} \frac{1}{n^3} (-1)^{\frac{n-1}{2}} \left[1 - \frac{\cosh\left(\frac{n\pi y}{2a}\right)}{\cosh\left(\frac{n\pi b}{2a}\right)}\right] \cos\left(\frac{n\pi z}{2a}\right) \tag{A.10}$$

The details of the analytical solution of the velocity profile comes from *Theory of Elasticity* by S.P. Timoshenko & J.N. Goodier [115].

The equation for the shear stress in the channel equals:

$$\tau_{yz} = \mu\left(\frac{\partial v_x}{\partial y} + \frac{\partial v_x}{\partial z}\right) \tag{A.11}$$

The flow rate of the fluid can be calculated by integrating the velocity profile over the cross-sectional area that is perpendicular to the direction of flow, the result of which is shown in (A.12) [116].

$$Q = \frac{4ba^3}{3\mu}\left(\frac{\Delta P}{L}\right)\left[1 - \frac{192a}{\pi^5 b}\sum_{n=1,3,5,\ldots}^{\infty}\frac{\tanh\left(\frac{n\pi b}{2a}\right)}{n^5}\right] \quad \text{(A.12)}$$

The shear rate can finally be calculated using the flow rate and channel dimensions (A.13), using f^* from approximations by Son et al [53], where the expression for f^* is given in Equation A.14.

$$\gamma_a = \frac{6Q}{WH^2}\left(1 + \frac{H}{W}\right) f^*\left(\frac{H}{W}\right) \quad \text{(A.13)}$$

$$f^*(x) = \left[\left(1 + \frac{1}{x}\right)^2\left(1 - \frac{192}{\pi^5 x}\sum_{i=1,3,5}^{\infty}\frac{\tanh\left(\frac{\pi}{2}ix\right)}{i^5}\right)\right]^{-1} \quad \text{(A.14)}$$

Appendix B

Flow Cytometry Raw Data

CFSE+ Events Gated on Size (Concentration: particles/μL)				
hr	**Loop Calcium**	**Time control calcium**	**Loop No calcium**	**Time Control NO calcium**
0	10089.47368	5068.421053	9739.473684	5386.842105
0	8984.210526	5857.894737	8715.789474	6528.947368
0	5823.684211	4373.684211	10386.84211	4523.684211
0	9702.631579	10181.57895	8702.631579	7555.263158
1	10018.42105	6839.473684	16976.31579	4902.631579
1	8228.947368	6221.052632	18839.47368	6221.052632
1	22952.63158	6373.684211	20405.26316	4894.736842
1	17507.89474	9781.578947	13692.10526	12455.26316
2	16615.78947	8218.421053	23034.21053	5978.947368
2	9784.210526	7368.421053	26489.47368	9105.263158
2	24723.68421	8765.789474	24050	5610.526316
2	26242.10526	6547.368421	15413.15789	16181.57895
3	19,805.26	7,292.11	18339.47368	7418.421053
3	13,057.89	6,250.00	28410.52632	9321.052632
3	36,568.42	-	27963.15789	9342.105263
3	35,510.53	9,613.16	30723.68421	14094.73684

6	14560.52632	7292.105263	20834.21053	6500
6	12228.94737	3092.105263	38389.47368	13550
6	24078.94737	8205.263158	22294.73684	8039.473684
6	44228.94737	12002.63158	21950	10581.57895

Table 18: CFSE-positive Events Gated on Size (Flow Cytometry Data)

Annexin V+ Events Gated on Size (Concentration: particles/µL)				
hr	**Loop Calcium**	**Time control calcium**	**Loop No calcium**	**Time Control NO calcium**
0	1518.421053	1055.263158	2136.842105	1207.894737
0	652.6315789	576.3157895	1028.947368	881.5789474
0	847.3684211	923.6842105	1344.736842	792.1052632
0	1547.368421	1342.105263	1236.842105	1402.631579
1	1176.315789	789.4736842	1718.421053	536.8421053
1	605.2631579	392.1052632	1413.157895	694.7368421
1	1428.947368	815.7894737	2065.789474	1105.263158
1	1613.157895	1505.263158	1792.105263	1286.842105
2	1505.263158	1028.947368	2494.736842	786.8421053
2	647.3684211	413.1578947	1915.789474	1213.157895
2	1147.368421	1186.842105	2213.157895	734.2105263
2	2163.157895	650	1484.210526	1921.052632
3	1,300.00	850.00	1763.157895	1073.684211
3	842.11	594.74	1552.631579	689.4736842
3	1,992.11	378.95	2447.368421	1086.842105
3	2,239.47	1,336.84	2047.368421	1357.894737
6	757.8947368	657.8947368	1700	807.8947368
6	560.5263158	378.9473684	1963.157895	1094.736842
6	1031.578947	618.4210526	1618.421053	1065.789474
6	1436.842105	1197.368421	1342.105263	1131.578947

Table 19: Annexin V-positive Events Gated on Size (Flow Cytometry Data)

CFSE+ and Annexin V+ Events Gated on Size (Concentration (particles/µL)				
	Loop Calcium	**Time control calcium**	**Loop No calcium**	**Time Control NO calcium**
0	1300	889.4736842	1997.368421	1081.578947
0	794.7368421	702.6315789	971.0526316	771.0526316
0	771.0526316	810.5263158	1231.578947	694.7368421
0	1455.263158	1234.210526	1144.736842	1321.052632
1	1052.631579	710.5263158	1681.578947	465.7894737
1	731.5789474	550	1386.842105	636.8421053
1	1344.736842	728.9473684	2002.631579	981.5789474

1	1557.894737	1363.157895	1673.684211	1197.368421
2	1428.947368	892.1052632	2386.842105	715.7894737
2	836.8421053	560.5263158	1836.842105	1134.210526
2	1094.736842	981.5789474	2113.157895	692.1052632
2	2110.526316	607.8947368	1413.157895	1815.789474
3	1,250.00	678.95	1681.578947	1023.684211
3	1,013.16	665.79	1523.684211	655.2631579
3	1,910.53	431.58	2373.684211	994.7368421
3	2,197.37	1,278.95	1947.368421	1284.210526
6	718.4210526	589.4736842	1642.105263	736.8421053
6	776.3157895	431.5789474	1892.105263	1031.578947
6	976.3157895	534.2105263	1565.789474	1002.631579
6	1400	1084.210526	1263.157895	1039.473684

Table 20: Events positive for both CFSE and Annexin V, gated on size (Flow Cytometry Data)

Statistics

Anova: Single Factor
CALCIUM TIME
SUMMARY

Groups	*Count*	*Sum*	*Average*	*Variance*
F02 MP T0	4	25481.57895	6370.394737	6823256.579
F06 MP T1	4	29215.78947	7303.947368	2797481.533
F07 MP T2	4	30900	7725	946890.5817
F09 MP T3	3	23155.26316	7718.421053	2964016.62
F10 MP T6	4	30592.10526	7648.026316	13385398.78

ANOVA

Source of Variation	*SS*	*df*	*MS*	*F*	*P-value*	*F crit*
Between Groups	5167065.717	4	1291766.429	0.232490045	0.915473	3.11225
Within Groups	77787115.65	14	5556222.546			
Total	82954181.37	18				

Anova: Single Factor
NO CALCIUM TIME
SUMMARY

Groups	*Count*	*Sum*	*Average*	*Variance*
F02 MP T0	4	23994.73684	5998.684211	1751364.266
F06 MP T1	4	28473.68421	7118.421053	13047216.07
F07 MP T2	4	36876.31579	9219.078947	24003155.01
F09 MP T3	4	40176.31579	10044.07895	8105814.289
F10 MP T6	4	38671.05263	9667.763158	9530957.41

ANOVA

Source of Variation	*SS*	*df*	*MS*	*F*	*P-value*	*F crit*
Between Groups	49557640.58	4	12389410.15	1.097602576	0.393414	3.055568
Within Groups	169315521.1	15	11287701.41			
Total	218873161.7	19				

Anova: Single Factor
CALCIUM CENTRIMAG
SUMMARY

Groups	*Count*	*Sum*	*Average*	*Variance*
F05 MP CM0	4	34600	8650	3759958.449
F04 MP CM1	4	58707.89474	14676.97368	46593261.2
F08 MP CM2	4	77365.78947	19341.44737	58452513.27
F11 MP CM3	4	104942.1053	26235.52632	135930865.7
F12 MP CM6	4	95097.36842	23774.34211	212224734

ANOVA

Source of Variation	*SS*	*df*	*MS*	*F*	*P-value*	*F crit*
Between Groups	799987033.9	4	199996758.5	2.188333501	0.119779	3.055568
Within Groups	1370883998	15	91392266.51			
Total	2170871032	19				

Anova: Single Factor
NO CALCIUM CENTRIMAG
SUMMARY

Groups	*Count*	*Sum*	*Average*	*Variance*
F05 MP CM0	4	37544.73684	9386.184211	680934.3259
F04 MP CM1	4	69913.15789	17478.28947	8335721.953
F08 MP CM2	4	88986.84211	22246.71053	22856829.99
F11 MP CM3	4	105436.8421	26359.21053	30048451.06
F12 MP CM6	4	103468.4211	25867.10526	70081756.69

ANOVA

Source of Variation	*SS*	*df*	*MS*	*F*	*P-value*	*F crit*
Between Groups	794258076.9	4	198564519.2	7.521172824	0.001563	3.055568
Within Groups	396011082.1	15	26400738.8			
Total	1190269159	19				

Table 21: One-way ANOVA results for 0 through 6 hours in CFSE-positive microvesicles

Anova: Single Factor
calcium centrimag 3 hours
SUMMARY

Groups	*Count*	*Sum*	*Average*	*Variance*
F05 MP CM0	4	34600	8650	3759958.449
F04 MP CM1	4	58707.89474	14676.97368	46593261.2
F08 MP CM2	4	77365.78947	19341.44737	58452513.27
F11 MP CM3	4	104942.1053	26235.52632	135930865.7

ANOVA

Source of Variation	*SS*	*df*	*MS*	*F*	*P-value*	*F crit*
Between Groups	662767972.6	3	220922657.5	3.610782512	0.045742	3.490295
Within Groups	734209795.7	12	61184149.64			
Total	1396977768	15				

Anova: Single Factor
no calcium centrimag 3 hours
SUMMARY

Groups	*Count*	*Sum*	*Average*	*Variance*
F05 MP CM0	4	37544.74	9386.184	680934.3
F04 MP CM1	4	69913.16	17478.29	8335722
F08 MP CM2	4	88986.84	22246.71	22856830
F11 MP CM3	4	105436.8	26359.21	30048451

ANOVA

Source of Variation	*SS*	*df*	*MS*	*F*	*P-value*	*F crit*
Between Groups	637480181.4	3	2.12E+08	13.72653	0.000348	3.490295
Within Groups	185765812	12	15480484			
Total	823245993.3	15				

Table 22: One-way ANOVA results for 0 through 3 hours in CFSE-positive microvesicles

Descriptive Statistics (CFSE+)		
Sample	Mean	Std. Deviation
calcium_time0_stagnant	7035.9649	2752.63200
calcium_time1_stagnant	7614.0351	1902.44473
calcium_time2_stagnant	7378.0702	835.56810
calcium_time3_stagnant	7718.4211	1721.63196
calcium_time6_stagnant	7462.2807	4457.70003
calcium_time0_loop	9592.1053	560.85979
calcium_time1_loop	11918.4211	4922.62289
calcium_time2_loop	17547.3684	8268.40095
calcium_time3_loop	22791.2281	11520.29323
calcium_time6_loop	23672.8070	17840.27031
nocalc_time0_stagnant	6490.3509	1084.72565
nocalc_time1_stagnant	7859.6491	4034.14301
nocalc_time2_stagnant	10421.9298	5227.20108
nocalc_time3_stagnant	10278.0702	3439.50724
nocalc_time6_stagnant	10210.5263	3539.61651
nocalc_time0_loop	9052.6316	594.85909
nocalc_time1_loop	16502.6316	2606.17209
nocalc_time2_loop	21645.6140	5667.21652
nocalc_time3_loop	25824.5614	6584.64718
nocalc_time6_loop	27057.8947	9829.28062

Table 23: Descriptive statistics for CFSE-positive microvesicles

Mauchly's test of sphericity (CFSE+)	
Within Subjects Effect	Mauchly's W

Media	1.000
Condition	1.000
Time	.000
Media * Condition	1.000
Media * Time	.000
Condition * Time	.000
Media * Condition * Time	.000

Table 24: Mauchly's test of sphericity results for CFSE-positive microvesicles

Repeated-Measures ANOVA (CFSE+)			
Source		Sig.	Partial Eta Squared
Media	Sphericity Assumed	.568	.187
	Greenhouse-Geisser	.568	.187
Condition	Sphericity Assumed	.003	.993
	Greenhouse-Geisser	.003	.993
Time	Sphericity Assumed	.003	.838
	Greenhouse-Geisser	.064	.838
Media * Condition	Sphericity Assumed	.858	.020
	Greenhouse-Geisser	.858	.020
Media * Time	Sphericity Assumed	.902	.111
	Greenhouse-Geisser	.689	.111
Condition * Time	Sphericity Assumed	.012	.768
	Greenhouse-Geisser	.110	.768

Media * Condition * Time	Sphericity Assumed	.973	.055
	Greenhouse-Geisser	.796	.055

Table 25: Repeated-measures ANOVA results with Greenhouse-Geisser correction for non-spherical groups (CFSE-positive microvesicles)

Paired Samples Correlations (CFSE+)			
Compared Samples		Correlation	Two-Sided p
Pair 1	calcium_time0_stagnant & calcium_time0_loop	.501	.499
Pair 2	calcium_time1_stagnant & calcium_time1_loop	.247	.753
Pair 3	calcium_time2_stagnant & calcium_time2_loop	-.021	.979
Pair 4	calcium_time3_stagnant & calcium_time3_loop	1.000	.007
Pair 5	calcium_time6_stagnant & calcium_time6_loop	.908	.092
Pair 6	nocalc_time0_stagnant & nocalc_time0_loop	-.950	.050
Pair 7	nocalc_time1_stagnant & nocalc_time1_loop	-.857	.143
Pair 8	nocalc_time2_stagnant & nocalc_time2_loop	-.813	.187
Pair 9	nocalc_time3_stagnant & nocalc_time3_loop	.772	.228
Pair 10	nocalc_time6_stagnant & nocalc_time6_loop	.861	.139

Table 26: Pearson correlation coefficients with significance values (CFSE-positive microvesicles)

Paired Sample T-Test (CFSE+)		
Compared samples		Two-Sided p-value
Pair 1	calcium_time0_stagnant - calcium_time0_loop	.147
Pair 2	calcium_time1_stagnant - calcium_time1_loop	.112
Pair 3	calcium_time2_stagnant - calcium_time2_loop	.057
Pair 4	calcium_time3_stagnant - calcium_time3_loop	.117
Pair 5	calcium_time6_stagnant - calcium_time6_loop	.066
Pair 6	nocalc_time0_stagnant - nocalc_time0_loop	.050
Pair 7	nocalc_time1_stagnant - nocalc_time1_loop	.046
Pair 8	nocalc_time2_stagnant - nocalc_time2_loop	.066
Pair 9	nocalc_time3_stagnant - nocalc_time3_loop	.003
Pair 10	nocalc_time6_stagnant - nocalc_time6_loop	.012

Table 27: Paired sample t-test (CFSE-positive microvesicles)

Anova: Single Factor
calcium time control
SUMMARY

Groups	Count	Sum	Average	Variance
F02 MP T0	4	3897.368	974.3421	100929.71
F06 MP T1	4	3502.632	875.6579	213745.96
F07 MP T2	4	3278.947	819.7368	124217.45
F09 MP T3	4	3998.246	999.5614	115714.84
F10 MP T6	4	2852.632	713.1579	119395.2

ANOVA

Source of Variation	SS	df	MS	F	P-value	F crit
Between Groups	218482.3792	4	54620.59	0.4051954	0.802024	3.055568
Within Groups	2022009.464	15	134800.6			
Total	2240491.844	19				

Anova: Single Factor
no calcium time control
SUMMARY

Groups	Count	Sum	Average	Variance
F02 MP T0	4	4284.211	1071.0526	80794.09
F06 MP T1	4	3623.684	905.92105	121885.39
F07 MP T2	4	4655.263	1163.8158	300837.37
F09 MP T3	4	4207.895	1051.9737	75560.365
F10 MP T6	4	4100	1025	21673.592

ANOVA

Source of Variation	SS	df	MS	F	P-value	F crit
Between Groups	138308.1717	4	34577.043	0.2877819	0.881337	3.055568
Within Groups	1802252.424	15	120150.16			
Total	1940560.596	19				

Anova: Single Factor
calcium centrimag
SUMMARY

Groups	Count	Sum	Average	Variance
F05 MP CM0	4	4565.789	1141.447	210768.12
F04 MP CM1	4	4823.684	1205.921	192416.32
F08 MP CM2	4	5463.158	1365.789	406361.96
F11 MP CM3	4	6373.684	1593.421	408968.14
F12 MP CM6	4	3786.842	946.7105	144073.75

ANOVA

Source of Variation	SS	df	MS	F	P-value	F crit
Between Groups	948216.759	4	237054.2	0.8698673	0.504568	3.055568
Within Groups	4087764.889	15	272517.7			
Total	5035981.648	19				

Anova: Single Factor
no calcium centrimag
SUMMARY

Groups	Count	Sum	Average	Variance
F05 MP CM0	4	5747.368	1436.8421	234953.83
F04 MP CM1	4	6989.474	1747.3684	71975.993
F08 MP CM2	4	8107.895	2026.9737	186806.9
F11 MP CM3	4	7810.526	1952.6316	149879.96
F12 MP CM6	4	6623.684	1655.9211	65408.01

ANOVA

Source of Variation	SS	df	MS	F	P-value	F crit
Between Groups	894907.8947	4	223726.97	1.5777093	0.231297	3.055568
Within Groups	2127074.1	15	141804.94			
Total	3021981.994	19				

Table 28: One-way ANOVA for 0 to 6 hours for AnnexinV-positive microvesicles

Descriptive Statistics (AnnexinV+)		
Sample	Mean	Std. Deviation
calcium_time0_stagnant	991.2281	386.88984
calcium_time0_loop	1239.4737	508.42623
calcium_time1_stagnant	895.6140	564.11830
calcium_time1_loop	1131.5789	505.43445
calcium_time2_stagnant	697.3684	310.61551
calcium_time2_loop	1438.5965	760.09063
calcium_time3_stagnant	927.1930	377.02669
calcium_time3_loop	1460.5263	712.38062
calcium_time6_stagnant	744.7368	416.06420
calcium_time6_loop	918.4211	459.68344
nocalc_time0_stagnant	839.4737	395.39419
nocalc_time0_loop	1641.2281	200.92124
nocalc_time1_stagnant	1307.0175	572.90104

nocalc_time1_loop	1964.9123	507.05093
nocalc_time2_stagnant	1040.3509	335.45493
nocalc_time2_loop	1787.7193	248.28126
nocalc_time3_stagnant	1011.4035	177.20384
nocalc_time3_loop	1668.4211	311.72827
nocalc_time6_stagnant	1467.5439	588.87619
nocalc_time6_loop	5649.1228	5239.57435

Table 29: Descriptive statistics for AnnexinV-positive microvesicles

Mauchly's test of sphericity (AnnexinV+)	
Within Subjects Effect	Mauchly's W
Condition	1.000
Media	1.000
Time	.000
Condition * Media	1.000
Condition * Time	.000
Media * Time	.000
Condition * Media * Time	.000

Table 30: Mauchly's test of sphericity results for AnnexinV-positive microvesicles

Repeated-Measures ANOVA (AnnexinV+)			
Source		Sig.	Partial Eta Squared
Condition	Sphericity Assumed	.262	.544
	Greenhouse-Geisser	.262	.544
Media	Sphericity Assumed	.232	.590
	Greenhouse-Geisser	.232	.590

Time	Sphericity Assumed	.494	.317
	Greenhouse-Geisser	.441	.317
Condition * Media	Sphericity Assumed	.408	.350
	Greenhouse-Geisser	.408	.350
Condition * Time	Sphericity Assumed	.114	.568
	Greenhouse-Geisser	.236	.568
Media * Time	Sphericity Assumed	.088	.599
	Greenhouse-Geisser	.222	.599
Condition * Media * Time	Sphericity Assumed	.222	.474
	Greenhouse-Geisser	.312	.474

Table 31: Repeated-measures ANOVA results with Greenhouse-Geisser correction for non-spherical groups (AnnexinV-positive microvesicles)

Paired Samples Correlations (AnnexinV+)			
Compared Samples		Correlation	Two-Sided p
Pair 1	calcium_time0_stagnant & calcium_time0_loop	.890	.110
Pair 2	calcium_time1_stagnant & calcium_time1_loop	.881	.119
Pair 3	calcium_time2_stagnant & calcium_time2_loop	.157	.843
Pair 4	calcium_time3_stagnant & calcium_time3_loop	1.000	.012
Pair 5	calcium_time6_stagnant & calcium_time6_loop	.937	.063
Pair 6	nocalc_time0_stagnant & nocalc_time0_loop	.576	.424
Pair 7	nocalc_time1_stagnant & nocalc_time1_loop	-.946	.054

Pair 8	nocalc_time2_stagnant & nocalc_time2_loop	.586	.414
Pair 9	nocalc_time3_stagnant & nocalc_time3_loop	-.205	.795
Pair 10	nocalc_time6_stagnant & nocalc_time6_loop	.033	.967

Table 32: Pearson correlation coefficients with significance values (AnnexinV-positive microvesicles)

Paired Sample T-Test (AnnexinV+)		
Compared Samples		Two-Sided p
Pair 1	calcium_time0_stagnant - calcium_time0_loop	.240
Pair 2	calcium_time1_stagnant - calcium_time1_loop	.058
Pair 3	calcium_time2_stagnant - calcium_time2_loop	.206
Pair 4	calcium_time3_stagnant - calcium_time3_loop	.110
Pair 5	calcium_time6_stagnant - calcium_time6_loop	.039
Pair 6	nocalc_time0_stagnant - nocalc_time0_loop	.011
Pair 7	nocalc_time1_stagnant - nocalc_time1_loop	.172
Pair 8	nocalc_time2_stagnant - nocalc_time2_loop	.011
Pair 9	nocalc_time3_stagnant - nocalc_time3_loop	.029
Pair 10	nocalc_time6_stagnant - nocalc_time6_loop	.303

Table 33: Paired sample t-test (AnnexinV-positive microvesicles)

Anova: Single Factor
calcium time control 3 hours
SUMMARY

Groups	Count	Sum	Average	Variance
F02 MP T0	4	3636.842	909.2105	52809.33
F06 MP T1	4	3352.632	838.1579	128958.9
F07 MP T2	4	3042.105	760.5263	43157.89
F09 MP T3	4	3787.018	946.7544	102640.2

ANOVA

Source of Variation	SS	df	MS	F	P-value	F crit
Between Groups	81065.77	3	27021.92	0.329972	0.803852	3.490295
Within Groups	982698.9	12	81891.57			
Total	1063765	15				

Anova: Single Factor
no calcium time control 3 hours
SUMMARY

Groups	Count	Sum	Average	Variance
F02 MP T0	4	3868.421	967.1053	83668.05
F06 MP T1	4	3281.579	820.3947	109175.3
F07 MP T2	4	4357.895	1089.474	275692.5
F09 MP T3	4	3957.895	989.4737	66588.18

ANOVA

Source of Variation	SS	df	MS	F	P-value	F crit
Between Groups	147989.5256	3	49329.84	0.368736	0.776966	3.490295
Within Groups	1605372.23	12	133781			
Total	1753361.756	15				

Anova: Single Factor
calcium loop 3 hours
SUMMARY

Groups	Count	Sum	Average	Variance
F05 MP CM0	4	4321.053	1080.263	122015.2
F04 MP CM1	4	4686.842	1171.711	128990.7
F08 MP CM2	4	5471.053	1367.763	303953.7
F11 MP CM3	4	6371.053	1592.763	306649.9

ANOVA

Source of Variation	SS	df	MS	F	P-value	F crit
Between Groups	620022.1	3	206674	0.959479	0.443281	3.490295
Within Groups	2584829	12	215402.4			
Total	3204851	15				

Anova: Single Factor
no calcium loop 3 hours
SUMMARY

Groups	Count	Sum	Average	Variance
F05 MP CM0	4	5344.737	1336.184	206026.7
F04 MP CM1	4	6744.737	1686.184	63307.36
F08 MP CM2	4	7750	1937.5	172610.2
F11 MP CM3	4	7526.316	1881.579	138194.8

ANOVA

Source of Variation	SS	df	MS	F	P-value	F crit
Between Groups	886001.991	3	295334	2.036298	0.162533	3.490295
Within Groups	1740417.244	12	145034.8			
Total	2626419.235	15				

Table 34: One-way ANOVA for 0 through 6 hours in CFSE & AnnexinV-positive microvesicles

Descriptive Statistics (CFSE & AnnexinV+)		
	Mean	Std. Deviation
calcium_time0_stagnant	942.1053	269.66944
calcium_time1_stagnant	874.5614	430.68210
calcium_time2_stagnant	686.8421	179.33394
calcium_time3_stagnant	874.5614	350.27031
calcium_time6_stagnant	701.7544	340.49554
calcium_time0_loop	1183.3333	345.37239
calcium_time1_loop	1114.0351	416.56601
calcium_time2_loop	1458.7719	637.36567
calcium_time3_loop	1486.8421	626.62531
calcium_time6_loop	964.9123	377.90732
nocalc_time0_stagnant	1057.8947	275.76386
nocalc_time1_stagnant	766.6667	382.67839

nocalc_time2_stagnant	1221.9298	555.22158
nocalc_time3_stagnant	987.7193	316.01235
nocalc_time6_stagnant	935.9649	172.49058
nocalc_time0_loop	1371.0526	549.31335
nocalc_time1_loop	1580.7018	167.93378
nocalc_time2_loop	1878.9474	488.20578
nocalc_time3_loop	1717.5439	214.11955
nocalc_time6_loop	1599.1228	316.66910

Table 35: Descriptive Statistics for CFSE & AnnexinV-positive microvesicles

Mauchly's test of sphericity (CFSE & AnnexinV+)	
Within Subjects Effect	Mauchly's W
Media	1.000
Condition	1.000
Time	.000
Media * Condition	1.000
Media * Time	.000
Condition * Time	.000
Media * Condition * Time	.000

Table 36: Mauchly's test of sphericity results for CFSE & AnnexinV-positive microvesicles

Repeated-Measures ANOVA (CFSE & AnnexinV+)			
Source		Sig.	Partial Eta Squared
Media	Sphericity Assumed	.206	.631
	Greenhouse-Geisser	.206	.631

Condition	Sphericity Assumed	.037	.928
	Greenhouse-Geisser	.037	.928
Time	Sphericity Assumed	.267	.443
	Greenhouse-Geisser	.310	.443
Media * Condition	Sphericity Assumed	.609	.153
	Greenhouse-Geisser	.609	.153
Media * Time	Sphericity Assumed	.173	.511
	Greenhouse-Geisser	.249	.511
	Lower-bound		
Condition * Time	Sphericity Assumed	.147	.535
	Greenhouse-Geisser	.236	.535
Media * Condition * Time	Sphericity Assumed	.628	.252
	Greenhouse-Geisser	.510	.252

Table 37: Repeated-measures ANOVA with Greenhouse-Geisser correction for non-spherical groups (CFSE & AnnexinV-positive microvesicles)

Paired Samples Correlations (CFSE & AnnexinV+)			
Compared Samples		Correlation	Two-Sided p
Pair 1	calcium_time0_stagnant & calcium_time0_loop	.860	.140
Pair 2	calcium_time1_stagnant & calcium_time1_loop	.842	.158
Pair 3	calcium_time2_stagnant & calcium_time2_loop	-.173	.827

Pair 4	calcium_time3_stagnant & calcium_time3_loop	.985	.109
Pair 5	calcium_time6_stagnant & calcium_time6_loop	.906	.094
Pair 6	nocalc_time0_stagnant & nocalc_time0_loop	.274	.726
Pair 7	nocalc_time1_stagnant & nocalc_time1_loop	.412	.588
Pair 8	nocalc_time2_stagnant & nocalc_time2_loop	-.952	.048
Pair 9	nocalc_time3_stagnant & nocalc_time3_loop	.468	.532
Pair 10	nocalc_time6_stagnant & nocalc_time6_loop	-.151	.849

Table 38: Pearson correlation coefficients with significance values (CFSE & AnnexinV-positive microvesicles)

Paired Sample T-Test (CFSE & AnnexinV+)		
Compared Samples		Two-Sided p
Pair 1	calcium_time0_stagnant - calcium_time0_loop	.173
Pair 2	calcium_time1_stagnant - calcium_time1_loop	.046
Pair 3	calcium_time2_stagnant - calcium_time2_loop	.146
Pair 4	calcium_time3_stagnant - calcium_time3_loop	.066
Pair 5	calcium_time6_stagnant - calcium_time6_loop	.018
Pair 6	nocalc_time0_stagnant - nocalc_time0_loop	.212

Pair 7	nocalc_time1_stagnant - nocalc_time1_loop	.013
Pair 8	nocalc_time2_stagnant - nocalc_time2_loop	.165
Pair 9	nocalc_time3_stagnant - nocalc_time3_loop	.013
Pair 10	nocalc_time6_stagnant - nocalc_time6_loop	.027

Table 39: Paired sample t-test (CFSE & AnnexinV-positive microvesicles)

Sample		Sig.
LoopCalcium	Between Groups	.033
TimeCtrlCalc	Between Groups	.722
LoopNOCalc	Between Groups	<.001
TimeCtrlNoCalc	Between Groups	.794

Table 40: One-way ANOVA for PFH from 0 to 6 hours

Descriptive Statistics (PFH)		
Sample	Mean (mg/dL)	Std. Deviation
pfh_calc_time0_stagnant	8.0395	3.34443
pfh_calcium_time1_stagnant	8.2207	1.82861
pfh_calcium_time2_stagnant	8.6596	2.04554
pfh_calcium_time3_stagnant	8.3900	2.52598
pfh_calcium_time6_stagnant	10.0529	2.85760

pfh_calcium_time0_loop	7.5658	1.74020
pfh_calcium_time1_loop	18.7821	11.01301
pfh_calcium_time2_loop	29.2879	19.90100
pfh_calcium_time3_loop	38.2350	26.73381
pfh_calcium_time6_loop	56.8550	40.14614
pfh_nocalc_time0_stagnant	9.4816	3.50865
pfh_nocalc_time1_stagnant	8.8059	2.48634
pfh_nocalc_time2_stagnant	9.9136	2.71385
pfh_nocalc_time3_stagnant	10.7008	2.22945
pfh_nocalc_time6_stagnant	11.6901	2.38337
pfh_nocalc_time0_loop	12.4285	2.12799
pfh_nocalc_time1_loop	21.7012	3.22543
pfh_nocalc_time2_loop	28.5703	6.41992
pfh_nocalc_time3_loop	34.8751	9.74660
pfh_nocalc_time6_loop	51.7066	19.77678

Table 41: Descriptive statistics for PFH in time control and CentriMag for 0 to 6 hours

Mauchly's test of sphericity (PFH)	
Within Subjects Effect	Mauchly's W
Media	1.000
Condition	1.000
Time	.000
Media * Condition	1.000
Media * Time	.000
Condition * Time	.000
Media * Condition * Time	.000

Table 42: Mauchly's test of sphericity results for PFH

Repeated-Measures ANOVA (PFH)			
Source		Sig.	Partial Eta Squared
Media	Sphericity Assumed	.927	.003
	Greenhouse-Geisser	.927	.003
Condition	Sphericity Assumed	.022	.866
	Greenhouse-Geisser	.022	.866
Time	Sphericity Assumed	<.001	.896
	Greenhouse-Geisser	.012	.896
Media * Condition	Sphericity Assumed	.891	.007
	Greenhouse-Geisser	.891	.007
Media * Time	Sphericity Assumed	.968	.042
	Greenhouse-Geisser	.757	.042
Condition * Time	Sphericity Assumed	<.001	.893
	Greenhouse-Geisser	.014	.893
Media * Condition * Time	Sphericity Assumed	.918	.070
	Greenhouse-Geisser	.675	.070

Table 43: Repeated-measures ANOVA results with Greenhouse-Geisser correction for non-spherical groups (PFH)

Post-hoc Pairwise Comparison for Time (PFH)

(I) Time	(J) Time	Mean Difference (I-J)	Std. Error	Sig.[a]	95% Confidence Interval for Difference[a]	
					Lower Bound	Upper Bound
1	2	-4.999	1.687	.594	-17.575	7.578
	3	-9.729	2.575	.325	-28.921	9.463
	4	-13.671	3.229	.241	-37.739	10.396
	5	-23.197	4.512	.143	-56.824	10.429
2	1	4.999	1.687	.594	-7.578	17.575
	3	-4.730	.964	.162	-11.913	2.452
	4	-8.673	1.684	.142	-21.220	3.875
	5	-18.199	3.034	.093	-40.815	4.418
3	1	9.729	2.575	.325	-9.463	28.921
	2	4.730	.964	.162	-2.452	11.913
	4	-3.942	.727	.123	-9.364	1.480
	5	-13.468	2.106	.077	-29.166	2.230
4	1	13.671	3.229	.241	-10.396	37.739
	2	8.673	1.684	.142	-3.875	21.220
	3	3.942	.727	.123	-1.480	9.364
	5	-9.526	1.429	.069	-20.177	1.125
5	1	23.197	4.512	.143	-10.429	56.824
	2	18.199	3.034	.093	-4.418	40.815
	3	13.468	2.106	.077	-2.230	29.166
	4	9.526	1.429	.069	-1.125	20.177
Based on estimated marginal means						
a. Adjustment for multiple comparisons: Bonferroni.						

Table 44: Post-hoc pairwise comparison for the time variable (PFH)

Post-hoc Pairwise Comparisons for Condition/Time Interaction							
Time	(I) Condition	(J) Condition	Mean Difference (I-J)	Std. Error	Sig.[b]	95% Confidence Interval for Difference[b]	
						Lower Bound	Upper Bound
1	1	2	-1.237	.955	.286	-4.274	1.801
	2	1	1.237	.955	.286	-1.801	4.274
2	1	2	-11.728*	2.978	.029	-21.206	-2.250
	2	1	11.728*	2.978	.029	2.250	21.206
3	1	2	-19.643*	4.969	.029	-35.456	-3.829
	2	1	19.643*	4.969	.029	3.829	35.456
4	1	2	-27.010*	5.986	.020	-46.060	-7.959
	2	1	27.010*	5.986	.020	7.959	46.060
5	1	2	-43.409*	8.964	.017	-71.936	-14.883
	2	1	43.409*	8.964	.017	14.883	71.936
Based on estimated marginal means							
*. The mean difference is significant at the .05 level.							
b. Adjustment for multiple comparisons: Bonferroni.							

Table 45: Post-hoc pairwise comparison for the Condition/Time interaction (PFH)

Paired Samples Correlations (PFH)			
Compared Samples		Correlation	Two-Sided p
Pair 1	pfh_calc_time0_stagnant & pfh_calcium_time0_loop	.319	.681
Pair 2	pfh_calcium_time1_stagnant & pfh_calcium_time1_loop	.306	.694
Pair 3	pfh_calcium_time2_stagnant & pfh_calcium_time2_loop	.366	.634
Pair 4	pfh_calcium_time3_stagnant & pfh_calcium_time3_loop	.683	.317
Pair 5	pfh_calcium_time6_stagnant & pfh_calcium_time6_loop	.719	.281
Pair 6	pfh_nocalc_time0_stagnant & pfh_nocalc_time0_loop	1.000	<.001
Pair 7	pfh_nocalc_time1_stagnant & pfh_nocalc_time1_loop	-.825	.175
Pair 8	pfh_nocalc_time2_stagnant & pfh_nocalc_time2_loop	-.982	.018
Pair 9	pfh_nocalc_time3_stagnant & pfh_nocalc_time3_loop	-.996	.004
Pair 10	pfh_nocalc_time6_stagnant & pfh_nocalc_time6_loop	-.878	.122

Table 46: Pearson correlation coefficients with significance values (PFH)

Paired Sample T-Test (PFH)		
Compared Samples		Two-Sided p
Pair 1	pfh_calc_time0_stagnant - pfh_calcium_time0_loop	.789
Pair 2	pfh_calcium_time1_stagnant - pfh_calcium_time1_loop	.140
Pair 3	pfh_calcium_time2_stagnant - pfh_calcium_time2_loop	.121
Pair 4	pfh_calcium_time3_stagnant - pfh_calcium_time3_loop	.098
Pair 5	pfh_calcium_time6_stagnant - pfh_calcium_time6_loop	.091
Pair 6	pfh_nocalc_time0_stagnant - pfh_nocalc_time0_loop	.024
Pair 7	pfh_nocalc_time1_stagnant - pfh_nocalc_time1_loop	.018
Pair 8	pfh_nocalc_time2_stagnant - pfh_nocalc_time2_loop	.026
Pair 9	pfh_nocalc_time3_stagnant - pfh_nocalc_time3_loop	.027
Pair 10	pfh_nocalc_time6_stagnant - pfh_nocalc_time6_loop	.035

Table 47: Paired sample t-test (PFH)

Anova: Single Factor
Calcium Loop

SUMMARY

Groups	Count	Sum	Average	Variance
Loop 0 Ca	4	277.5101	69.37753	43.78424
Loop 1 Ca	4	283.431	70.85775	30.08147
Loop 3 Ca	4	276.5852	69.14631	63.39576
Loop 6 Ca	4	275.1784	68.7946	36.62332

ANOVA

Source of Variation	SS	df	MS	F	P-value	F crit
Between Groups	9.893635	3	3.297878	0.075864	0.971832	3.490295
Within Groups	521.6544	12	43.4712			
Total	531.548	15				

Anova: Single Factor
No Calcium Loop

SUMMARY

Groups	Count	Sum	Average	Variance
Loop 0 No	4	299.5676	74.89191	124.3426
Loop 1 No	4	293.7762	73.44406	81.35549
Loop 3 No	4	298.4995	74.62488	74.64293
Loop 6 No	4	298.4995	74.62488	74.64293

ANOVA

Source of Varia	SS	df	MS	F	P-value	F crit
Between G	5.027558	3	1.675853	0.018884	0.996275	3.490295
Within Gro	1064.952	12	88.74599			
Total	1069.979	15				

Anova: Single Factor
Calcium Time Control

SUMMARY

Groups	Count	Sum	Average	Variance
Time 0 Ca	4	273.5887	68.39718	53.03855
Time 1 Ca	4	280.6982	70.17456	43.42226
Time 3 Ca	4	279.4476	69.86191	53.29217
Time 6 Ca	4	273.6883	68.42208	38.93539

ANOVA

Source of Variation	SS	df	MS	F	P-value	F crit
Between Groups	10.54719	3	3.515731	0.07453	0.972532	3.490295
Within Groups	566.0651	12	47.17209			
Total	576.6123	15				

Anova: Single Factor

SUMMARY

Groups	Count	Sum	Average	Variance
Time 0 No	4	304.4803	76.12008	139.4339
Time 1 No	4	289.2902	72.32254	67.0303
Time 3 No	4	301.5191	75.37978	127.9904
Time 6 No	4	291.6801	72.92003	113.5922

ANOVA

Source of Varia	SS	df	MS	F	P-value	F crit
Between G	40.96369	3	13.65456	0.121903	0.945414	3.490295
Within Gro	1344.14	12	112.0117			
Total	1385.104	15				

Table 48: One-way ANOVA for mean cell volume from 0 to 6 hours in the CentriMag (Calc/NoCalc) and time control (Calc/NoCalc)

Appendix C

Critical diameter calculation for bovine and human red blood cell

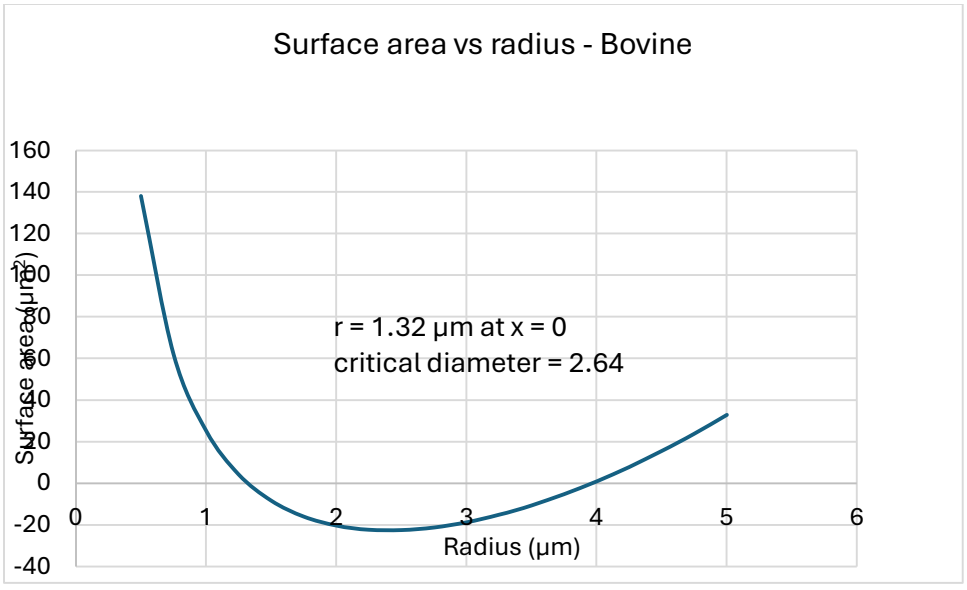

Figure 32: Surface area as a function of radius, plotted to determine critical diameter of a bovine red blood cell

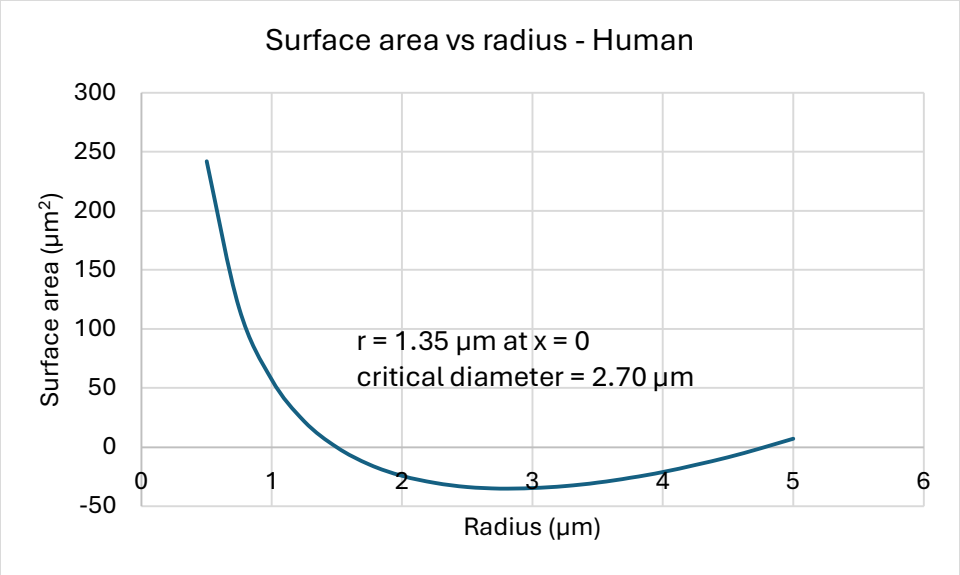

Figure 33: Surface area as a function of radius, plotted to determine critical diameter of a human red blood cell

LabView VI Code for Pressure Recording

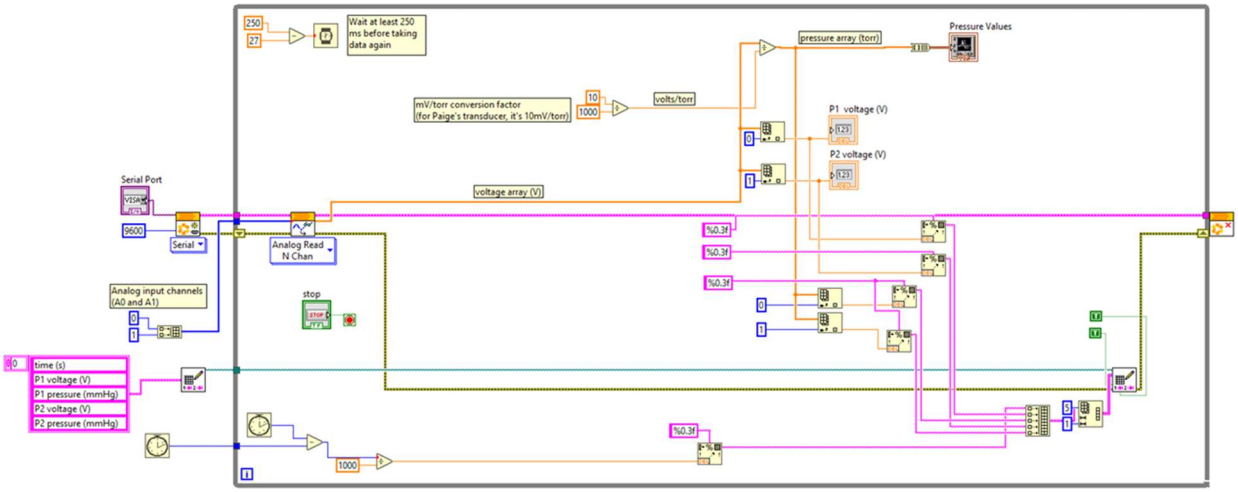

Figure 34: LabView VI Code for Pressure Recording

Raw Data: Pressure Drop vs. Time Plots

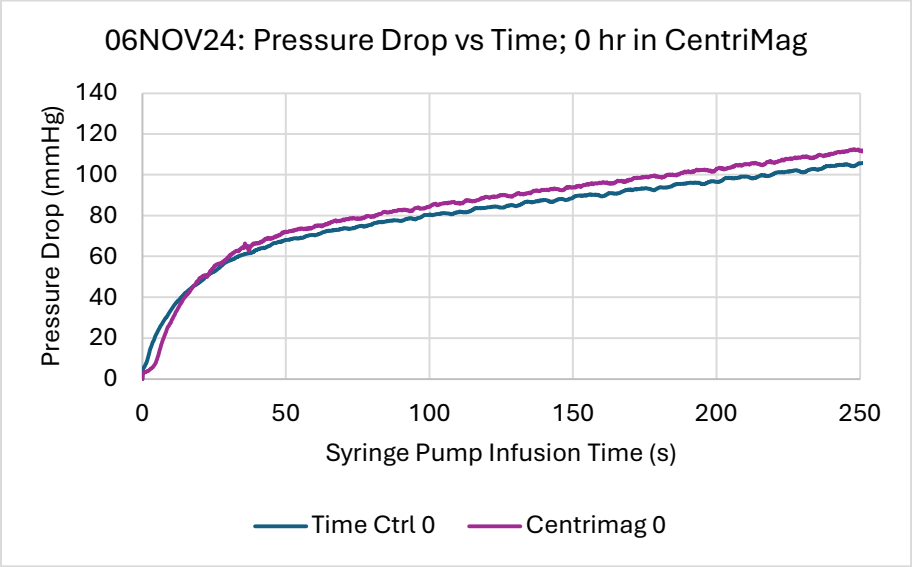

Figure 35: 06NOV24: Pressure Drop vs Time; 0 hr in CentriMag

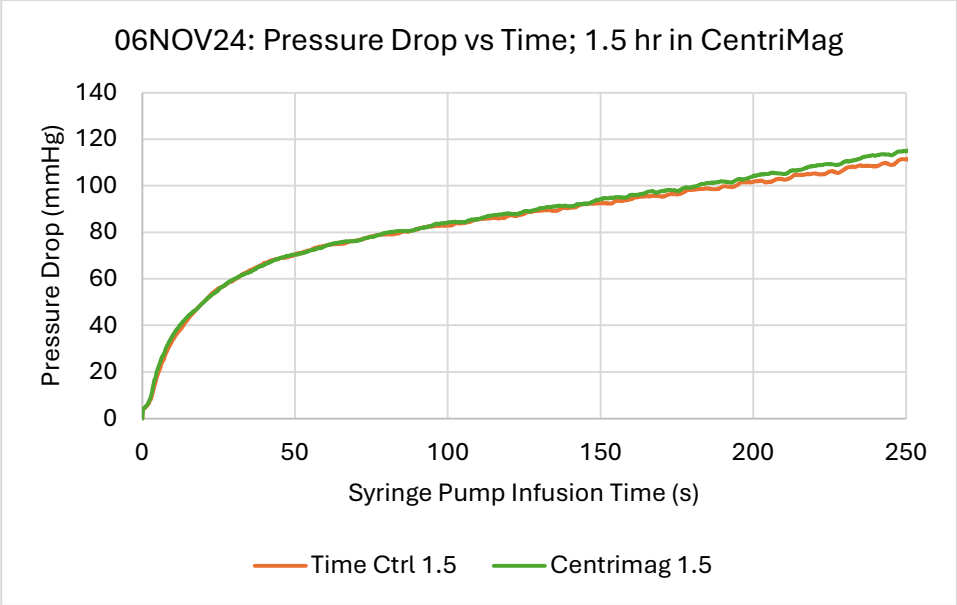

Figure 36: 06NOV24: Pressure Drop vs Time; 1.5 hr in CentriMag

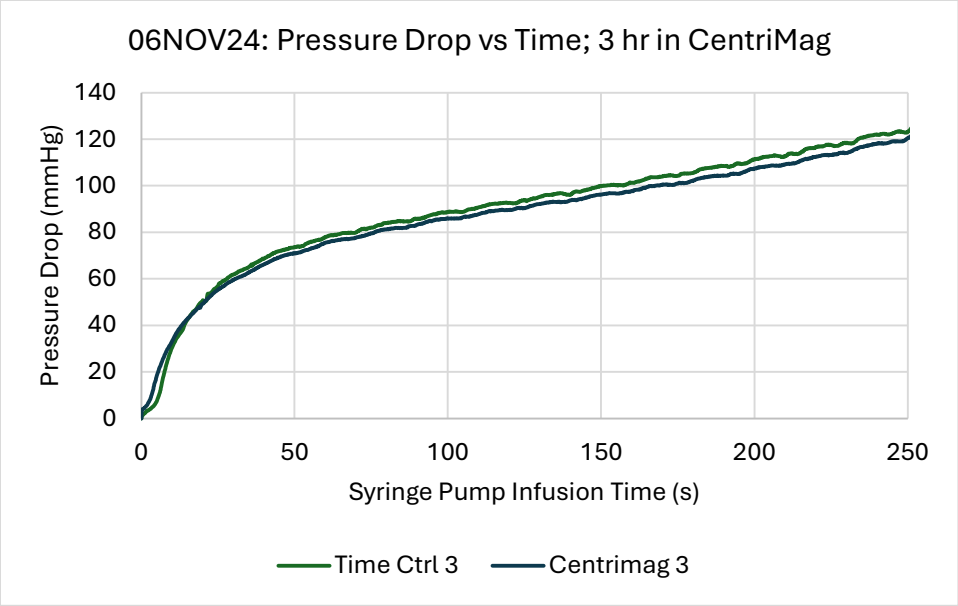

Figure 37: 06NOV24: Pressure Drop vs Time; 3 hr in CentriMag

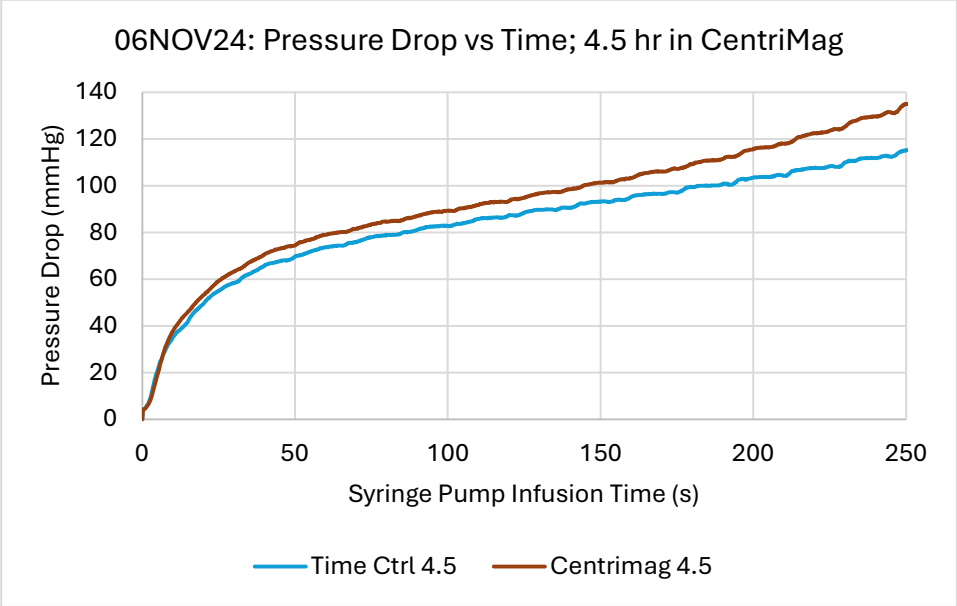

Figure 38: 06NOV24: Pressure Drop vs Time; 4.5 hr in CentriMag

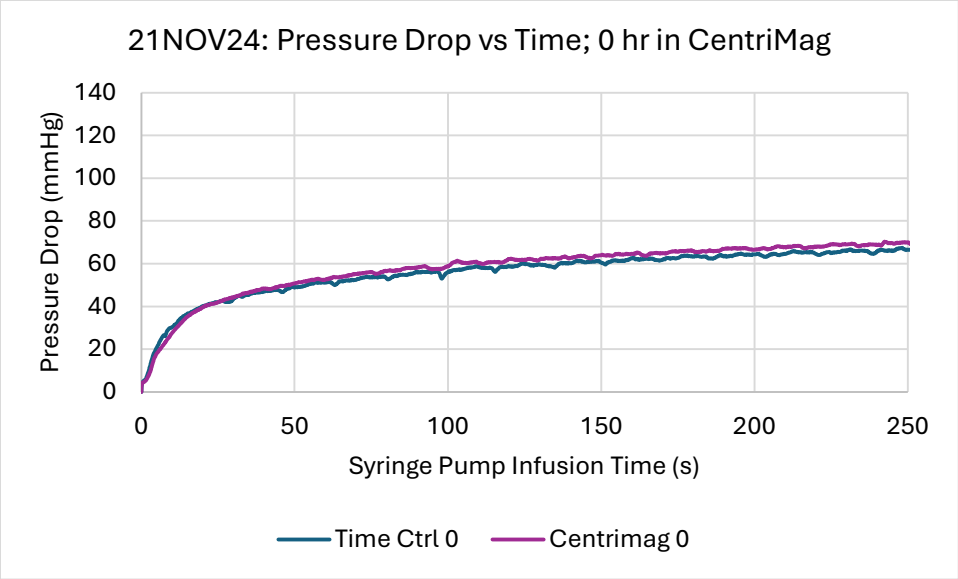

Figure 39: 21NOV24: Pressure Drop vs Time; 0 hr in CentriMag

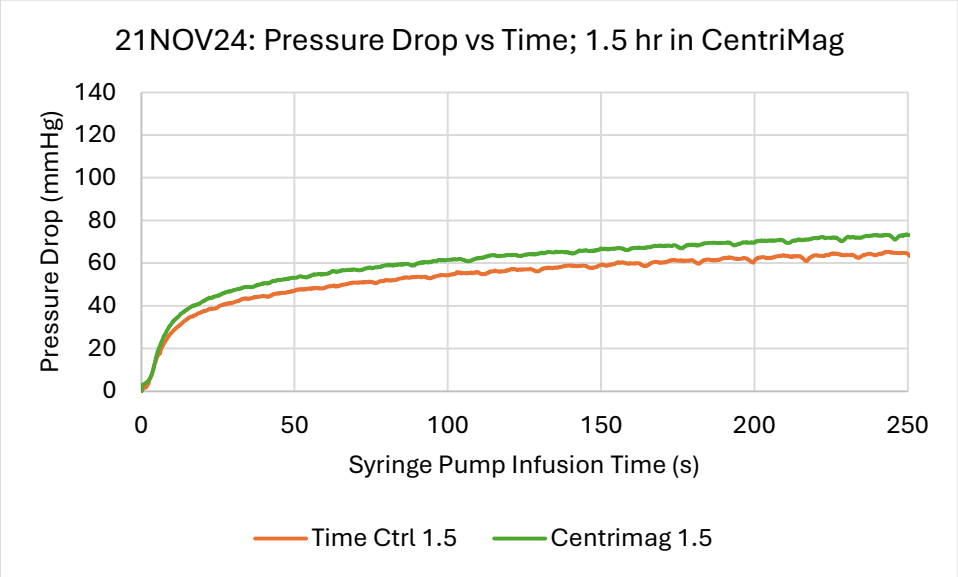

Figure 40: 21NOV24: Pressure Drop vs Time; 1.5 hr in CentriMag

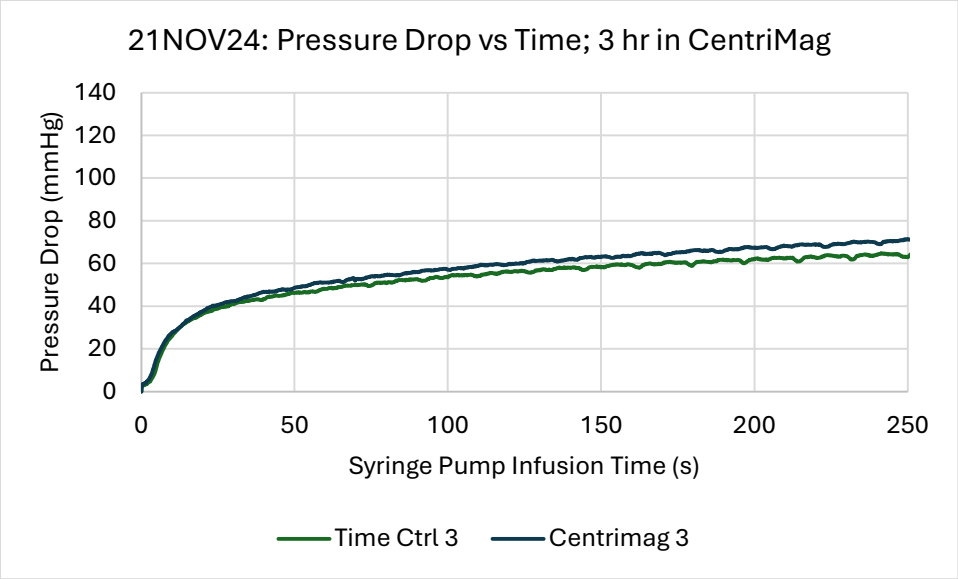

Figure 41: 21NOV24: Pressure Drop vs Time; 3 hr in CentriMag

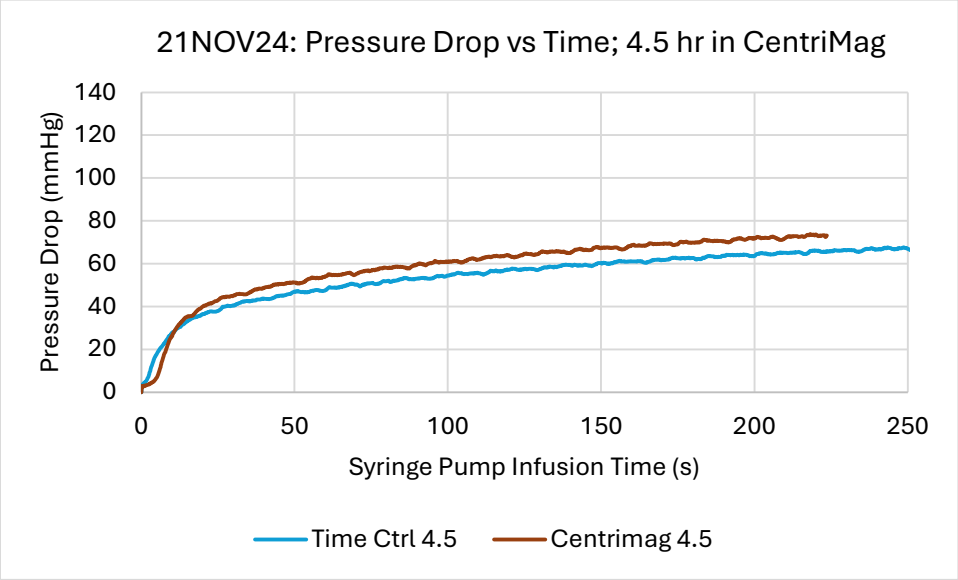

Figure 42: 21NOV24: Pressure Drop vs Time; 4.5 hr in CentriMag

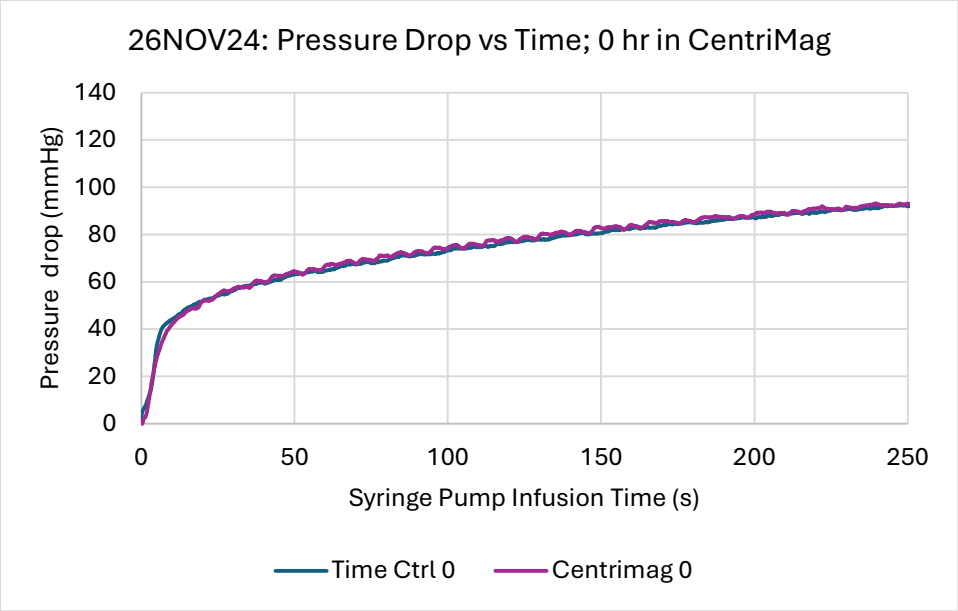

Figure 43: 26NOV24: Pressure Drop vs Time; 0 hr in CentriMag

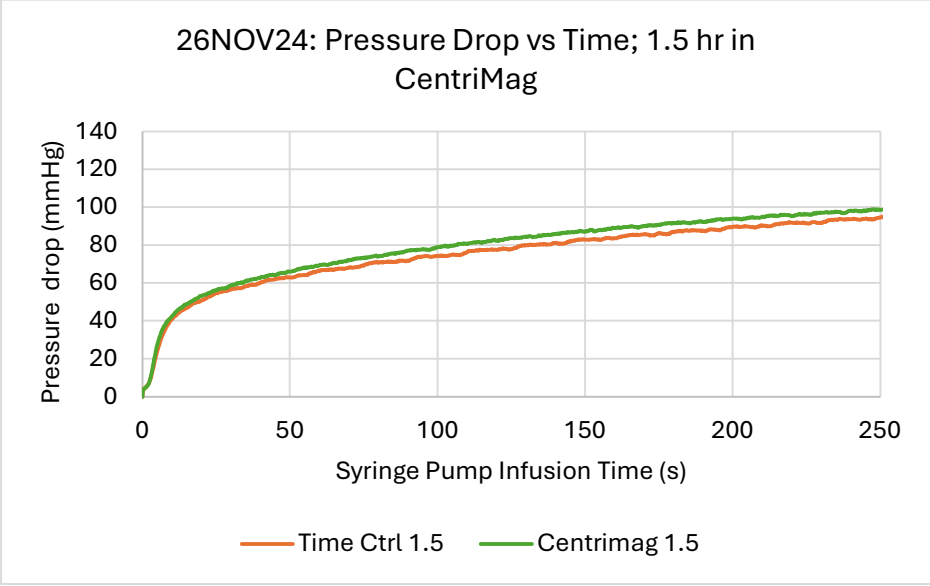

Figure 44: 26NOV24: Pressure Drop vs Time; 1.5 hr in CentriMag

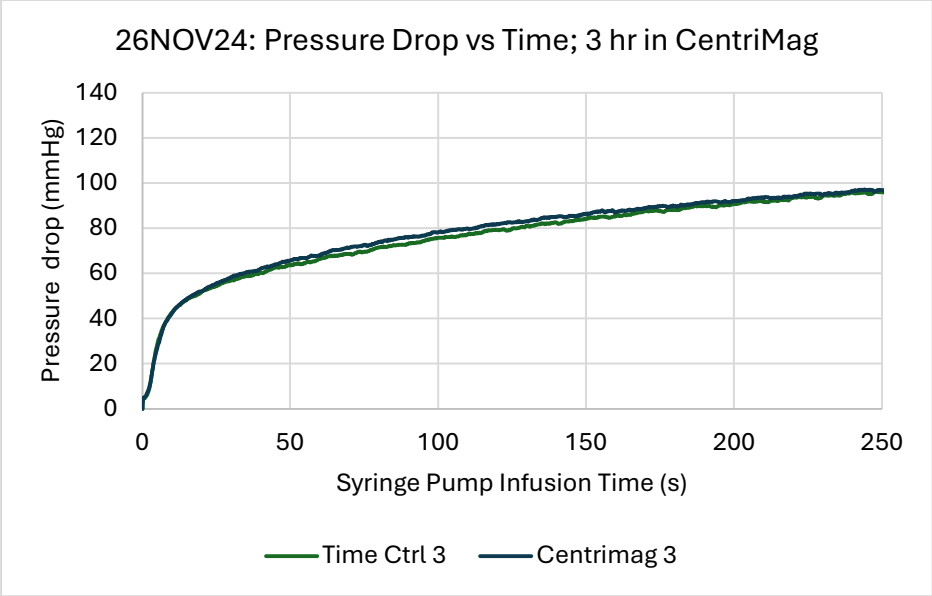

Figure 45: 26NOV24: Pressure Drop vs Time; 3 hr in CentriMag

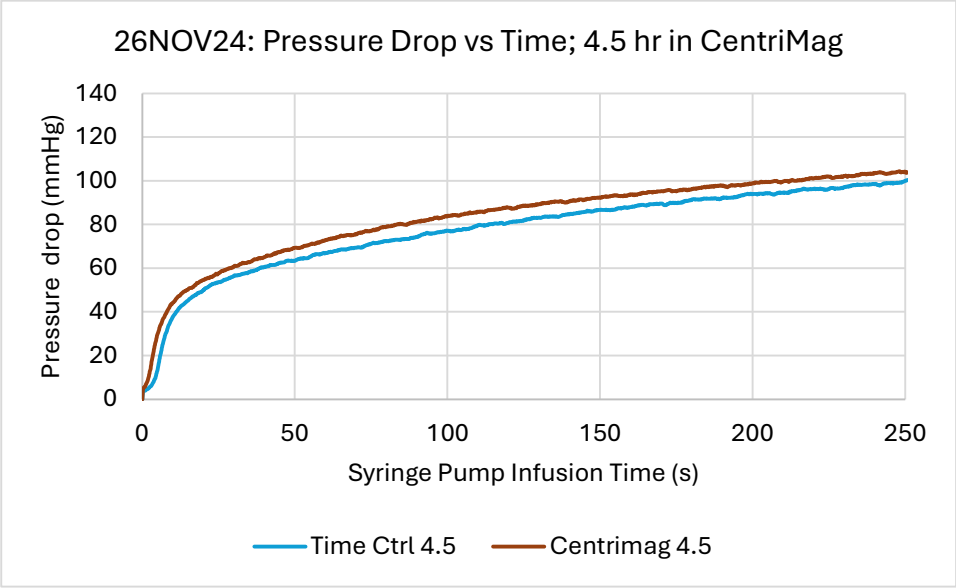

Figure 46: 26NOV24: Pressure Drop vs Time; 4.5 hr in CentriMag

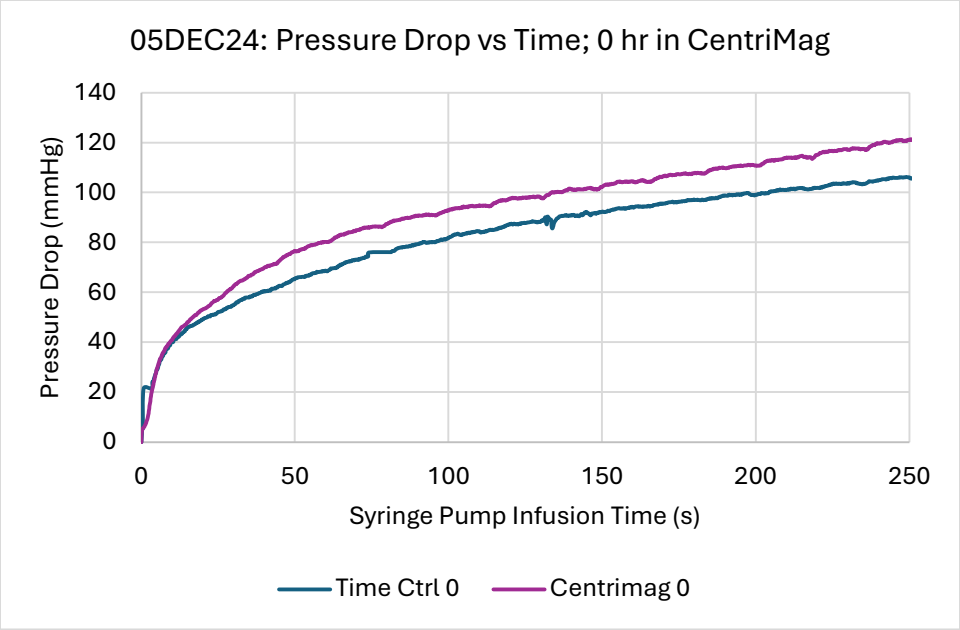

Figure 47: 05DEC24: Pressure Drop vs Time; 0 hr in CentriMag

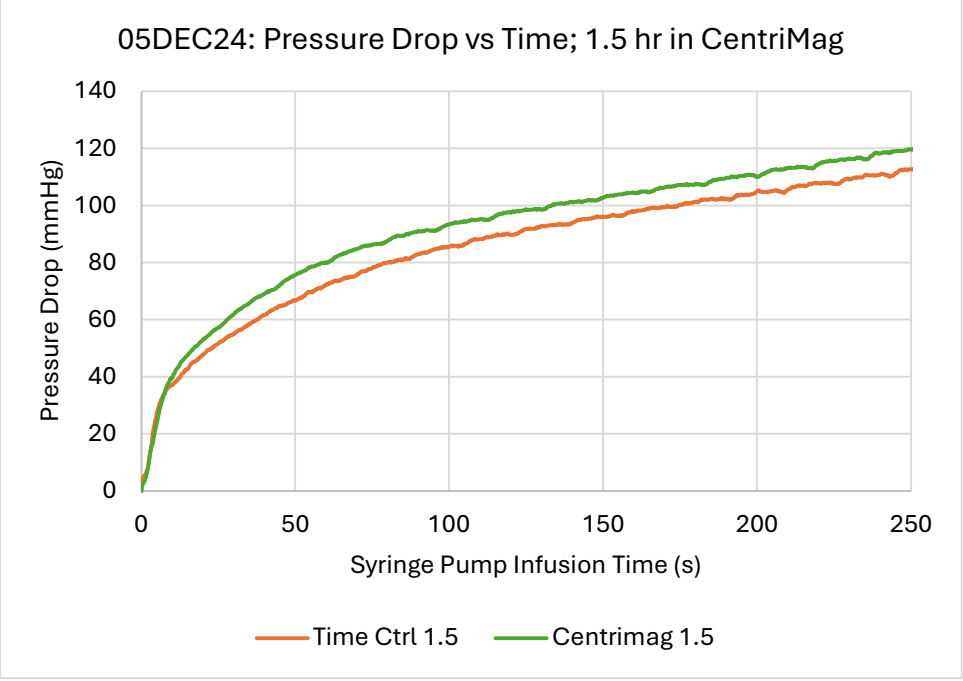

Figure 48: 05DEC24: Pressure Drop vs Time; 1.5 hr in CentriMag

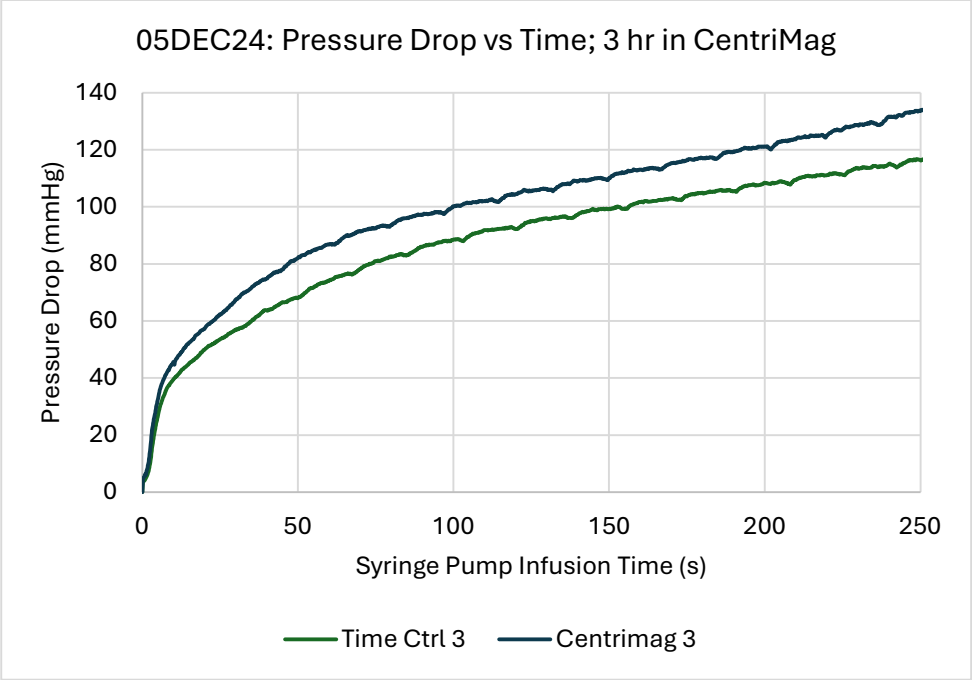

Figure 49: 05DEC24: Pressure Drop vs Time; 3 hr in CentriMag

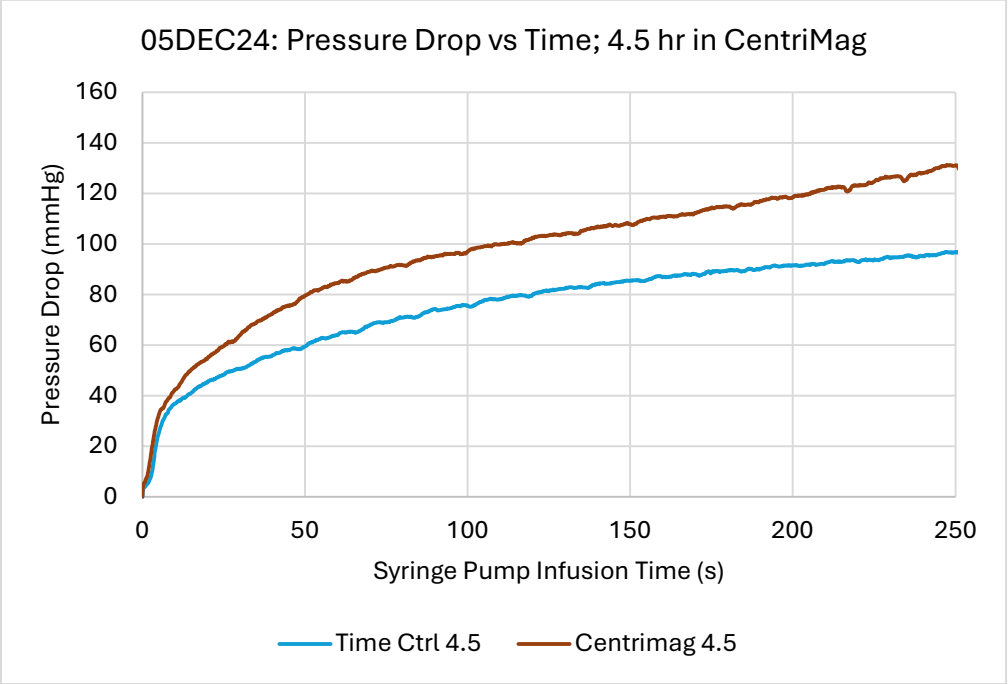

Figure 50: 05DEC24: Pressure Drop vs Time; 4.5 hr in CentriMag

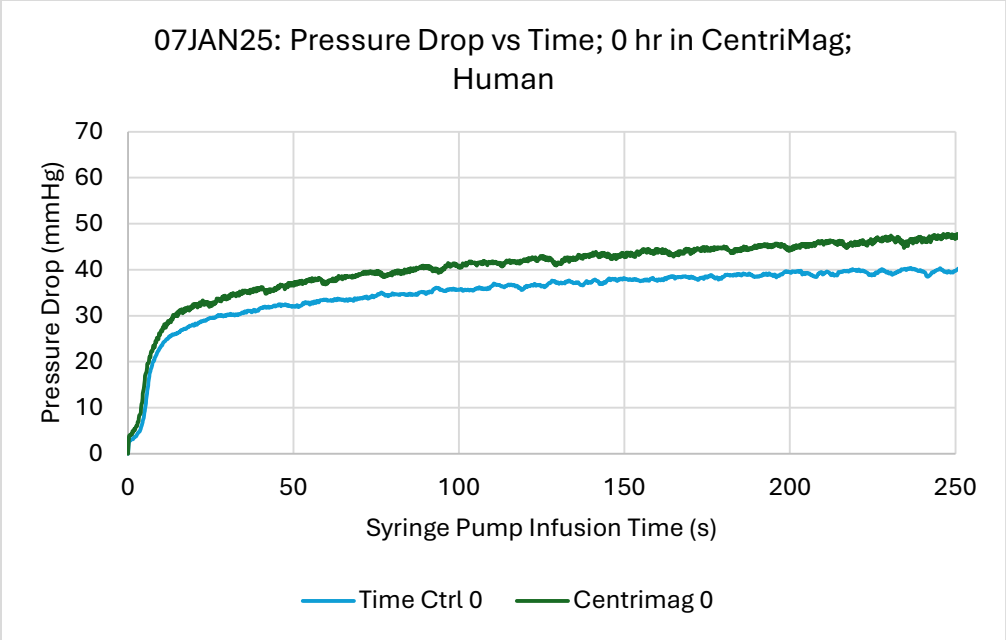

Figure 51: 07JAN25: Pressure Drop vs Time; 0 hr in CentriMag; Human

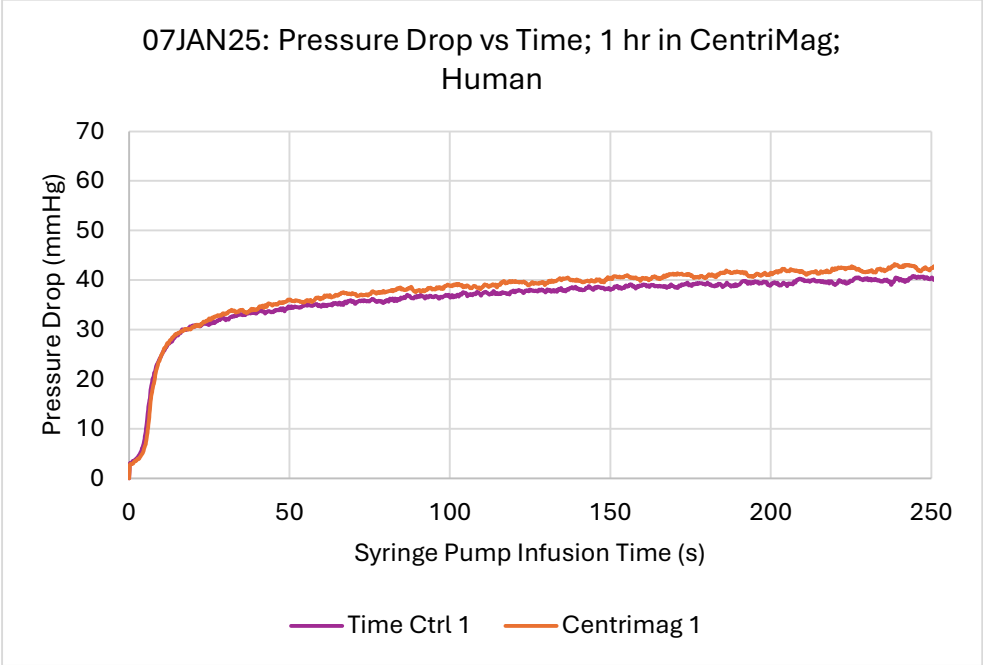

Figure 52: 07JAN25: Pressure Drop vs Time; 1 hr in CentriMag; Human

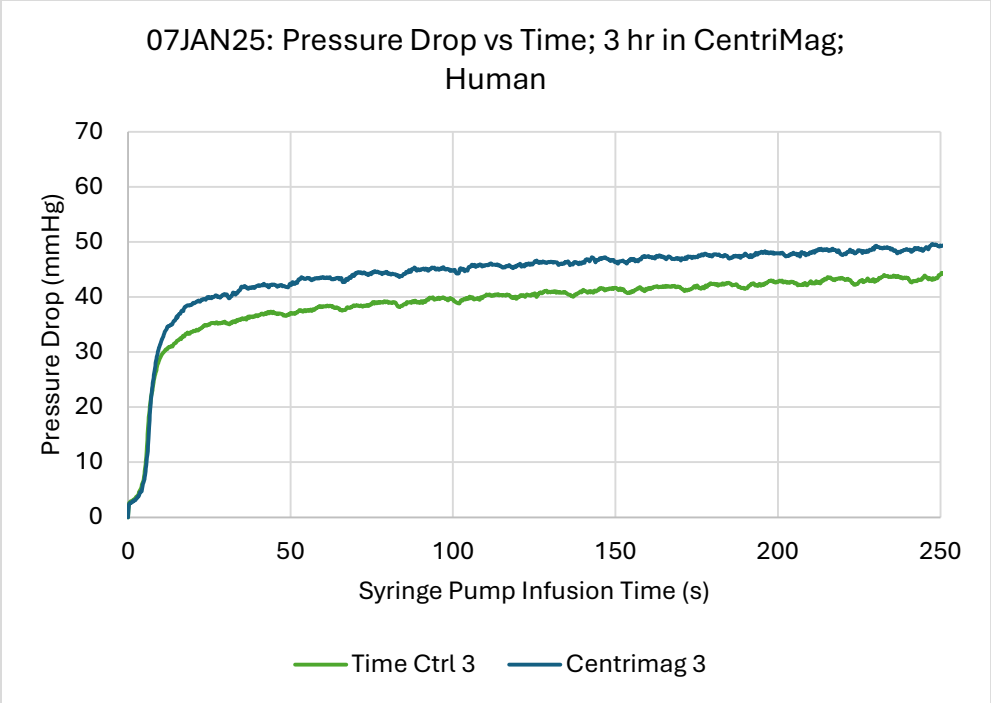

Figure 53: 07JAN25: Pressure Drop vs Time; 3 hr in CentriMag; Human

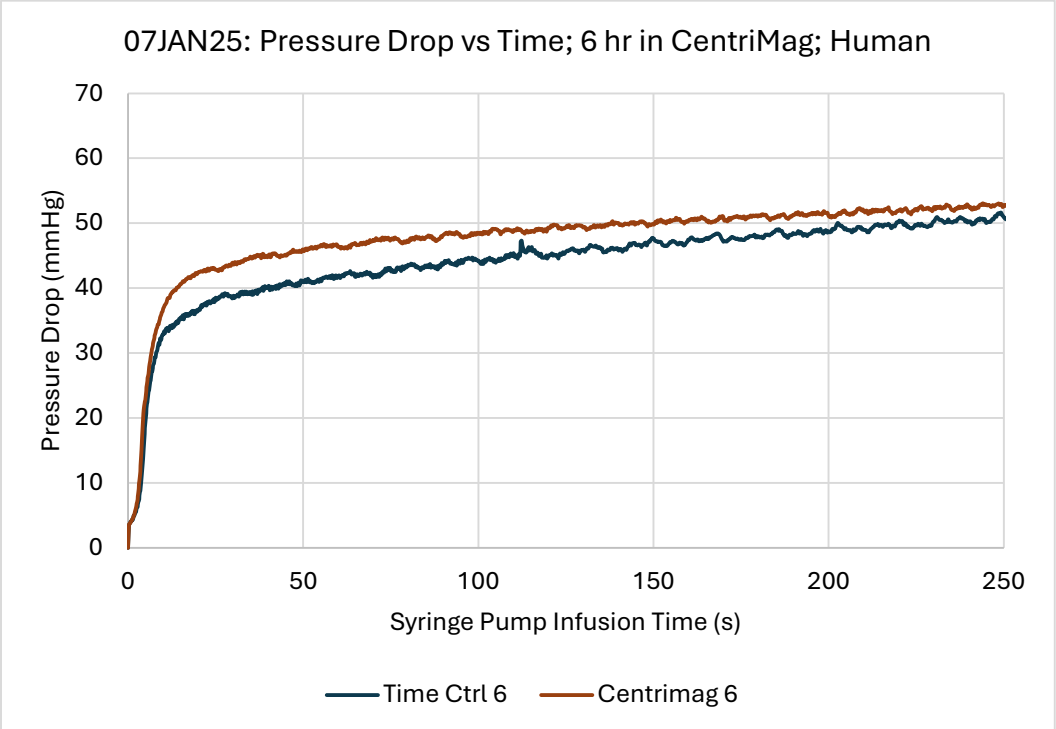

Figure 54: 07JAN25: Pressure Drop vs Time; 6 hr in CentriMag; Human

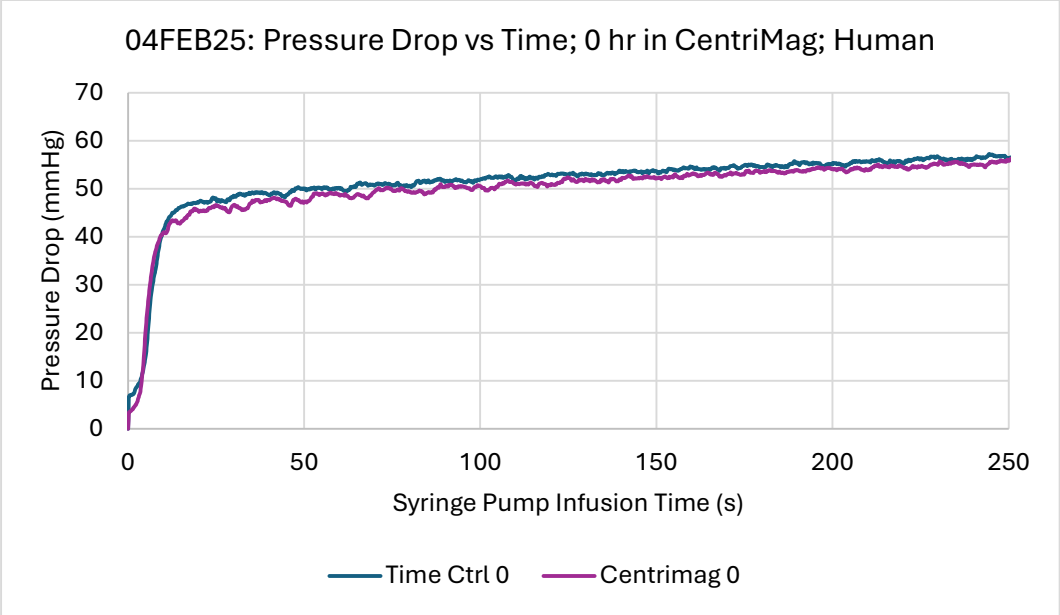

Figure 55: 04FEB25: Pressure Drop vs Time; 0 hr in CentriMag; Human

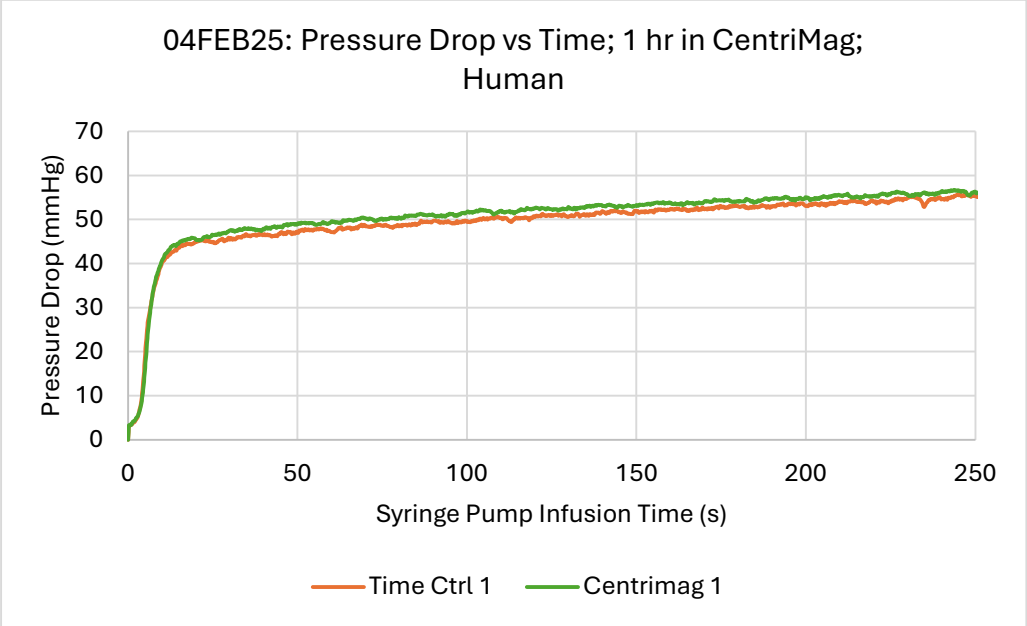

Figure 56: 04FEB25: Pressure Drop vs Time; 1 hr in CentriMag; Human

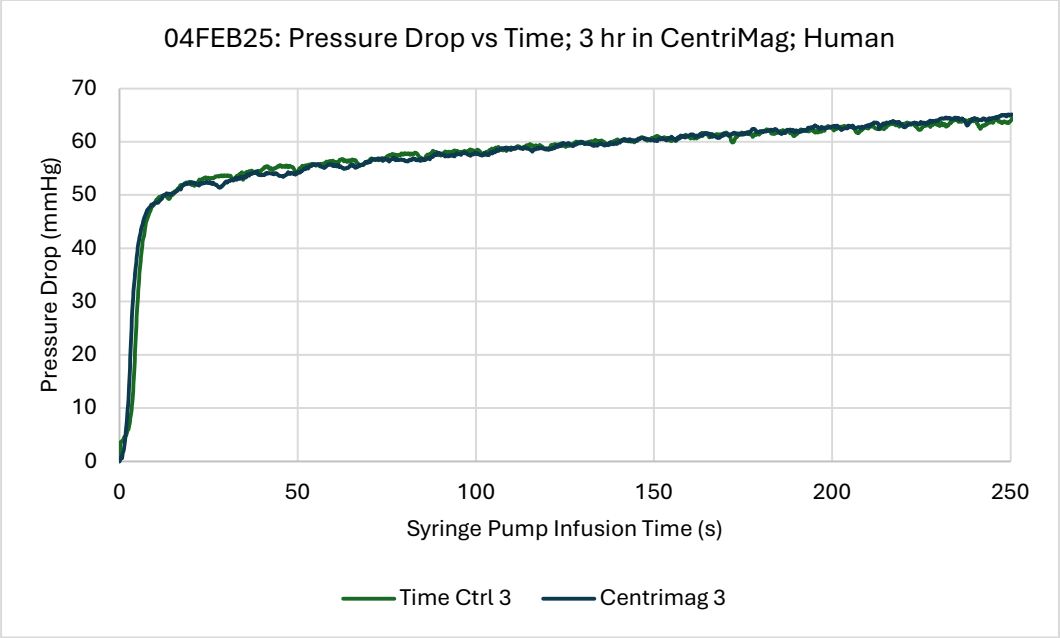

Figure 57: 04FEB25: Pressure Drop vs Time; 3 hr in CentriMag; Human

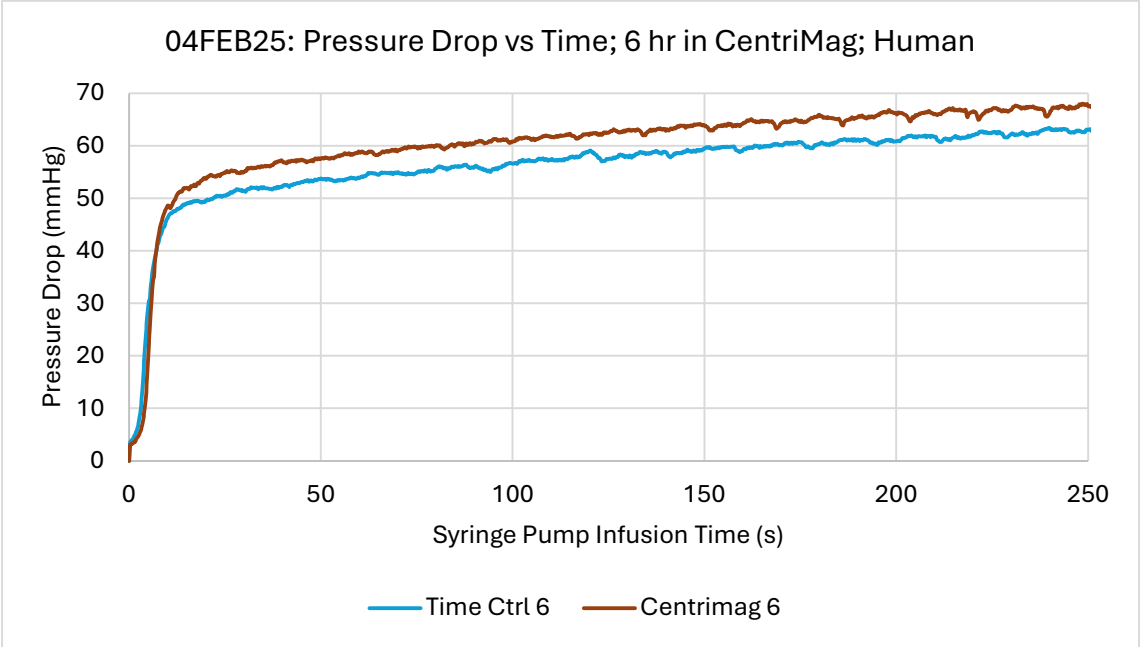

Figure 58: 04FEB25: Pressure Drop vs Time; 6 hr in CentriMag; Human

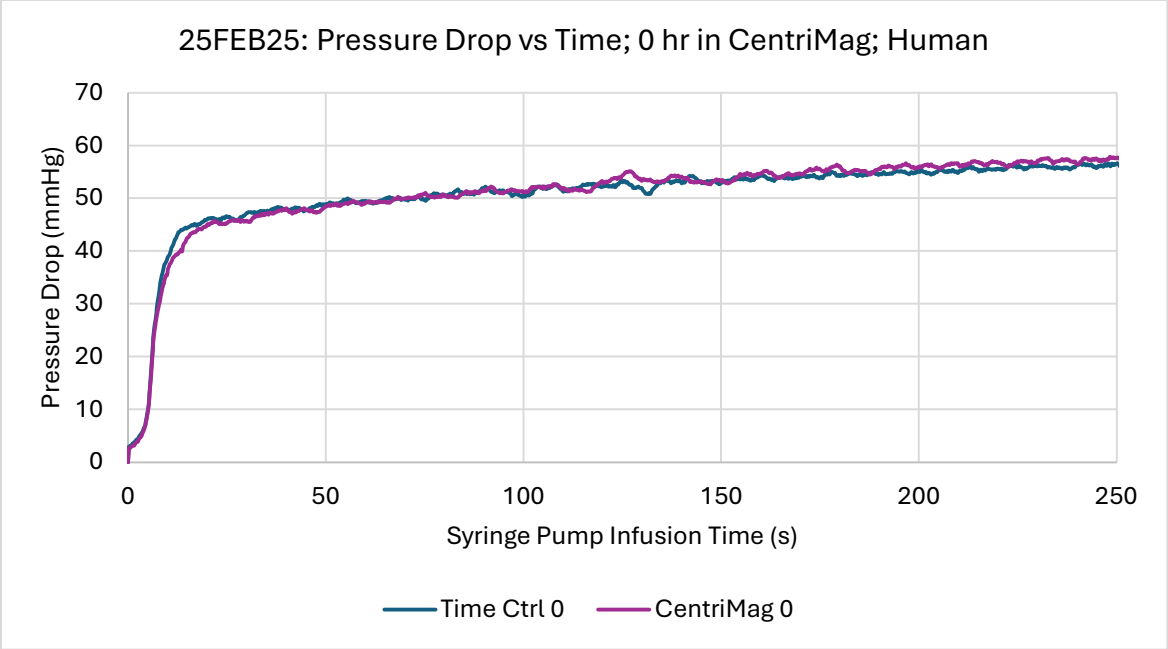

Figure 59: 25FEB25: Pressure Drop vs Time; 0 hr in CentriMag; Human

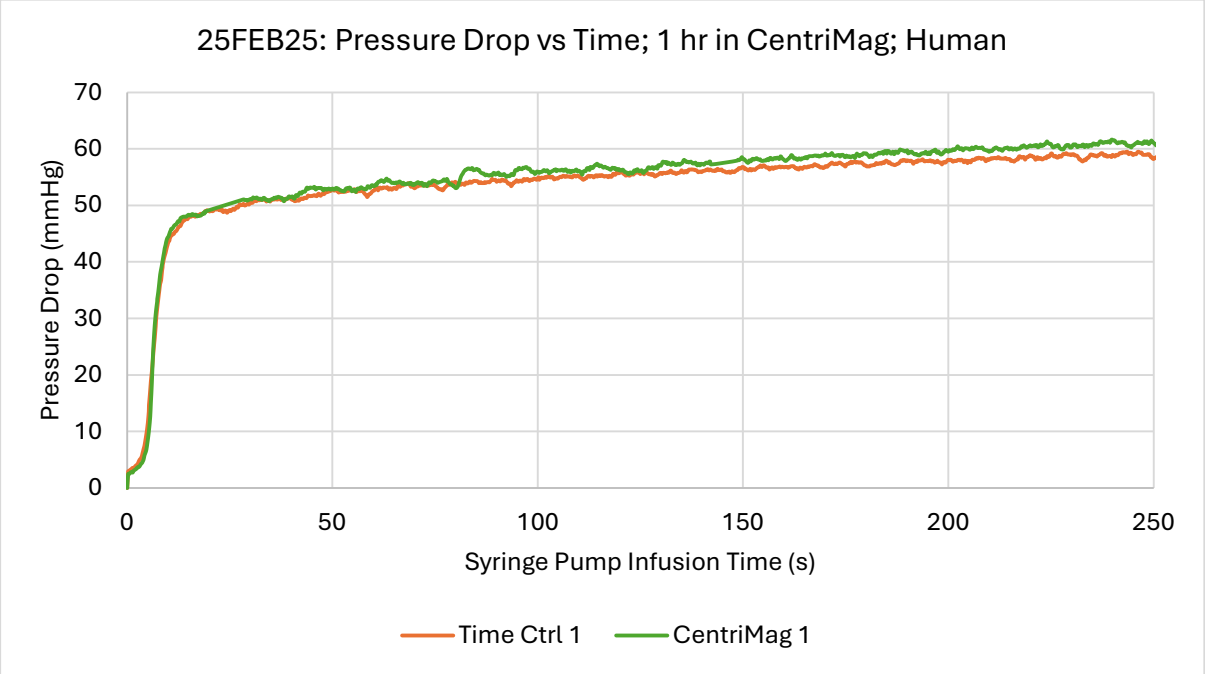

Figure 60: 25FEB25: Pressure Drop vs Time; 1 hr in CentriMag; Human

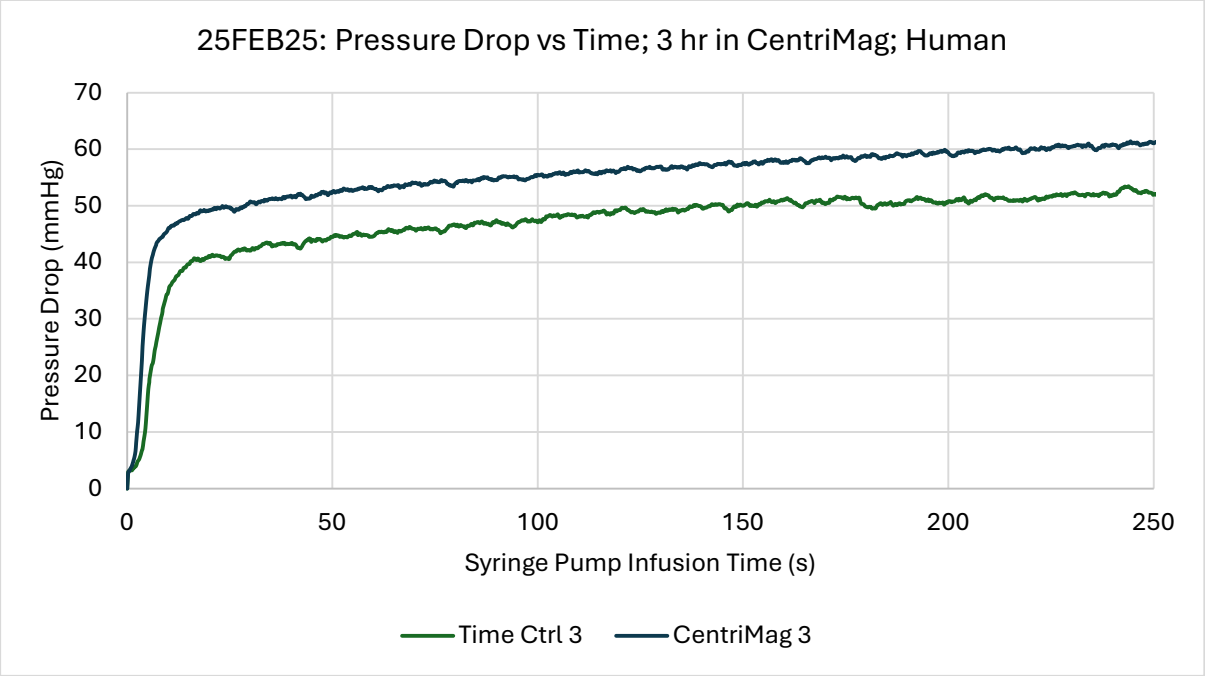

Figure 61: 25FEB25: Pressure Drop vs Time; 3 hr in CentriMag; Human

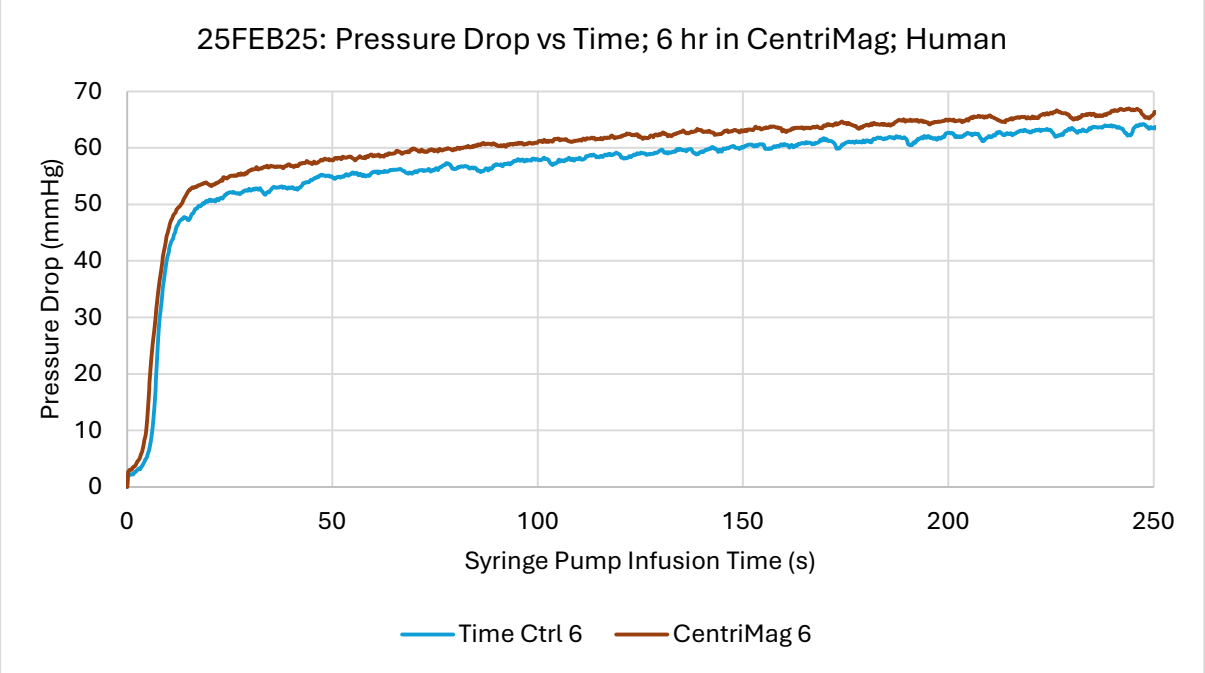

Figure 62: 25FEB25: Pressure Drop vs Time; 6 hr in CentriMag; Human

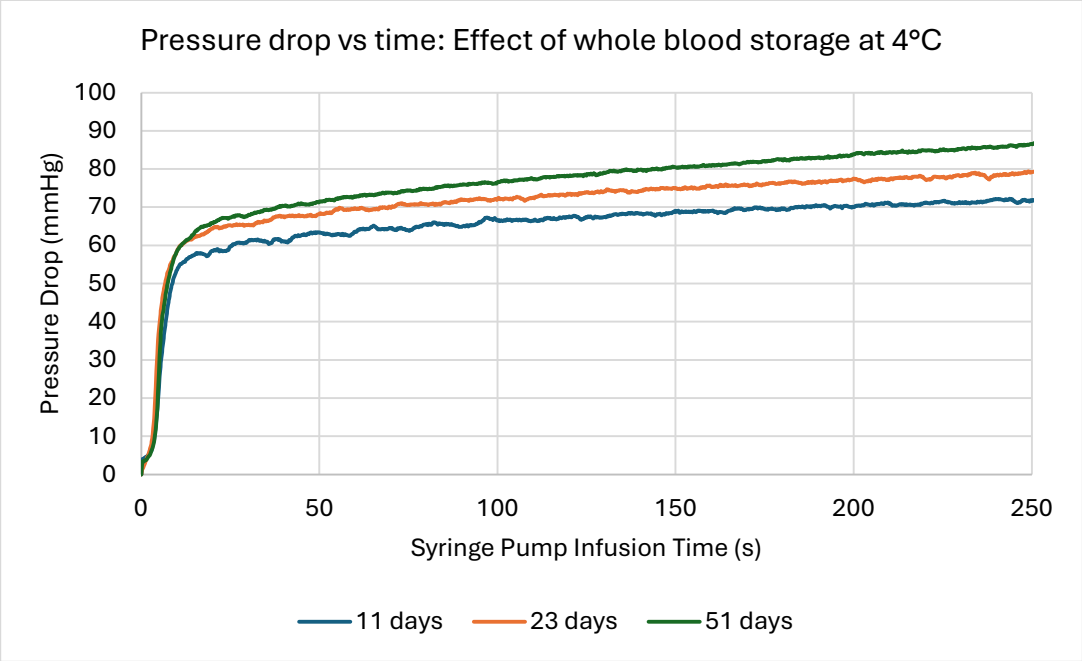

Figure 63: Pressure drop vs time: Effect of whole blood storage at 4°C

Statistics

Bovine

Anova: Single Factor
Bovine Loop
SUMMARY

Groups	*Count*	*Sum*	*Average*	*Variance*
0	4	256	64	88.66667
1.5	4	264	66	114
3	4	259	64.75	150.9167
4.5	4	270	67.5	133.6667

ANOVA

Source of Variation	*SS*	*df*	*MS*	*F*	*P-value*	*F crit*
Between Groups	28.1875	3	9.395833	0.077134	0.971162	3.490295
Within Groups	1461.75	12	121.8125			
Total	1489.938	15				

Anova: Single Factor
Bovine Time Control
SUMMARY

Groups	*Count*	*Sum*	*Average*	*Variance*
0	4	247	61.75	72.25
1.5	4	245	61.25	78.25
3	4	246	61.5	83
4.5	4	246	61.5	87

ANOVA

Source of Variation	*SS*	*df*	*MS*	*F*	*P-value*	*F crit*
Between Groups	0.5	3	0.166667	0.00208	0.999861	3.490295
Within Groups	961.5	12	80.125			
Total	962	15				

Table 49: One-way ANOVA results for 0 through 4.5 hours (bovine P_0) (loop and time control)

Descriptive Statistics (Bovine P_0)		
Sample	Mean	Std. Deviation
time0_stagnant	61.7500	8.50000
time0_loop	64.0000	9.41630
time1.5_stagnant	61.2500	8.84590

time1.5_loop	66.0000	10.67708
Time3_stagnant	61.5000	9.11043
time3_loop	64.7500	12.28481
time4.5_stagnant	61.5000	9.32738
time4.5_loop	67.5000	11.56143

Table 50: Descriptive statistics for bovine P_0

Mauchly's test of sphericity (Bovine P_0)	
Within Subjects Effect	Mauchly's W
Time	.241
Condition	1.000
Time * Condition	.387

Table 51: Mauchly's test of sphericity results for bovine P_0

Repeated-Measures ANOVA (Bovine P_0)			
Source		Sig.	Partial Eta Squared
Time	Sphericity Assumed	.505	.219
	Greenhouse-Geisser	.459	.219
Condition	Sphericity Assumed	.078	.698
	Greenhouse-Geisser	.078	.698
Time * Condition	Sphericity Assumed	.155	.426
	Greenhouse-Geisser	.195	.426

Table 52: Repeated-measures ANOVA results with Greenhouse-Geisser correction for non-spherical groups (bovine P_0)

Paired Samples Correlations (Bovine P_0)			
Compared Samples		Correlation	Two-Sided p
Pair 1	loop0 & time0	.979	.021
Pair 2	loop1.5 & time1.5	.900	.100
Pair 3	loop3 & time3	.972	.028
Pair 4	loop4.5 & time4.5	.977	.023

Table 53: Pearson correlation coefficients with significance values (bovine P_0)

Paired T-Test (Bovine P_0)		
Compared Samples		Two-Sided p
Pair 1	loop0 - time0	.117
Pair 2	loop1.5 - time1.5	.137
Pair 3	loop3 - time3	.205
Pair 4	loop4.5 - time4.5	.032

Table 54: Paired sample t-test (bovine P_0)

Anova: Single Factor						
Time Control						
SUMMARY						
Groups	*Count*	*Sum*	*Average*	*Variance*		
Row 1	4	30.54187	7.635467	0.4944042		
Row 2	4	34.08093	8.520233	0.5603463		
Row 3	4	38.17733	9.544333	3.1898131		
Row 4	4	38.40027	9.600067	1.1888998		
ANOVA						
rce of Variat	*SS*	*df*	*MS*	*F*	*P-value*	*F crit*
Between Gr	10.50416421	3	3.501388	2.5776473	0.1023302	3.49029482
Within Grou	16.30039024	12	1.358366			
Total	26.80455444	15				

Anova: Single Factor						
CentriMag						
SUMMARY						
Groups	*Count*	*Sum*	*Average*	*Variance*		
Row 1	3	26.2504	8.750133	2.582032		
Row 2	4	50.8288	12.7072	2.942093		
Row 3	4	75.8252	18.9563	15.70309		
Row 4	4	96.61373	24.15343	40.92754		
ANOVA						
Source of Varia	*SS*	*df*	*MS*	*F*	*P-value*	*F crit*
Between G	495.8849	3	165.295	9.888092	0.001866	3.587434
Within Gr	183.8823	11	16.71657			
Total	679.7672	14				

Table 55: One-way ANOVA for bovine PFH over 4.5 hours

Descriptive Statistics (Bovine PFH)		
Sample	Mean	Std. Deviation
bovine_pfh0_stagnant	7.9048	.55337
bovine_pfh0_loop	8.7501	1.60687
bovine_pfh1.5_stagnant	8.6480	.86177
bovine_pfh1.5_loop	12.4750	2.02227
bovine_pfh3_stagnant	9.8462	2.05862
bovine_pfh3_loop	18.2712	4.55399
bovine_pfh4.5_stagnant	9.8555	1.17976
bovine_pfh4.5_loop	23.0829	7.38342

Table 56: Descriptive statistics for bovine PFH

Mauchly's test of sphericity (Bovine PFH)	
Within Subjects Effect	Mauchly's W
Time	.000
Condition	1.000
Time * Condition	.000

Table 57: Mauchly's test of sphericity results for bovine PFH

Repeated-Measures ANOVA (Bovine PFH)			
Source		Sig.	Partial Eta Squared
Time	Sphericity Assumed	.004	.871
	Greenhouse-Geisser	.066	.871
Condition	Sphericity Assumed	.114	.785
	Greenhouse-Geisser	.114	.785
Time * Condition	Sphericity Assumed	.050	.704
	Greenhouse-Geisser	.157	.704

Table 58: Repeated-measures ANOVA results with Greenhouse-Geisser correction for non-spherical groups (bovine PFH)

Paired Samples Correlations (Bovine PFH)			
Compared Samples		Correlation	Two-Sided p
Pair 1	bovine_pfh0_stagnant & bovine_pfh0_loop	.677	.527
Pair 2	bovine_pfh1.5_stagnant & bovine_pfh1.5_loop	-.920	.080
Pair 3	bovine_pfh3_stagnant & bovine_pfh3_loop	-.992	.008
Pair 4	bovine_pfh4.5_stagnant & bovine_pfh4.5_loop	-.989	.011

Table 59: Pearson correlation coefficients with significance values (bovine PFH)

Paired t-test (Bovine PFH)		
Compared Samples		Two-Sided p

		Std. Deviation	
Pair 1	bovine_pfh0_stagnant - bovine_pfh0_loop	1.29792	.376
Pair 2	bovine_pfh1.5_stagnant - bovine_pfh1.5_loop	2.42161	.041
Pair 3	bovine_pfh3_stagnant - bovine_pfh3_loop	5.73929	.046
Pair 4	bovine_pfh4.5_stagnant - bovine_pfh4.5_loop	7.47760	.030

Table 60: Paired sample t-test (bovine PFH)

Descriptive Statistics (Bovine MCV)		
Sample	Mean	Std. Deviation
time0_stagnant	61.4033	6.40984
time1_stagnant	61.8500	5.87945
time3_stagnant	59.6567	6.82016
time6_stagnant	62.0467	10.82731
time0_loop	58.6200	7.64702
time1_loop	59.3400	6.24741
time3_loop	59.1033	8.82581
time6_loop	61.8700	14.64254

Table 61: Descriptive statistics for bovine MCV

Paired t-test (Bovine MCV)		
Compared Samples		Two-Sided p
Pair 1	time0_stagnant - time0_loop	.278

Pair 2	time1_stagnant - time1_loop	.009
Pair 3	time3_stagnant - time3_loop	.825
Pair 4	time6_stagnant - time6_loop	.956

Table 62: Paired sample t-test for bovine MCV

Human

Anova: Single Factor

Human Time Control

SUMMARY

Groups	*Count*	*Sum*	*Average*	*Variance*
0	3	131	43.66667	70.33333
1	3	132.5	44.16667	79.08333
3	3	137	45.66667	64.33333
6	3	146	48.66667	57.33333

ANOVA

Source of Variation	*SS*	*df*	*MS*	*F*	*P-value*	*F crit*
Between Groups	45.5625	3	15.1875	0.224101	0.877044	4.066181
Within Groups	542.166667	8	67.77083			
Total	587.729167	11				

Anova: Single Factor

Human Loop

SUMMARY

Groups	*Count*	*Sum*	*Average*	*Variance*
0	3	131	43.66667	46.33333
1	3	136	45.33333	74.33333
3	3	149	49.66667	44.33333
6	3	159	53	37

ANOVA

Source of Varia	*SS*	*df*	*MS*	*F*	*P-value*	*F crit*
Between G	160.9167	3	53.63889	1.062156	0.417463	4.066181
Within Gr	404	8	50.5			
Total	564.9167	11				

Table 63: One-way ANOVA results for 0 to 4.5 hours (human P_0) (loop and time control)

Descriptive Statistics (Human P_0)		
Sample	Mean	Std. Deviation
human_time0_stagnant	43.6667	8.38650
human_time0_loop	43.6667	6.80686
human_time1_stagnant	44.1667	8.89288
human_time1_loop	45.3333	8.62168
human_time3_stagnant	45.6667	8.02081
human_time3_loop	49.6667	6.65833
human_time6_stagnant	48.6667	7.57188
human_time6_loop	53.0000	6.08276

Table 64: Descriptive statistics for human P_0

Mauchly's test of sphericity (Human P_0)

Within Subjects Effect	Mauchly's W
Time	.000
Condition	1.000
Time * Condition	.000

Table 65: Mauchly's test of sphericity results for human P_0

Repeated-Measured ANOVA (Human P_0)			
Source		Sig.	Partial Eta Squared
Time	Sphericity Assumed	.038	.731
	Greenhouse-Geisser	.140	.731
Condition	Sphericity Assumed	.101	.808
	Greenhouse-Geisser	.101	.808
Time * Condition	Sphericity Assumed	.128	.587
	Greenhouse-Geisser	.218	.587

Table 66: Repeated-measures ANOVA results with Greenhouse-Geisser correction for non-spherical groups (human P_0)

Paired Samples Correlations (Human P_0)			
Compared Samples		Correlation	Two-Sided p
Pair 1	human_time0_stagnant & human_time0_loop	.987	.103
Pair 2	human_time1_stagnant & human_time1_loop	1.000	.007
Pair 3	human_time3_stagnant & human_time3_loop	.868	.331

Pair 4	human_time6_stagnant & human_time6_loop	.999	.032

Table 67: Pearson correlation coefficients with significance values (human P_0)

Paired t-test (Human P_0)		
Compared Samples		Two-Sided p
Pair 1	human_time0_stagnant - human_time0_loop	1.000
Pair 2	human_time1_stagnant - human_time1_loop	.020
Pair 3	human_time3_stagnant - human_time3_loop	.225
Pair 4	human_time6_stagnant - human_time6_loop	.039

Table 68: Paired sample t-test (human P_0)

Anova: Single Factor

Time Control

SUMMARY

Groups	*Count*	*Sum*	*Average*	*Variance*
Time0	3	33.16133	11.05378	3.016383
Time1	3	34.83333	11.61111	4.869234
Time3	3	36.89547	12.29849	3.339429
Time6	3	42.44093	14.14698	1.356117

ANOVA

ce of Varia	*SS*	*df*	*MS*	*F*	*P-value*	*F crit*
Between G	16.31087	3	5.436958	1.728603	0.238178	4.066181
Within Gr	25.16233	8	3.145291			
Total	41.4732	11				

Anova: Single Factor

CentriMag

SUMMARY

Groups	*Count*	*Sum*	*Average*	*Variance*
CM0	3	31.9352	10.64507	11.14817
CM1	3	48.1536	16.0512	10.49043
CM3	3	70.66986667	23.55662	37.62882
CM6	3	98.53653333	32.84551	55.49027

ANOVA

Source of Variati	*SS*	*df*	*MS*	*F*	*P-value*	*F crit*
Between Gro	835.09349	3	278.3645	9.702688	0.0048349	4.0661806
Within Grou	229.51538	8	28.68942			
Total	1064.6089	11				

Table 69: One-way ANOVA for human PFH over 6 hours

Descriptive Statistics (Human PFH)		
Sample	Mean	Std. Deviation
human_pfh0_stagnant	11.0538	1.73677

human_pfh0_loop	10.6451	3.33889
human_pfh1_stagnant	11.6111	2.20663
human_pfh1_loop	16.0512	3.23889
human_pfh3_stagnant	12.2985	1.82741
human_pfh3_loop	23.5566	6.13423
human_pfh6_stagnant	14.1470	1.16452
human_pfh6_loop	32.8455	7.44918

Table 70: Descriptive statistics for human PFH

Mauchly's test of sphericity (Human PFH)	
Within Subjects Effect	Mauchly's W
Time	.000
Condition	1.000
Time * Condition	.000

Table 71: Mauchly's test of sphericity results for human PFH

Repeated-Measures ANOVA (Human PFH)			
Source		Sig.	Partial Eta Squared
Time	Sphericity Assumed	<.001	.988
	Greenhouse-Geisser	.002	.988
Condition	Sphericity Assumed	.062	.880
	Greenhouse-Geisser	.062	.880
Time * Condition	Sphericity Assumed	.003	.892
	Greenhouse-Geisser	.055	.892

Table 72: Repeated-measures ANOVA results with Greenhouse-Geisser correction for non-spherical groups (human PFH)

Post-hoc Pairwise Comparison for Time (Human PFH)						
(I) Time	(J) Time	Mean Difference (I-J)	Std. Error	Sig.[b]	95% Confidence Interval for Difference[b]	
					Lower Bound	Upper Bound
1	2	-2.982*	.124	.010	-4.330	-1.634
	3	-7.078	.868	.088	-16.523	2.366
	4	-12.647*	.630	.015	-19.507	-5.786
2	1	2.982*	.124	.010	1.634	4.330
	3	-4.096	.747	.190	-12.225	4.033
	4	-9.665*	.519	.017	-15.316	-4.014
3	1	7.078	.868	.088	-2.366	16.523
	2	4.096	.747	.190	-4.033	12.225
	4	-5.569*	.507	.049	-11.091	-.046
4	1	12.647*	.630	.015	5.786	19.507
	2	9.665*	.519	.017	4.014	15.316
	3	5.569*	.507	.049	.046	11.091
Based on estimated marginal means						
*. The mean difference is significant at the .05 level.						
b. Adjustment for multiple comparisons: Bonferroni.						

Table 73: Post-hoc Pairwise Comparison for Time (human PFH)

Paired Samples Correlations (Human PFH)			
Compared Samples		Correlation	Two-Sided p
Pair 1	human_pfh0_stagnant & human_pfh0_loop	.997	.046

Pair 2	human_pfh1_stagnant & human_pfh1_loop	.977	.137
Pair 3	human_pfh3_stagnant & human_pfh3_loop	.938	.226
Pair 4	human_pfh6_stagnant & human_pfh6_loop	-.920	.256

Table 74: Pearson correlation coefficient with significant values (human PFH)

Paired t-test (Human PFH)		
Compared Samples		Two-Sided p
Pair 1	human_pfh0_stagnant - human_pfh0_loop	.703
Pair 2	human_pfh1_stagnant - human_pfh1_loop	.023
Pair 3	human_pfh3_stagnant - human_pfh3_loop	.049
Pair 4	human_pfh6_stagnant - human_pfh6_loop	.063

Table 75: Paired sample t-test (human PFH)

Descriptive Statistics (Human MCV)		
	Mean	Std. Deviation
human_time0_stagnant	128.2500	1.48492
human_time1_stagnant	135.7220	4.03733
human_time3_stagnant	129.3300	1.34584
human_time6_stagnant	134.1515	4.28877
human_time0_loop	133.9746	9.56875
human_time1_loop	141.1452	4.36360
human_time3_loop	133.4586	2.65830

human_time6_loop	125.4371	.61810

Table 76: Descriptive statistics for human MCV

Paired t-test (Human MCV)		
Compared Samples		Two-Sided p
Pair 1	human_time0_stagnant - human_time0_loop	.500
Pair 2	human_time1_stagnant - human_time1_loop	.983
Pair 3	human_time3_stagnant - human_time3_loop	.606
Pair 4	human_time6_stagnant - human_time6_loop	.028

Table 77: Paired sample t-test for human MCV

Paired samples correlations for human MCV			
Compared Samples		Correlation	Two-Sided p
Pair 1	human_time0_stagnant & human_time0_loop	1.000	<.001
Pair 2	human_time1_stagnant & human_time1_loop	.293	.811
Pair 3	human_time3_stagnant & human_time3_loop	1.000	.010
Pair 4	human_time6_stagnant & human_time6_loop	.947	.209

Table 78: Pearson correlation coefficients for human MCV

Correlations for cholesterol content and average P_0

		Cholesterol	Deformability_Loop_Average	Deformability_TimeControl_average
Cholesterol	Pearson Correlation	1	.885	.949
	Sig. (2-tailed)		.309	.205
	N	3	3	3
Deformability_Loop_Average	Pearson Correlation	.885	1	.987
	Sig. (2-tailed)	.309		.104
	N	3	3	3
Deformability_TimeControl_average	Pearson Correlation	.949	.987	1
	Sig. (2-tailed)	.205	.104	
	N	3	3	3

Table 79: Pearson correlation for donor total plasma cholesterol content and average P_0